

การสังเคราะห์ตัวเร่งปฏิกิริยาแซดเอสเอ็ม-5 ที่มีขนาดผลึกระดับนาโน  
สำหรับการผลิตแก๊สโซลีนจากพอลิโอเลฟินเหลือทิ้ง

นางสาวสินีนาด อุทโท

วิทยานิพนธ์นี้เป็นส่วนหนึ่งของการศึกษาตามหลักสูตรปริญญาวิทยาศาสตรมหาบัณฑิต  
สาขาวิชาปิโตรเคมี และวิทยาศาสตร์พอลิเมอร์  
คณะวิทยาศาสตร์ จุฬาลงกรณ์มหาวิทยาลัย  
ปีการศึกษา 2551  
ลิขสิทธิ์ของจุฬาลงกรณ์มหาวิทยาลัย

SYNTHESIS OF NANOCRYSTALLINE ZSM-5 CATALYST FOR PRODUCTION  
OF GASOLINE FROM POLYOLEFIN WASTE

Miss Sineenat Utto

A Thesis Submitted in Partial Fulfillment of the Requirements  
for the Degree of Master of Science Program in Petrochemistry and Polymer Science  
Faculty of Science  
Chulalongkorn University  
Academic Year 2008  
Copyright of Chulalongkorn University

Thesis Title                   SYNTHESIS OF NANOCRYSTALLINE ZSM-5 CATALYST FOR  
  PRODUCTION OF GASOLINE FROM POLYOLEFIN WASTE

By                                 Miss Sineenat Utto

Field of Study                 Petrochemistry and Polymer Science

Advisor                         Aticha Chaisuwan, Ph.D.

---

Accepted by the Faculty of Science, Chulalongkorn University in Partial Fulfillment  
of the Requirements for the Master's Degree

.....Dean of the Faculty of Science  
(Professor Supot Hannongbua, Dr.rer.nat.)

#### THESIS COMMITTEE

.....Chairman  
(Professor Pattarapan Prasassarakich, Ph.D.)

.....Advisor  
(Aticha Chaisuwan, Ph.D.)

.....Examiner  
(Assistant Professor Warinthorn Chavasiri, Ph.D.)

.....Examiner  
(Kongkrapan Intarajang, Ph.D.)

ลินีนาถ อุทโท : การสังเคราะห์ตัวเร่งปฏิกิริยาแซดเอสเอ็ม-5 ที่มีขนาดผลึกระดับนาโน สำหรับการผลิตแก๊สลิ้นจากพอลิโอเลฟินเหลือทิ้ง. (SYNTHESIS OF NANOCRYSTALLINE ZSM-5 CATALYST FOR PRODUCTION OF GASOLINE FROM POLYOLEFIN WASTE) อ. ที่ปริกษาวิทยานิพนธ์หลัก : ดร.อิริษา ฉายสุวรรณ, 121 หน้า.

ได้สังเคราะห์แซดเอสเอ็ม-5 ด้วยวิธีที่แตกต่างกันสองวิธีคือ วิธีไฮโดรเทอร์มัลและวิธีเซโรเจล วิธีไฮโดรเทอร์มัลทำได้โดยการผสมสารละลายโซเดียมเมตาซิลิเกตเพนทะไฮเดรต สารละลายโซเดียมอะลูมิเนตและสารละลายเททระเอทิลแอมโมเนียมโบรไมด์ ตามด้วยการตกผลึกที่ 170 องศาเซลเซียสเป็นเวลาต่าง ๆ กัน ได้ศึกษาวิธีเซโรเจลด้วยการสังเคราะห์แซดเอสเอ็ม-5 จากซิลิกาที่เตรียมขึ้นใหม่ ได้สำรวจอิทธิพลของชนิดของสารต้นแบบ ค่าพีเอชของเจลและอัตราส่วนของสารต้นแบบต่อซิลิกาต่อการสังเคราะห์แซดเอสเอ็ม-5 ซึ่งเป็นซีโอไลต์ที่มีโครงสร้างแบบเอ็มเอฟไอเททระโพรฟิลแอมโมเนียมโบรไมด์ และเททระโพรฟิลแอมโมเนียมไฮดรอกไซด์ ถูกนำมาใช้เป็นสารต้นแบบ ได้แปรค่าพีเอชจาก 9.0 ถึง 11.0 และอัตราส่วนโดยโมลของสารต้นแบบต่อซิลิกาจาก 0.1 ถึง 0.5 นอกจากนี้ยังได้ศึกษาอิทธิพลของการใช้คลื่นอัลตราซาวนด์ระหว่างขั้นตอนการเกิดเจลเปรียบเทียบกับแซดเอสเอ็ม-5 ที่เตรียมโดยไม่ได้ใช้คลื่นอัลตราซาวนด์ สารต้นแบบอินทรีย์ถูกกำจัดออกจากตัวอย่างแซดเอสเอ็ม-5 ด้วยการเผาในเตาเผาที่ 550 องศาเซลเซียส นำแซดเอสเอ็ม-5 ที่สังเคราะห์ได้ไปตรวจสอบลักษณะเฉพาะด้วยเทคนิคการเลี้ยวเบนของรังสีเอ็กซ์ กล้องจุลทรรศน์อิเล็กตรอนแบบส่องกราด ไอซีพี-เออีเอส อะลูมิเนียมนิวเคลียร์แมกเนติกเรโซแนนซ์ชนิดสปินมูมเฉพาะ การดูดซับไนโตรเจน เอ็กซ์เรย์ฟลูออเรสเซนส์และการคายแอมโมเนียโดยใช้อุณหภูมิที่ตั้งโปรแกรม ได้นำแซดเอสเอ็ม-5 ไปทดสอบสมบัติเชิงเร่งปฏิกิริยาของปฏิกิริยาการแตกย่อยพอลิเอทิลีนชนิดความหนาแน่นสูงในรีแอกเตอร์ชนิดไม่ต่อเนื่องภายใต้ภาวะต่าง ๆ ค่าการเปลี่ยนและปริมาณของผลิตภัณฑ์ส่วนที่เป็นแก๊สและส่วนที่เป็นของเหลวขึ้นกับอุณหภูมิของปฏิกิริยาและอัตราส่วนของซิลิกอนต่ออะลูมิเนียมในตัวเร่งปฏิกิริยา ความเลือกจำเพาะต่อชนิดผลิตภัณฑ์ที่ได้รับผลจากตัวแปรเหล่านั้นเพียงเล็กน้อย ผลิตภัณฑ์ที่เป็นแก๊สที่ได้จากการแตกตัวของพอลิเอทิลีนชนิดความหนาแน่นสูงส่วนใหญ่เป็นโพรพิน นอมัลบิวเทน ไอโซบิวทิน และไอสารที่มีจุดหลอมเหลวสูงกว่านอมัลเพนเทน ผลิตภัณฑ์ส่วนที่เป็นของเหลวที่ได้จากการแตกย่อยพอลิเอทิลีนชนิดความหนาแน่นสูงส่วนใหญ่อยู่ในช่วง  $C_6$  ถึง  $C_9$  ตัวเร่งปฏิกิริยาแซดเอสเอ็ม-5 ที่ใช้งานแล้วสามารถทำให้กลับคืนสภาพเดิมได้ด้วยการเผาธรรมชาติและความว่องไวยังคงไม่เปลี่ยนแปลงมากนัก

สาขาวิชา ปิโตรเคมีและวิทยาศาสตร์พอลิเมอร์ .....ลายมือชื่อนิติศ.....

ปีการศึกษา .....2551.....ลายมือชื่อ อ. ที่ปริกษาวิทยานิพนธ์หลัก.....

# # 4872507623: MAJOR PETROCHEMISTRY AND POLYMER SCIENCE

KEYWORDS: MICROPOROUS MATERIAL / ZSM-5 / CATALYTIC CRACKING  
/ HDPE

SINEENAT UTTO: SYNTHESIS OF NANOCRYSTALLINE ZSM-5  
CATALYST FOR PRODUCTION OF GASOLINE FROM POLYOLEFIN  
WASTE. ADVISOR: ATICHA CHAISUWAN, Ph.D., 121 pp.

ZSM-5 was synthesized using two different methods: hydrothermal and xerogel methods. The hydrothermal synthesis method was carried out by mixing sodium metasilicate pentahydrate solution, a sodium aluminate solution and a solution of tetrapropylammonium bromide, followed by crystallization at 170°C for various periods. The xerogel method was studied by synthesizing ZSM-5 from freshly prepared silica. Influences of type of the templates, pH of gel and template/SiO<sub>2</sub> ratio on the synthesis of ZSM-5, MFI structure zeolite, were investigated. Tetrapropylammonium bromide and tetrapropylammonium hydroxide were used as templates. The values of pH from 9.0 to 11.0 and template/SiO<sub>2</sub> mole ratios from 0.1 to 0.5 were varied. Furthermore, the influence of sonication during the gel formation step was also studied in comparison with zeolite ZSM-5 prepared without sonication. The organic template was removed from the ZSM-5 samples by calcination in a muffle furnace at 550°C. The ZSM-5 catalysts were characterized by X-ray power diffraction, scanning electron microscope, ICP-AES, <sup>27</sup>Al-MAS-NMR, nitrogen adsorption, X-ray fluorescence and ammonia-temperature programmed desorption techniques. The obtained ZSM-5 were tested for their catalytic activity in the cracking of HDPE waste in a batch reactor under different conditions. The conversions and the yields of gas fraction and liquid fraction depend on the reaction temperature and the Si/Al ratios in catalyst. The product selectivity is affected by those factors only slightly. The gas products obtained by HDPE cracking are mainly propene, n-butane, i-butene and C<sub>5</sub>+. The liquid fraction obtained by cracking of HDPE waste composes mainly in the range of C<sub>6</sub> to C<sub>9</sub>. The used ZSM-5 catalyst can be regenerated by simple calcination and its activity still does not change significantly.

Field of Study: Petrochemistry and Polymer Science Student's Signature: .....

Academic Year: .....2008..... Advisor's Signature:.....

## ACKNOWLEDGEMENTS

The success of this thesis can be attributed to the extensive support and assistance from Dr. Aticha Chaisuwan, the author's thesis advisor. She deeply thanks her for valuable advice and guidance in this research as well as extraordinary experiences throughout the work.

She would like to gratitude to Professor Dr. Pattarapan Prasassrakich, Assistant Professor Dr. Warinthorn Chavasiri and Dr. Kongkrapan Intarajang as the chairman and examiner of this thesis committee, respectively, for all of their kindness and useful advice in the research.

She would like to gratefully thank PTT Chemical Public Company Limited for supporting the standard mixtures for GC analysis. Moreover, she would like to thank Department of Chemistry and Program of Petrochemistry and Polymer Science, Faculty of Science, Chulalongkorn University for the valuable knowledge and experience. In addition, Thailand Japan Technology Transfer Project supported by Japan Banks for International Cooperation (TJTTP-JBIC) is appreciated for instrument support. Furthermore, she would like to thank the members of Materials Chemistry and Catalysis Research Unit for consideration and generosity.

Finally, she greatly thanks for her family and all of my friends for their help and encouragement during her graduate study.

# CONTENTS

	Page
<b>ABSTRACT (THAI)</b> .....	iv
<b>ABSTRACT (ENGLISH)</b> .....	v
<b>ACKNOWLEDGEMENTS</b> .....	vi
<b>CONTENTS</b> .....	vii
<b>LIST OF TABLES</b> .....	xi
<b>LIST OF FIGURES</b> .....	xiii
<b>LIST OF SCHEMES</b> .....	xix
<b>LIST OF ABBREVIATIONS</b> .....	xx
<b>CHAPTER I INTRODUCTION</b> .....	1
<b>CHAPTER II THEORY</b> .....	9
2.1 Zeolites .....	9
2.1.1 Zeolite structures .....	10
2.1.2 Acid sites of zeolites .....	10
2.1.3 Shape selectivity .....	12
2.1.4 Zeolite synthesis .....	13
2.1.4.1 Temperature .....	14
2.1.4.2 Time .....	14
2.1.4.3 Gross composition .....	15
2.1.5 Zeolite ZSM-5 .....	16
2.1.5.1 Shape selectivity properties of zeolite ZSM-5 .....	16
2.1.5.2 Chemical composition of zeolite ZSM-5 .....	18
2.1.6 The templating process .....	18
2.1.7 Characterization of zeolit ZSM-5 .....	20
2.1.7.1 Powder x-ray diffraction (XRD) .....	20
2.1.7.2 Scanning electron microscopy (SEM) .....	21
2.1.7.3 Nitrogen adsorption-desorption isotherm .....	22
2.1.7.4 Temperature-programmed desorption of ammonia .....	25
2.1.7.5 <sup>27</sup> Al-MAS-NMR .....	26
2.2 The refining process .....	26
2.3 Catalytic cracking mechanisms .....	29

	Page
2.3.1 General cracking mechanisms .....	29
2.3.2 Reactions of olefins .....	30
2.3.3 Proposed cracking mechanisms of polymer .....	32
2.3.4 Reactions of paraffins .....	34
<b>CHAPTER III EXPERIMENTS</b> .....	<b>35</b>
3.1 Instruments and apparatus .....	35
3.2 Chemicals and gases .....	37
3.3 Synthesis of ZSM-5 by hydrothermal method .....	38
3.4 Synthesis of ZSM-5 by xerogel method .....	38
3.5 Preparation of ZSM-5 with two different types of template .....	41
3.6 Preparation of ZSM-5 at various pH values .....	41
3.7 Preparation of ZSM-5 with various template/SiO <sub>2</sub> mole ratios .....	41
3.8 Preparation of ZSM-5 with and without sonication .....	41
3.9 Preparation of ZSM-5 with various crystallization times .....	43
3.10 Preparation of ZSM-5 with various Si/Al mole ratios .....	43
3.11 Removal of organic template from the ZSM-5 catalysts .....	43
3.12 Ammonium ion exchange of zeolite samples .....	44
3.13 Sample preparation for ICP-AES analysis .....	45
3.14 Activities of HZSM-5 catalysts in HDPE cracking .....	45
3.14.1 Catalytic cracking of HDPE .....	45
3.14.2 Effect of crystallization time .....	46
3.14.3 Effect of preparation of ZSM-5 and temperature .....	46
3.14.4 Effect of Si/Al mole ratios .....	47
3.15 Catalyst regeneration .....	47
<b>CHAPTER IV RESULTS AND DISSCUSSIONS</b> .....	<b>49</b>
4.1 Parameters affecting formation of ZSM-5 synthesized by hydrothermal method .....	49
4.1.1 Effect of template type on formation of ZSM-5 .....	49
4.1.1.1 XRD results .....	49
4.1.1.2 SEM images .....	49
4.1.1.3 Nitrogen adsorption .....	51
4.1.2 Effect of pH of gel on formation of ZSM-5 .....	52
4.1.2.1 XRD results .....	52



	Page
4.1.2.2 SEM images .....	52
4.1.2.3 Nitrogen adsorption .....	53
4.1.3 Effect of template/SiO <sub>2</sub> on formation of ZSM-5 .....	57
4.1.3.1 XRD results .....	57
4.1.3.2 SEM images .....	58
4.1.3.3 Nitrogen adsorption .....	59
4.1.3.4 NH <sub>3</sub> -TPD profiles .....	60
4.1.4 Effect of sonication on formation of ZSM-5 .....	62
4.1.4.1 XRD results .....	62
4.1.4.2 SEM images .....	63
4.1.4.3 Nitrogen adsorption .....	64
4.1.5 Effect of crystallization time on formation of ZSM-5 .....	65
4.1.5.1 XRD results .....	65
4.1.5.2 SEM images .....	65
4.1.5.3 Nitrogen adsorption .....	66
4.1.6 Effect of the Si/Al ratios on formation of ZSM-5 .....	69
4.1.6.1 Elemental analysis .....	69
4.1.6.2 XRD results .....	70
4.1.6.3 <sup>27</sup> Al-MAS-NMR spectra .....	70
4.1.6.4 SEM images .....	71
4.1.6.5 Nitrogen adsorption .....	73
4.1.6.6 NH <sub>3</sub> -TPD profiles .....	73
4.2 Parameters affecting formation of ZSM-5 synthesized by xerogel method .....	76
4.2.1 Effect of crystallization time on formation of ZSM-5 .....	76
4.2.1.1 XRD results .....	76
4.2.1.2 SEM images .....	76
4.2.1.3 Nitrogen adsorption .....	76
4.2.1.4 XRF analysis .....	82
4.2.1.5 <sup>27</sup> Al-MAS-NMR spectra .....	83
4.3 Activity of various ZSM-5 catalysts in HDPE cracking .....	84
4.3.1 Effect of crystallization time .....	84
4.3.2 Effect of preparation methods and temperature .....	88
4.3.3 Effect of Si/Al ratios .....	93

	Page
4.3.4 Reactivity of regenerated catalyst on HDPE cracking .....	97
4.3.4.1 Characterization of regenerated catalyst .....	97
4.3.4.1.1 XRD results .....	97
4.3.4.1.2 SEM images .....	98
4.3.4.1.3 Nitrogen adsorption .....	99
4.3.4.2 Reactivity of regenerated catalysts on HDPE cracking .....	101
<b>CHAPTER V CONCLUSION</b> .....	<b>105</b>
<b>REFERENCES</b> .....	<b>108</b>
<b>APPENDICE</b> .....	<b>114</b>
<b>VITAE</b> .....	<b>121</b>

## LIST OF TABLES

<b>Table</b>	<b>Page</b>
1.1 Commodity plastics and their uses .....	3
2.1 Factors influencing zeolite crystallization .....	14
2.2 The effects of selected variables of gross composition on the final crystalline product in zeolite synthesis .....	15
2.3 Features of adsorption isotherms .....	24
2.4 IUPAC classification of pores .....	24
3.1 Required amounts of sodium aluminate in the preparation of ZSM-5 samples with various Si/Al mole ratios in gel .....	43
4.1 Textural properties of Sample HTBr compared with Sample HTOH .....	52
4.2 Particle size and morphology of calcined Samples HTOH with the Si/Al in gel of 20 prepared at various pH values .....	54
4.3 BET specific surface area and external surface area of calcined Samples HTOH prepared at various pH values .....	54
4.4 BET specific surface area, external surface area and pore size of Samples HTOH-10.5 with various template/SiO <sub>2</sub> mole ratios .....	60
4.5 Number of acid sites from NH <sub>3</sub> -TPD analysis of the calcined Samples HTOH-10.5 with various template/SiO <sub>2</sub> ratios .....	61
4.6 Textural properties of Sample HTOH-10.5-0.1ns and Sample HTOH-10.5-0.1so .....	65
4.7 BET specific surface area, external surface area and pore size distribution of calcined Samples HTOH-10.5-0.1so with various crystallization time .....	69
4.8 Si/Al molar ratios in gel and in catalyst of calcined Samples HTOH-10.5-0.1so-24h with different Si/Al ratios .....	69
4.9 Textural properties of Samples HTOH-10.5-0.1so-24h with various Si/Al ratios in gel .....	73
4.10 Number of acid sites from NH <sub>3</sub> -TPD analysis of calcined Samples HTOH-10.5-0.1so-24h with various Si/Al ratios .....	75

<b>Table</b>	<b>Page</b>
<b>4.11</b> Textural properties of Samples XGOH prepared with various crystallization periods .....	82
<b>4.12</b> Si/Al ratios of Samples XGOH with various crystallization periods by XRF...	83
<b>4.13</b> Values of %conversion and %yield obtained by catalytic cracking of HDPE over XGOH catalysts with various crystallization time (Condition: 10 wt% catalyst of plastic, N <sub>2</sub> flow of 20 cm <sup>3</sup> /min, 380°C and reaction time of 40 min) .....	84
<b>4.14</b> Values of %conversion and %yield obtained by thermal cracking and catalytic cracking of HDPE over Samples XGOH-12h and HTOH-10.5-0.1-24h-60 at 380°C and 400°C (Condition: 10 wt% catalyst of plastic, N <sub>2</sub> flow of 20 cm <sup>3</sup> /min and reaction of 40 min) .....	89
<b>4.15</b> Values of %conversion and %yield obtained by catalytic cracking of HDPE over Samples HTOH-10.5-0.1-24h with different Si/Al ratios at 380°C (Condition: 10 wt% catalyst of plastic, N <sub>2</sub> flow of 20 cm <sup>3</sup> /min and reaction time of 40 min) .....	94
<b>4.16</b> The physical properties of fresh and regenerated XGOH-12h catalysts .....	100
<b>4.17</b> Values of %conversion and %yield obtained by catalytic cracking of HDPE over fresh and regenerated XGOH-12h catalysts (Condition: 10 wt% catalyst of plastic, N <sub>2</sub> flow of 20 cm <sup>3</sup> /min, 400°C and reaction time of 40 min) .....	101

## LIST OF FIGURES

<b>Figure</b>	<b>Page</b>
1.1 Thailand plastic consumption per capita in 1980-2004 .....	4
2.1 The structure of zeolites .....	9
2.2 A primary building unit of zeolites .....	10
2.3 Secondary building units found in zeolite structures .....	11
2.4 The structure of zeolite A and faujasite-type zeolites .....	11
2.5 The generation of Brønsted and Lewis acid sites in zeolite .....	12
2.6 Three types of selectivity in zeolites: reactant, product and transitionstate shape selectivity .....	13
2.7 The 5-1 secondary building unit (a) to form the chain units (b) found in the ZSM-5 and ZSM-11 structure .....	16
2.8 (a) Structure of ZSM-5 (MFI). View shows the straight channel. The sinusoidal channels run perpendicular to the straight channels. (b) Schematic illustration of the three-dimensional channels in ZSM-5 .....	17
2.9 Correlation between pore size of various zeolites and kinetic diameter of some molecules .....	18
2.10 The formation of zeolite ZSM-5 according to the idea by which it is the interaction of organics ion and silicate .....	19
2.11 The formation of a solid displaying a hexagonal array of pores prepared from a cationic surfactant liquid crystal arrangement and anionic inorganic precursor .....	20
2.12 Diffraction of X-ray by regular planes of atoms .....	21
2.13 Scanning electron micrograph of a ZSM-5 sample .....	22
2.14 The IUPAC classification of adsorption isotherm .....	23
2.15 Distilling crude and product disposition .....	27
2.16 Cracking mechanisms illustrated by the reaction of n-heptene .....	30
2.17 Monomolecular cracking mechanisms (only mechanism possible with ZSM-5) .....	32
2.18 Bimolecular cracking mechanism that can occur on zeolite Y in addition to the monomolecular mechanism .....	33

<b>Figure</b>	<b>Page</b>
<b>3.1</b> Apparatus for synthesis of ZSM-5 .....	40
<b>3.2</b> Apparatus for reduce pressure distillation .....	48
<b>4.1</b> XRD patterns of the calcined ZSM-5 prepared from different templates : (a) TPABr and (b) TPAOH .....	50
<b>4.2</b> SEM images of the calcined ZSM-5 prepared from different templates: (a) TPABr and (b) TPAOH .....	50
<b>4.3</b> N <sub>2</sub> adsorption-desorption isotherms of (a) Sample HTBr and (b) Sample HTOH .....	51
<b>4.4</b> XRD patterns of calcined Samples HTOH (the Si/Al ratio in gel of 20) prepared at various pH gel values: (a) 9.0, (b) 9.5, (c) 10.0, (d) 10.5 and (e) 11.0 .....	53
<b>4.5</b> SEM images of calcined Samples HTOH with different pH: (a) pH = 9.0 (3500x), (b) pH = 9.5 (3500x), (c) pH = 10.0 (3500x), (d) pH = 10.0 (20000x), (e) pH = 10.5 (3500x), (f) pH = 10.5 (20000x), (g) pH = 11.0 (3500x) and (h) pH = 11.0 (20000x) .....	55
<b>4.6</b> N <sub>2</sub> adsorption-desorption isotherms of calcined HTOH samples prepared at different pH values of (a) 9.0, (b) 9.5, (c) 10.0, (d) 10.5 and (e) 11.0 .....	56
<b>4.7</b> XRD patterns of calcined Samples HTOH-10.5 prepared from various TPAOH/SiO <sub>2</sub> mole ratios: (a) 0.1, (b) 0.2 and (c) 0.5 .....	57
<b>4.8</b> SEM images of calcined Samples HTOH-10.5 (the Si/Al ratio in gel of 20) with various ratios of TPAOH/SiO <sub>2</sub> : (a) 0.1 (3500x), (b) 0.1 (20000x), (c) 0.2 (3500x), (d) 0.2 (20000x), (e) 0.5 (3500x) and (f) 0.5 (20000x) .....	58
<b>4.9</b> N <sub>2</sub> adsorption-desorption isotherms of Samples HTOH-10.5 with different TPAOH/SiO <sub>2</sub> mole ratios: (a) 0.1, (b) 0.2 and (c) 0.5 .....	59
<b>4.10</b> NH <sub>3</sub> -TPD profiles of Samples HTOH-10.5 with various template/SiO <sub>2</sub> ratios in gel .....	61
<b>4.11</b> XRD patterns of calcined Samples HTOH-10.5-0.1 prepared (a) without sonication and (b) with sonication .....	62
<b>4.12</b> SEM images of the calcined Samples HTOH-10.5-0.1 prepared (a) without sonication (3500x), (b) without sonication (20000x), (c) with sonication (3500x) and (d) with sonication (20000x) .....	63

<b>Figure</b>	<b>Page</b>
<b>4.13</b> N <sub>2</sub> adsorption-desorption isotherms of the the calcined HTOH-10.5-0.1 prepared (a) without sonication and (b) with sonication .....	64
<b>4.14</b> XRD patterns of calcined Samples HTOH-10.5-0.1so crystallized for various periods: (a) 24 h, (b) 48 h, (c) 72 h and (d) 96 h .....	66
<b>4.15</b> SEM images of calcined Samples HTOH-10.5-0.1so with different crystallization periods: (a), (b) 24 h, (c), (d) 48 h, (e), (f) 72 h and (g), (h) 96 h. The right images are correspondent to the left one at high magnification .....	67
<b>4.16</b> N <sub>2</sub> adsorption-desorption isotherms of Samples HTOH-10.5-0.1so with different crystallization time: (a) 24 h, (b) 48 h, (c) 72 h and (d) 96 h .....	68
<b>4.17</b> XRD patterns of calcined Samples HTOH-10.5-0.1so-24h with different Si/Al ratios in gel (a) 20, (b) 40 and (c) 60 .....	70
<b>4.18</b> <sup>27</sup> Al-MAS-NMR spectra of calcined Samples HTOH-10.5-0.1so-24h with different Si/Al ratios in gel (a) 20, (b) 40 and (c) 60 .....	71
<b>4.19</b> SEM images of calcined Samples HTOH-10.5-0.1so-24h with various Si/Al ratios in gel of (a) 20 (3500x), (b) 20 (20000x), (c) 40 (3500x), (d) 40 (20000x), (e) 60 (3500x) and (f) 60 (20000x) .....	72
<b>4.20</b> N <sub>2</sub> adsorption-desorption isotherms of calcined Samples HTOH-10.5-0.1so-24h with various Si/Al mole ratios: (a) 20, (b) 40 and (c) 60 .....	74
<b>4.21</b> NH <sub>3</sub> -TPD profiles of Samples HTOH-10.5-0.1so-24h with various Si/Al ratios in gel (a) 20, (b) 40 and (c) 60 .....	75
<b>4.22</b> XRD patterns of as-synthesized XGOH with ultrasound irradiation and crystallized for various periods: (a) 2 h, (b) 6 h, (c) 12 h, (d) 18 h, (e) 24 h, (f) 48 h, (g) 72 h and (h) 96 h .....	77
<b>4.23</b> Relationship between the intensity of characteristic peak at 2θ of 23° and crystallization time .....	78

<b>Figure</b>	<b>Page</b>
<b>4.24</b> SEM images of calcined Samples XGOH crystallized at 170°C for various periods: (a) 6 h (10000x), (b) 6 h (50000x), (c) 12 h (10000x), (d) 12 h (50000x), (e) 18 h (10000x), (f) 18 h (50000x), (g) 24 h (10000x), (h) 24 h (50000x), (i) 48 h (10000x), (j) 48 h (50000x), (k) 72 h (10000x), (l) 72 h (50000x), (m) 96 h (10000x) and (n) 96 h (50000x) .....	79
<b>4.25</b> N <sub>2</sub> adsorption-desorption isotherms of calcined Samples XGOH crystallized at 170°C for various crystallization periods: (a) 6 h, (b) 12 h, (c) 18 h, (d) 24 h, (e) 48 h, (f) 72 h and (g) 96 h .....	81
<b>4.26</b> <sup>27</sup> Al-MAS-NMR spectra of calcined Samples XGOH with different crystallization time: (a) 6 h, (b) 12 h, (c) 48 h and (d) 96 h .....	83
<b>4.27</b> Accumulative volume of liquid fractions obtained by catalytic cracking of HDPE over Samples XGOH with various crystallization time at 380°C (Condition: 10 wt% catalyst of plastic, N <sub>2</sub> flow of 20 cm <sup>3</sup> /min and reaction of 40 min) .....	85
<b>4.28</b> Distribution of gas fraction obtained by thermal cracking and catalytic cracking of HDPE over Samples XGOH with various crystallization time at 380°C (Condition: 10 wt% catalyst of plastic, N <sub>2</sub> flow of 20 cm <sup>3</sup> /min and reaction of 40 min) .....	86
<b>4.29</b> Carbon number distribution of distillate oil obtained by catalytic cracking of HDPE over Samples XGOH with various crystallization time at 380°C (Condition: 10 wt% catalyst of plastic, N <sub>2</sub> flow of 20 cm <sup>3</sup> /min and reaction of 40 min) .....	87
<b>4.30</b> Accumulative volume of liquid fractions obtained by catalytic cracking of HDPE over Samples XGOH-12h and HTOH-10.5-0.1-24h-60 at 380°C and 400°C (Condition: 10 wt% catalyst of plastic, N <sub>2</sub> flow of 20 cm <sup>3</sup> /min and reaction of 40 min) .....	90
<b>4.31</b> Distribution of gas fraction obtained by the thermal cracking and catalytic cracking of HDPE over XGOH-12h at 380°C and 400°C (Condition: 10 wt% catalyst of plastic, N <sub>2</sub> flow of 20 cm <sup>3</sup> /min and reaction of 40 min) .....	91



<b>Figure</b>	<b>Page</b>
<b>4.32</b> Distribution of gas fraction obtained by the thermal cracking and catalytic cracking of HDPE over HTOH-10.5-0.1-24h-60 at 380°C and 400°C (Condition: 10 wt% catalyst of plastic, N <sub>2</sub> flow of 20 cm <sup>3</sup> /min and reaction of 40 min) .....	92
<b>4.33</b> Carbon number distribution of liquid fractions from catalytic cracking of HDPE over Samples XGOH-12h and HTOH-10.5-0.1-24h-60 at 380°C and 400°C (Condition: 10 wt% catalyst of plastic, N <sub>2</sub> flow of 20 cm <sup>3</sup> /min and reaction of 40 min) .....	92
<b>4.34</b> Accumulative volume of liquid fractions obtained by catalytic cracking of HDPE over Samples HTOH-10.5-0.1-24h with different Si/Al ratio at 380°C (Condition: 10 wt% catalyst of plastic, N <sub>2</sub> flow of 20 cm <sup>3</sup> /min and reaction of 40 min) .....	95
<b>4.35</b> Distribution of gas fraction obtained by thermal cracking and catalytic cracking of HDPE over Samples HTOH-10.5-0.1-24h with different Si/Al ratios at 380°C (Condition: 10 wt% catalyst of plastic, N <sub>2</sub> flow of 20 cm <sup>3</sup> /min and reaction of 40 min) .....	95
<b>4.36</b> Carbon number distribution of liquid fraction from catalytic cracking of HDPE over Samples HTOH-10.5-0.1-24h with different Si/Al ratios at 380°C (Condition: 10 wt% catalyst of plastic, N <sub>2</sub> flow of 20 cm <sup>3</sup> /min and reaction of 40 min) .....	96
<b>4.37</b> Carbon number distribution of commercial SUPELCO standard gasoline fraction .....	96
<b>4.38</b> XRD patterns of (a) fresh XGOH-12h, (b) the 1 <sup>st</sup> regenerated, (c) the 2 <sup>nd</sup> regenerated, (d) the 3 <sup>rd</sup> regenerated and (e) the 4 <sup>th</sup> regenerated XGOH-12h catalysts .....	97
<b>4.39</b> SEM images of fresh and regenerated XGOH-12h catalysts: (a) fresh XGOH-12h, (b) 1 <sup>st</sup> regenerated, (c) 2 <sup>nd</sup> regenerated, (d) 3 <sup>rd</sup> regenerated and (e) 4 <sup>th</sup> regenerated XGOH-12h catalysts .....	98
<b>4.40</b> N <sub>2</sub> adsorption-desorption isotherms of (a) fresh, (b) 1 <sup>st</sup> regenerated, (c) 2 <sup>nd</sup> regenerated, (d) 3 <sup>rd</sup> regenerated and (e) 4 <sup>th</sup> regenerated XGOH-12h catalysts .....	100

<b>Figure</b>	<b>Page</b>
<b>4.41</b> Accumulative volume of liquid fractions obtained by catalytic cracking of HDPE over fresh and regenerated XGOH-12h catalysts at 400°C (Condition: 10 wt% catalyst of plastic, N <sub>2</sub> flow of 20 cm <sup>3</sup> /min and reaction of 40 min) .....	102
<b>4.42</b> Distribution of gas fraction obtained by the thermal cracking and catalytic cracking of HDPE over fresh and regenerated XGOH-12h catalysts at 400°C (Condition: 10 wt% catalyst of plastic, N <sub>2</sub> flow of 20 cm <sup>3</sup> /min and reaction of 40 min) .....	103
<b>4.43</b> Carbon number distribution of liquid fractions from catalytic cracking of HDPE over fresh and regenerated XGOH-12h catalysts at 400°C (Condition: 10 wt% catalyst of plastic, N <sub>2</sub> flow of 20 cm <sup>3</sup> /min and reaction of 40 min) .....	104
<b>A-1</b> Gas chromatogram of standard mixture gas .....	116
<b>A-2</b> Gas chromatogram of gas product obtained from catalytic cracking of HDPE over XGOH-12h (Si/Al ratio = 60) at 400°C .....	117
<b>A-3</b> Liquid chromatogram of standard gasoline (SUPELCO) .....	118
<b>A-4</b> Gas chromatogram of gas product obtained from catalytic cracking of HDPE over XGOH-12h (Si/Al ratio = 60) at 400°C .....	119
<b>A-5</b> XRD pattern of a HDPE bottle used as a representation plastic waste .....	120

## LIST OF SCHEMES

<b>Scheme</b>	<b>Page</b>
3.1 The heating program for the GC column used in gas analysis.....	37
3.2 The heating program for the GC column used in liquid analysis.....	37
3.3 Schematic diagram for the synthesis of ZSM-5 by hydrothermal method.....	39
3.4 Schematic diagram for the synthesis of ZSM-5 by xerogel method.....	42
3.5 A heating program for removal of the organic templates from the pores of ZSM-5.....	44
3.6 The heating program for ammonia removal from ZSM-5.....	44
3.7 Apparatus for catalytic cracking.....	47
3.8 Catalytic cracking of HDPE using HZSM-5 as catalyst.....	48

## LIST OF ABBREVIATIONS

TPABr	Tetrapropylammonium Bromide
TPAOH	Tetrapropylammonium Hydroxide
BET	Brunauer- Emmett-Teller
BJH	Barret, Joyner, and Halenda
XRD	X-ray Diffraction
XRF	X-ray Fluorescence
SEM	Scanning Electron Microscopy
TPD	Temperature-Programmed Desorption
GC	Gas Chromatography
ICP-AES	Inductively Coupled plasma-Atomic Emission Spectrometer
MAS-NMR	Magic-angle-spinning-nuclear magnetic resonance
HDPE	High density polyethylene
°C	degree Celsius
g	gram (s)
h	hour (s)
mg	milligram (s)
min	minute (s)
ppm	part per million or mg/l
M	molar
cps	counts per second
%	percent

# CHAPTER I

## INTRODUCTION

Today, plastics are very important materials having widespread use in the manufacture of a variety of products including packaging, textiles, pipes, cars and furniture components. Plastics are synthesized mainly from petroleum-derived chemicals, although only about 4% of total petroleum production is used in the manufacture of plastics. The main reasons for the continuous increase in the demand for commodity plastics are as follows [1]:

- Plastics are low density solids, which makes it possible to produce lightweight objects.
- Plastics have low thermal and electric conductivities; hence they are widely used for insulation purposes.
- Plastics are easily moulded into desired shapes.
- Plastics usually exhibit high corrosion resistance and low degradation rates and are highly durable materials.
- Plastics are low-cost materials.

Plastics are divided into two major groups depending on their behaviour when they are heated [2]:

- Thermoplastics are plastics which undergo a softening when heated to a particular temperature. This thermoplastic behaviour is a consequence of the absence of covalent bonds between the polymeric chains, which remain as practically independent units linked only by weak electrostatic forces. Therefore, waste thermoplastics can be easily reprocessed by heating and forming into a new shape. From a commercial point of view, the most important thermoplastics are high density polyethylene (HDPE), low density

polyethylene (LDPE), polypropylene (PP), polystyrene (PS), polyvinyl chloride (PVC), polyethylene terephthalate (PET), polyamide (PA), etc.

- Thermosets are plastics whose polymeric chains are chemically linked by strong covalent bonds, which lead to three-dimensional network structures. Once formed into a given shape, thermosets cannot be reprocessed or remoulded by heating. Examples of thermosets with significant commercial applications are polyurethanes (PU), epoxy resins, unsaturated polyester and phenol-formaldehyde resins. Thermosets are produced in smaller amounts than thermoplastics.

There are about 50 different groups of plastics, with hundreds of different varieties. All types of plastic are recyclable. To make sorting and thus recycling easy, the American Society of Plastics Industry developed a standard marking code to help consumers identify and sort the main types of plastics. These types and their most common uses are shown in Table 1.1 [3].

By examining the two largest plastics markets, polyethylene and polypropylene (Figure 1.1), supply managers can track what accounts for 60 percent of global commodity plastics consumption.

Polyethylene is by far the world's most used plastic (about 39% of the plastics used in 2004 were polyethylene and its consumption is constantly growing). Polyethylene can be found in the market in several grades: [5]

1. Low density polyethylene (LDPE), is an ethylene homopolymer produced in a high pressure uncatalyzed process, which contains long and short branches; these branches in LDPE prevent a good packing of polymer molecules and in consequence the polymer melts at low temperatures.

2. High density polyethylene (HDPE), was firstly obtained in 1958 by the use of Phillips and Ziegler-Natta catalysts. This grade, which consists in unbranched polyethylene molecular chains, has a higher melting temperature, but also a higher fragility.

3. Linear low density polyethylene (LLDPE), was produced in the 1980s by copolymerization of ethylene with other olefins like 1-hexene. Thus, a great quantity of short branches was added to the main polyethylene chain, achieving intermediate properties between HDPE and LDPE.

**Table 1.1** Commodity plastics and their uses

Code and symbol	Abbreviation	Major Uses
	PET	<b>Polyethylene terephthalate:</b> Plastic soft drink, water, sport drink, beer, prepared food trays and film that is used to cook frozen foods and roast.
	HDPE	<b>High-density polyethylene:</b> Milk, water, juice, cosmetic, shampoo, dish and laundry detergent bottles.
	PVC	<b>Polyvinyl chloride:</b> Clear food and non-food packaging, medical tubing, wire and cable insulation, construction products such as plastic pipes.
	LDPE	<b>Low density polyethylene:</b> Dry cleaning bags, product bags, food storage containers, trash can liners, bread and frozen food bags.
	PP	<b>Polypropylene:</b> Catsup bottles, yogurt containers and margarine tubs, medicine bottles, aerosol caps, drinking straws.
	PS	<b>Polystyrene:</b> Compact disc jackets, food service applications, grocery store meat trays, egg cartons, aspirin bottles.
	OTHER	<b>Any other plastics</b> that do not fall into any of the above categories: Three and five gallon reusable water bottles, some citrus juice and catsup bottles.

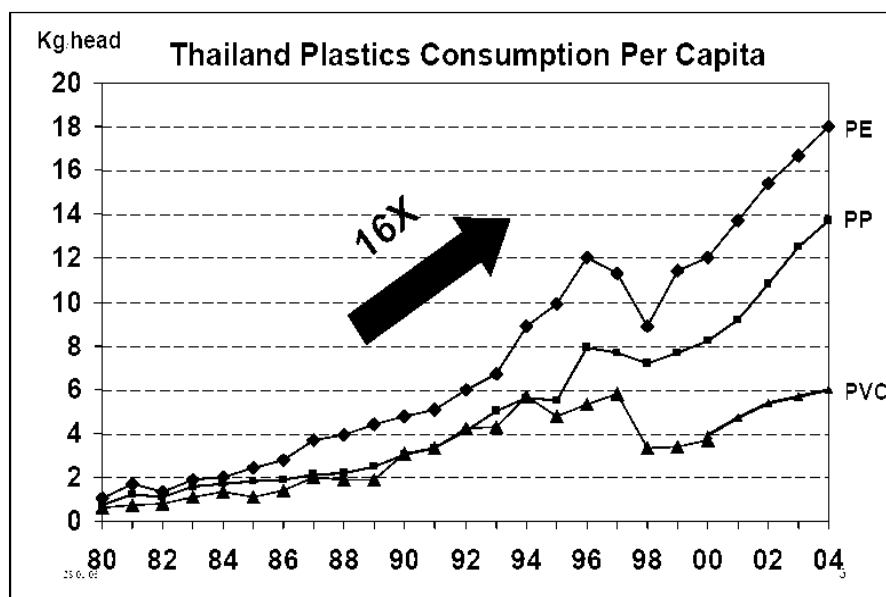


**Figure 1.1** Thailand plastic consumption per capita in 1980-2004 [4].

The increase in plastic materials consumption has led to a parallel rise in the generation of plastic wastes. The most common alternative for the management of these wastes in Western Europe was deposition in landfills (75%) and incineration (14%) [6]. However, the available space in landfill is decreasing, whereas incineration is strongly rejected public opinion, due the risk of the possible emission of toxic chemical, mainly polychlorinated aromatic species for example dioxins, furans. For this reason, the search for different recycling alternative is more and more necessary.

Though several methods have been proposed for recycling of waste plastics, it is generally accepted that material recovery is not a long-term solution to the present problem, and that energy or chemical recovery is a more attractive one. One approach to chemical recovery is to employ inert gas pyrolysis to produce gasoline-like materials. In this method, the waste plastics are thermally or catalytically degraded into gasses and oils, which can be used as sources in fuels or chemicals.

Thermal cracking involves the degradation of the polymeric materials by means of temperature when it is applied under inert atmospheric conditions. In the case of polyolefins like polyethylene, this process has been reported to proceed through a random scission mechanism that generates a heterogeneous mixture of linear paraffins and olefins over a wide range of molecular weights. Catalytic cracking involves several advantages over a purely thermal process. First, catalysts promote the degradation reaction to occur at lower temperatures, with implies lower



energy consumptions. Second and most importantly, the shape selectivity exhibited by certain catalysts allows the formation of a narrower distribution of products, which may be directed towards light and aromatic hydrocarbons with higher market values [7, 8].

Catalytic degradation is usually carried out on acid sites with sufficient strength, and thus various solid acids have been tested as catalysts [9]. One of the most commonly used solid catalysts in polymer degradation studies are zeolites due to their strong acidity, pore size and specific pore structure effects [10]. Some studies have been reported on catalytic pyrolysis of polyolefins with natural and synthetic zeolites [11, 12]. ZSM-5 zeolite has proved to be an efficient catalyst for catalytic degradation of polymers because of its strong acidity for the carbon-carbon bond scission and unique pore structure to reduce coke formation [13]. Several works have been published using ZSM-5 as solid catalyst [14-17]. Some of the studies reported in the literature will be reviewed below.

Y. Sakata *et al.* [18] studied degradation of polyethylene and polypropylene into fuel oil over various types of catalysts such as silica-alumina, ZSM-5, silicalite, amorphous mesoporous silica gel and mesoporous silica FSM-16 at 430°C for polyethylene and 380°C for polypropylene. ZSM-5 possessing strong acid sites produced less liquid products and more gaseous products than other acid catalysts. These results are in agreement with the fact that strong acid catalysts catalyze the cracking of heavier hydrocarbons into lighter or gaseous hydrocarbons than the weak acid catalysts.

G. Manos *et al.* [19] reported about catalytic cracking of high-density polyethylene over ZSM-5, mordenite, Y, ultrastable Y (US-Y) and zeolite  $\beta$  at 360°C. ZSM-5 zeolite showed the highest conversion and the lowest coke occurring. Furthermore, the presence of supercages (2.5 nm) in the Y and US-Y frameworks accounted for the lower conversions obtained. The heaviest hydrocarbons were formed with large-pore zeolites (Y, US-Y,  $\beta$ ). The presence of large supercages in the Y-type structure should account for this as well as for the higher coking. Significantly lighter products were formed with medium-pore zeolites (mordenite, ZSM-5). The product order was the following : (light products) ZSM-5 < mordenite <  $\beta$  < Y < US-Y (heavy products).

K. Gobin *et al.* [20] studied polymer degradation to fuels over microporous catalysts as a novel tertiary plastic recycling method. The catalysts employed were ZSM-5 and US-Y. The low coking level of ZSM-5 was reflected on the higher conversion value achieved by this catalyst in comparison to US-Y. This was able to be attributed to the shape selectivity properties of its relatively small pore structure that did not allow the growth of large coke molecules. With US-Y, the majority of the liquid boiling range was C<sub>6</sub>-C<sub>10</sub>. The distribution over ZSM-5 showed a sharp peak corresponding to C<sub>8</sub> and lighter products than US-Y due to its smaller pore size.

J. Aguado *et al.* [21] investigated the catalytic conversion of LDPE, HDPE and PP using Al-MCM-41, ZSM-5 and amorphous silica-alumina as catalyst. The catalytic cracking of HDPE and LDPE was investigated at 400°C in a batch reactor with duration of the experiments of 30 min. In the catalytic cracking of HDPE and LDPE, the highest activity was observed with ZSM-5 due to its stronger acidity.

R.A. Garcia *et al.* [22] investigated and compared the behavior of hybrid ZSM-5/MCM-41 materials with pure Al-MCM-41 and HZSM-5 samples for catalytic cracking of HDPE. The samples obtained exhibited remarkable catalytic activity in the HDPE cracking despite the low temperature (380°C) and catalyst loadings used (plastic/catalyst mass ratio=100), leading to polyolefin conversions higher than both Al-MCM-41 and HZSM-5. Light hydrocarbons with a narrow product distribution and rich in olefins (C<sub>3</sub>-C<sub>5</sub>) were the main components obtained over the hybrid and HZSM-5 catalysts. The superior catalytic activity of the hybrid materials for the HDPE cracking regarding to the Al-MCM-41 and pure HZSM-5 samples were assigned to a right combination of acid strength and accessibility of the acid sites.

P. Zhang *et al.* [23] studied of the performance of modified nanosized ZSM-5 zeolite on olefins reduction in FCC gasoline. Compared with the microsized HZSM-5, the nanosized HZSM-5 had much larger surface area. The activity and the stability of the nanosized HZSM-5 catalyst were much better than those of the microsized HZSM-5 catalyst. Although the amount of deposited cokes (time on stream of 10h) caused by olefin reduction reaction on the nanosized HZSM-5 catalyst was the nearly same as that on the microsized HZSM-5 catalyst, the performance on olefin reduction of the nanosized HZSM-5 catalyst was satisfactory. Surface area decreased in the spent microsized HZSM-5 catalyst was very large in comparison with that of the

spent nanosized one. The mainly reason was that the pores were blocked by coke deposited on the microscale HZSM-5 catalyst.

D.P. Serrano *et al.* [24] reported the catalytic cracking of polyolefin mixture consisting of 46.5 wt% LDPE, 25 wt% HDPE and 28.5 wt% PP at 400°C over a variety of acid solids as catalysts. The activity order was found as follow:

n-HZSM-5>H beta>HMCM-41>>SiO<sub>2</sub>-Al<sub>2</sub>O<sub>3</sub>>HZSM-5>HY>thermal degradation

The activity order found for the different catalysts was related to their respective properties and the nature of the polyolefin mixture. HMCM-41 also led to a high conversion because of its large pore size, which promoted the access of the polymer molecules to the acid sites. In the case of n-HZSM-5 and H-beta, the presence of a high external surface area enhanced its cracking activity, because the external acid sites were not sterically hindered for the conversion of the bulky polyolefin molecules. Significant differences were observed in the product distribution: n-HZSM-5 showed the highest selectivity toward C<sub>1-4</sub>(50 wt %), H beta leded mainly to liquid hydrocarbon C<sub>5-12</sub>(60 wt %), whereas HMCM-41 yielded both C<sub>5-12</sub>(54 wt %) and C<sub>13-30</sub>(32 wt %) fractions. Regarding the selectivity by carbon atom number, in all cases C<sub>4</sub> fraction was the major products, although its value changed widely depending on the catalyst.

Recently, J. Aguado *et al.* [25] investigated the catalytic activity of six acid solids of varying acid and textural properties in the cracking of pure high and low-density polyethylene and also of waste polyolefins of agricultural and urban origins using thermogravimetric and differential thermal analysis. The catalysts were three zeolitic materials (standard ZSM-5, nanocrystalline n-ZSM-5 and Beta) and three mesostructured solids (sol-gel Al-MCM-41 (sg), hydrothermal Al-MCM-41 (hy) and Al-SBA-15). The smaller crystal size contributed favorably to the formation of an extended external surface area and a consequently higher share of external acid sites, fully accessible to the bulky polymer macromolecules. Furthermore, a small crystal size also reduced diffusional hindrances to internal acid sites. Despite its strong acid properties, standard ZSM-5 showed the lowest catalytic activity of all acid solids, except when used on pure HDPE. This behaviour was attributed to steric impediments related to its microporous texture and large crystal size that hinder the access of large polymeric molecules to its internal acid sites. On the contrary, nanocrystalline zeolite n-ZSM-5 was the most active catalyst as it combined a strong acid character with

favorable accessibility into its active sites resulting from its small crystal size. The catalytic activity of all the acid solids tested in that work was significantly reduced when they were used for waste plastics. This effect might be associated with the cross-linking reactions occurring in the waste polymer during its use, which made it more resilient to catalytic degradation. This deactivating effect was particularly strong in materials with larger pore and weaker acid properties.

From the previous works, zeolite ZSM-5 has efficiency in the catalytic cracking of polyolefin. The strong acidity of this catalyst allows plastic wastes to be degraded with high activity. The obtained products were controlled by pore size, acid strength, and particle size of the catalyst. This work intends to develop method for the synthesis of ZSM-5 and to study the influence of ultrasound application during the gel formation step on physico-chemical properties and on the use in catalytic cracking of high density polyethylene waste. Moreover, this catalyst was selected in order to study the influence of template type, template/SiO<sub>2</sub> ratios, crystallization time, Si/Al ratios of the catalyst to improve the activity and product distribution in the conversion of the high density polyethylene and polypropylene wastes.

### **Objectives**

1. To synthesize nanocrystalline ZSM-5.
2. To investigate the efficiency and stability of ZSM-5 for cracking of high density polyethylene waste.
3. To study activity of regenerated ZSM-5 catalyst.

## CHAPTER II

### THEORY

#### 2.1 Zeolites

Zeolites are ordered, porous, and rigid crystalline aluminosilicates having a definite structure with a framework based on an extensive three-dimensional network of  $\text{SiO}_4$  and  $\text{AlO}_4$  tetrahedral. The tetrahedral are cross-linked by the sharing of oxygen atoms as shown in Figure 2.1

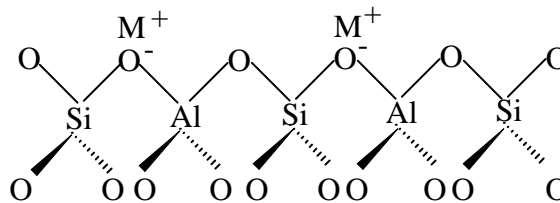
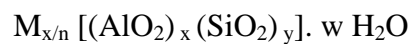


**Figure 2.1** The partial structure of zeolites [26].

The  $\text{AlO}_2^-$  tetrahedra in the structure determine the framework charge. This is balanced by cations that occupy nonframework positions. The general formula for the composition of zeolites is



where M is the cation of valence n, generally from the group I or II ions, although other metals, nonmetals, and organic cations are also possible, w is the number of water molecules. Water molecules presented are located in the channels and cavities, by surrounding the cations that neutralize the negative charge created by the presence of the  $\text{AlO}_2^-$  tetrahedral unit in the structure.

### 2.1.1 Zeolite structures [26]

The structure of zeolite consisted of a three-dimension framework of the tetrahedral primary building units when tetrahedral atoms are silicon or aluminum as shown in Figure 2.2

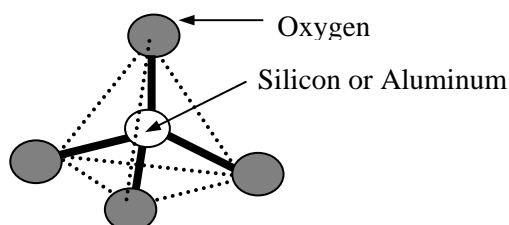


**Figure 2.2** A primary building unit of zeolites.

Zeolites have a common subunit of structure so called primary building units of tetrahedral  $(Al,Si)O_4$ , therein the Si or Al distribution is neglected. A secondary building unit (SBU) consists of selected geometric groupings of those tetrahedral. There are several building units, which can be used to describe all of the known zeolite structures. The secondary building units (SBU's) consist of 4,6 and 8-member single rings, 4-4, 6-6 and 8-8-member double rings, and 4-1,5-1 and 4-4-1 branched rings as illustrated in Figure 2.3

Most zeolite frameworks can be generated from several different SBUs. For example, the sodalite framework can be build from either the single 6-member ring or the single 4-member ring. Some of them are shown in Figure 2.4

### 2.1.2 Acid sites of zeolites

Most industrial application of zeolites are based upon technology adapted from the acid silica/alumina catalysts originally developed for the cracking reaction. This means that the activity required is based upon the production of Brønsted acid sites arising from the creating 'hydroxyls' within the zeolite pore structures. These hydroxyls are formed by ammonium exchange followed by a calcination step. Zeolites as normally synthesized usually have  $Na^+$  balancing the framework charges, but these can be readily exchanged for protons by direct reaction

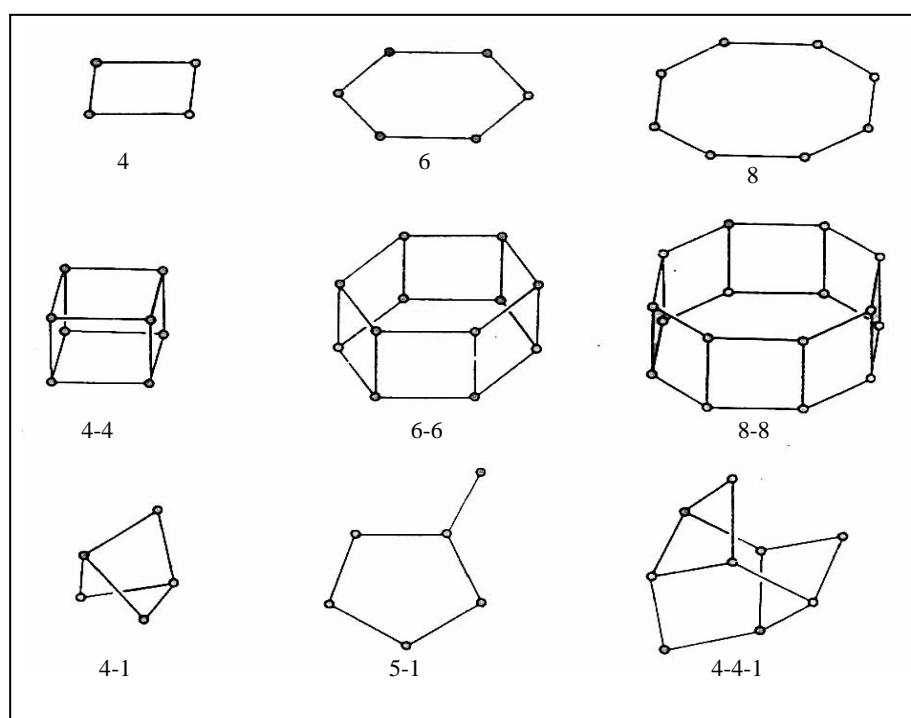


**Figure 2.3** Secondary building units found in zeolite structures [27].

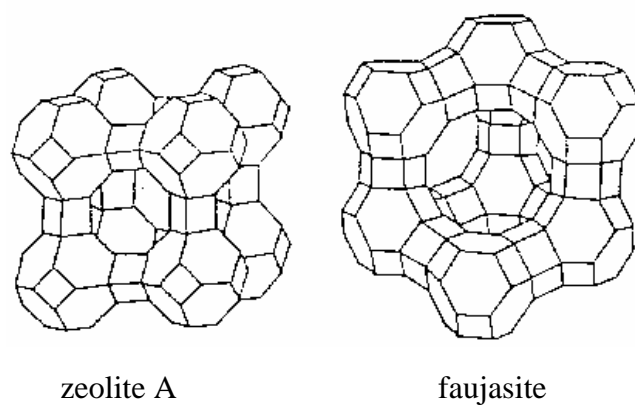


**Figure 2.4** The structure of zeolite A and faujasite-type zeolites [27].

with an acid, giving hydroxyl groups, the Brønsted acid sites. Alternatively, if the zeolite is not stable in acid solution, it is common to use the ammonium,  $\text{NH}_4^+$ , salt, and then heat it so that ammonia is driven off, leaving a proton. Further heating removes water from Brønsted site, exposing a tricoordinated Al ion, which has

electron-pair acceptor properties; this is identified as a Lewis acid site. A scheme for the formation of these sites is shown in Figure 2.5. The surfaces of zeolites can thus display either Brønsted or Lewis acid sites, or both, depending on how the zeolite is prepared. Brønsted sites are converted into Lewis sites as the temperature is increased above 500°C, and water is driven off.

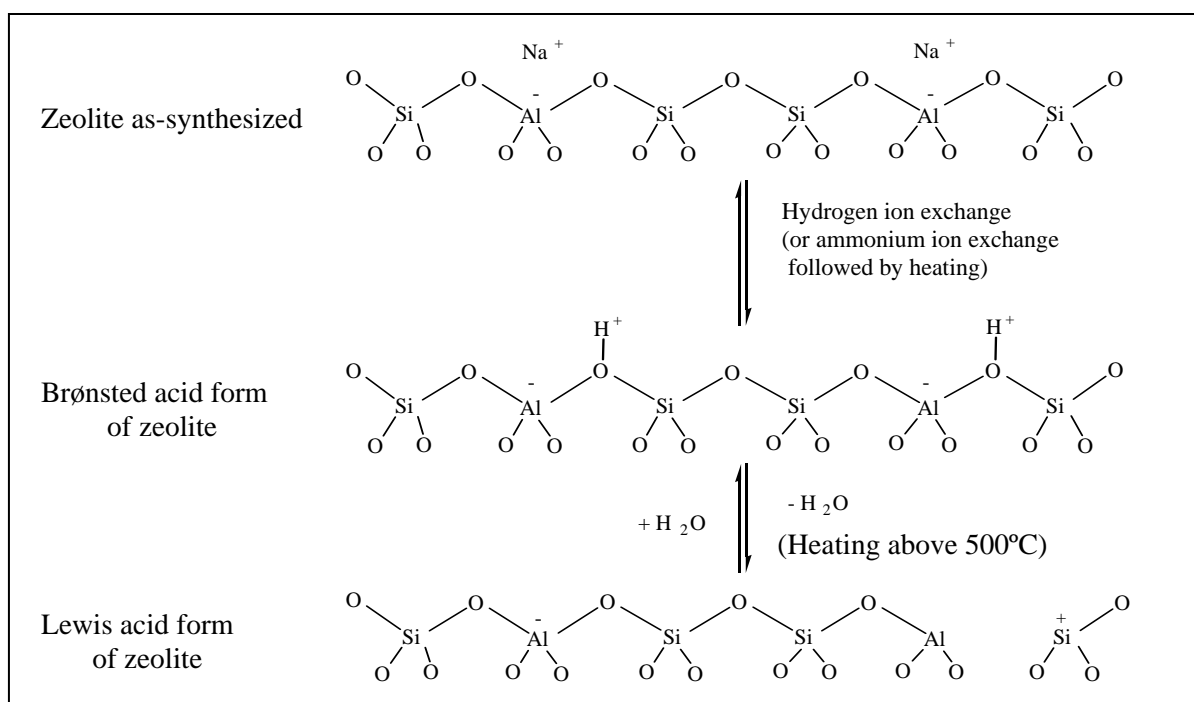


**Figure 2.5** The generation of Brønsted and Lewis acid sites in zeolite [28].

### 2.1.3 Shape selectivity

Shape selectivity plays a very important role in catalysis. Highly crystalline and regular channel structures are among the principal features that zeolite used as catalysts offer over other materials. Shape selectivity is divided into 3 types: reactant shape selectivity, product shape selectivity and transition-state shape selectivity. These types of selectivities are shown in Figure 2.6. Reactant shape selectivity results from the limited diffusivity of some reactants, which cannot effectively enter and diffuse inside the zeolites. Product shape selectivity occurs when diffusing product molecules cannot rapidly escape from the crystal, and undergo secondary reactions. Restricted transition-state shape selectivity is a kinetic effect arising from the local environment around the active site: the rate constant for a



certain reaction mechanism is reduced if the necessary transition state is too bulky to form readily.

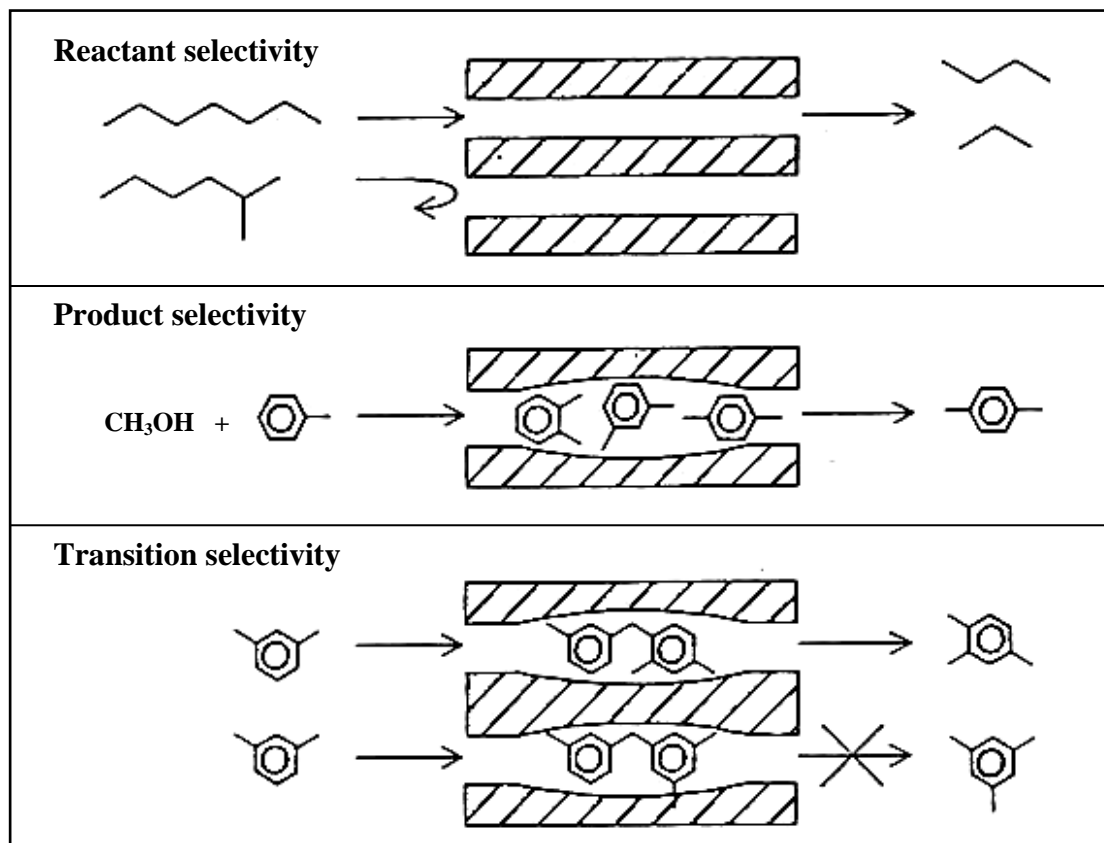


**Figure 2.6** Three types of selectivity in zeolites: reactant, product and transition-state shape selectivity [29].

#### 2.1.4 Zeolite synthesis

Many factors have a major influence on the zeolite structure crystallized, e.g., temperature, time and gross composition. These factors are listed in Table 2.1 and are briefly discussed below [27].

**Table 2.1** Factors influencing zeolite crystallization

- 
- Temperature
  - Time
  - Gross composition
    1.  $\text{SiO}_2/\text{Al}_2\text{O}_3$
    2. Cations
      - (a) Inorganic
      - (b) Organic
    3.  $[\text{H}_2\text{O}]$
    4. Anions (excluding  $[\text{OH}^-]$ )
    5.  $[\text{OH}^-]$
  - History-dependent factor
    1. Aging
    2. Stirring
    3. Nature of mixture
    4. Order of mixing
- 

#### 2.1.4.1 Temperature

To approximate their natural occurrence, zeolites are generally crystallized under high pressure and at moderately high temperatures (120-200°C) [27]. High pressure can be usually achieved using a closed vessel called an autoclave. Concerning temperature, higher temperature yields more condensed but not zeolitic phases, whereas lower temperature prohibits convenient synthesis process. As an example for the influence of temperature on zeolite synthesis, ZSM-5 and ZSM-11 were reported to co-exist at temperatures of 130-180°C [27], where percentage of ZSM-5 varied with temperatures as follows: <5% (130°C), 50-55% (145°C), 60-65% (160°C) and 75-80% (180°C).

#### 2.1.4.2 Time

Time is also important in systems where one phase metastable with respect to another, as in the case of zeolite synthesis [27]. Generally, at constant temperature and initial mixture composition, the transformation proceeds from amorphous, to metastable, to more stable phase. Argauer and Landolt [30] claimed a

wide range of temperature of 100-175°C at time ranging from six hours to sixty days for synthesis of ZSM-5 in an original patent. Clearly, time requires varies widely, and is often optimized to yield the desired zeolitic phase in a reasonable period.

#### 2.1.4.3 Gross composition

Each component in the reactant mixture contributes to specific characteristic of the gel and to the final material obtained. Table 2.2 provides a broad listing of individual components of the mixture and the primary influence each component has within that reactant mixture.

**Table 2.2** The effects of selected variables of gross composition on the final crystalline product in zeolite synthesis [27]

Variables	Primary influence
SiO <sub>2</sub> /Al <sub>2</sub> O <sub>3</sub>	Framework composition
H <sub>2</sub> O/SiO <sub>2</sub>	Rate, crystallization mechanism
OH <sup>-</sup> /SiO <sub>2</sub>	Silicate molecular weight, OH <sup>-</sup> concentration
Inorganic cation(s)/SiO <sub>2</sub>	Structure, cation distribution
Organic additives/SiO <sub>2</sub>	Structure, framework aluminium content

The SiO<sub>2</sub>/Al<sub>2</sub>O<sub>3</sub> mole ratio, the hydroxide content of the gel, and the presence of inorganic cations, also contribute to determining which structure(s) would finally crystallize besides the organic additives as crystal-directing agent or template [27]. For example, zeolite ZSM-5 generally crystallized in the TPA<sup>+</sup> (tetrapropylammonium cation) system at the SiO<sub>2</sub>/Al<sub>2</sub>O<sub>3</sub> ratio between 20 and infinity. However, at the ratio below 20 the mordenite phase appears. However, tetrapropylammonium cation was considered to be a strong structure director for ZSM-5. The crystallization of a particular zeolite structure from the gel system containing these four components strongly depends on the mole ratio of the starting gel mixture. The inorganic or organic cations influence not only the structure crystallized but also other features of the final crystalline products produced, such as morphology and crystal size.

### 2.1.5 ZSM-5

The oil company Mobil first synthesized ZSM-5, Zeolite Socony Mobil-Five, in 1972 and its structure code is MFI [27, 30-33]. The tetrahedral units are linked to form the chain-type building block as shown in Figure 2.7. Rings consisted of five oxygen atoms are evident in this structure; the name pentasil is therefore used for describing its structure. ZSM-5 is a medium-pore zeolite having an orthorhombic crystal structure. The pore opening is composed of a 10-member ring. The ZSM-5 framework contains two types of intersection channels: one type is straight, has elliptical (0.51 nm x 0.58 nm) opening, and run parallel to the b-axis of the orthorhombic unit cell, while the other has near-circular (0.54 nm x 0.56 nm) opening, is sinusoidal (zigzag) and directed along the a-axis. Figure 2.8 exhibits the structure of ZSM-5 and schematic illustration of three-dimensional channels.

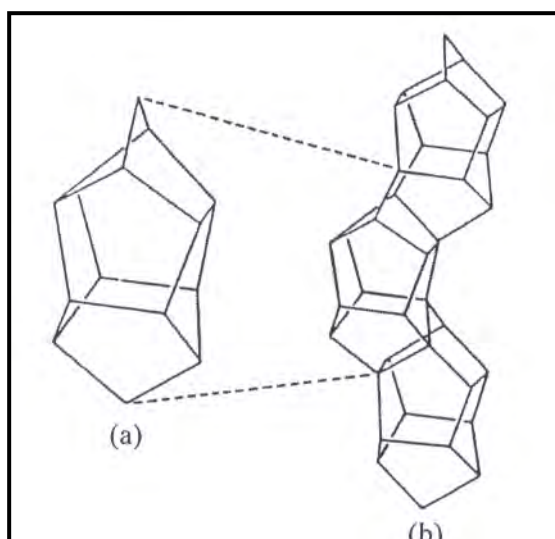


**Figure 2.7** The 5-1 secondary building unit (a) to form the chain units (b) found in the ZSM-5 and ZSM-11 structure [27].

#### 2.1.5.1 Shape selectivity of zeolite ZSM-5

The accessibility to the catalytic active sites in ZSM-5 is best viewed by considering its channel system as illustrated in Figure 2.8 (b) [32]. The particular shape-selective properties of ZSM-5 result from the conjugation of four different structurally interrelated features:

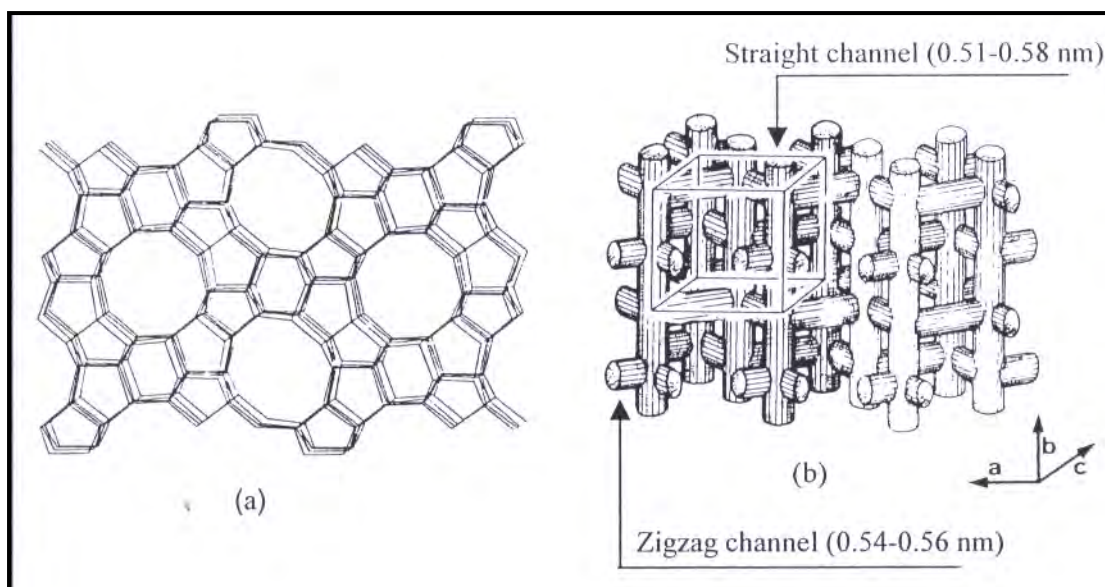


**Figure 2.8** (a) Structure of ZSM-5 (MFI). View shows the straight channel. The sinusoidal channels run perpendicular to the straight channels [33]. (b) Schematic illustration of the three-dimensional channels in ZSM-5 [32].

(a) A channel (or pore) opening consisting of a 10-member oxygen ring which is intermediate between that of classical shape-selective zeolites (such as erionite, ferrierite, gmelinite and zeolite A) and that of large pore zeolites (such as faujasite, mordenite and fault-free offretite) as shown in Figure 2.9.

(b) The presence of channel intersections (or intersecting elements) which offer a free space of larger dimensions (about 0.9 nm); the latter may play a distinct role in the ordering of simple molecules and could be the site for catalytic activity.

(c) The absence of cages along the channel, such cages which offer a larger available space may be detrimental to catalytic activity, as shown in the case of erionite, being the preferential site for the formation of carbonaceous residues.

(d) The occurrence of slightly differentiated channel networks. Aromatic and branched paraffins were indeed found to preferentially be adsorbed in the linear channels which are elliptical. This may be led to preferential diffusion paths and eventually prevent major counter diffusion effects.

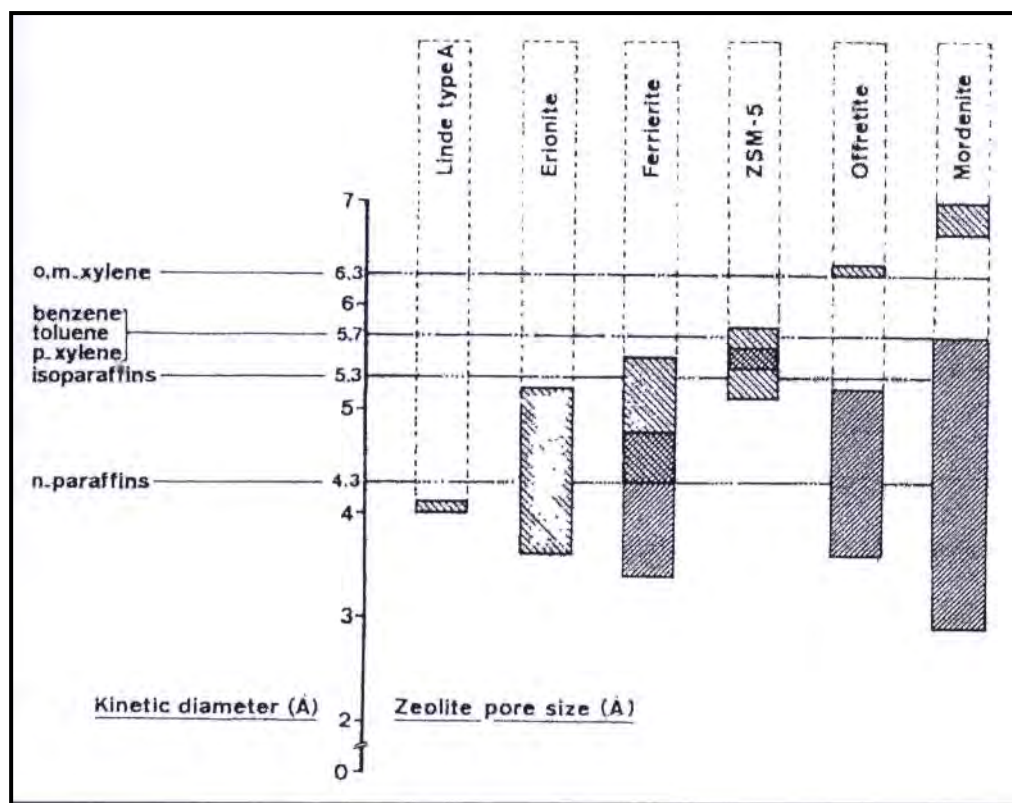
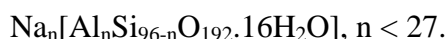


**Figure 2.9** Correlation between pore size of various zeolites and kinetic diameter of some molecules [32].

### 2.1.5.2 Chemical composition of ZSM-5

The chemical formula of a typical unit cell of hydrated Na-ZSM-5 is



That seems to be a limit on the Al incorporation in the framework. The lowest Si/Al ratio known in the ZSM-5 lattice is 10. ZSM-5 is used in many industrially catalytic processes [33]. The catalytic activity of the material is inextricably linked to its composition and structure.

### 2.1.6 The templating process

For a long time, more than 40 years, the templating process has been taken as the process responsible for the production of zeolites and molecular sieves. It was not until 1994 that Burkett and Davis [34] showed that the formation of molecular sieves depended heavily on the bonding of amines or quaternary

ammonium ions first to water and then to small silicate species, as shown in Figure 2.10.

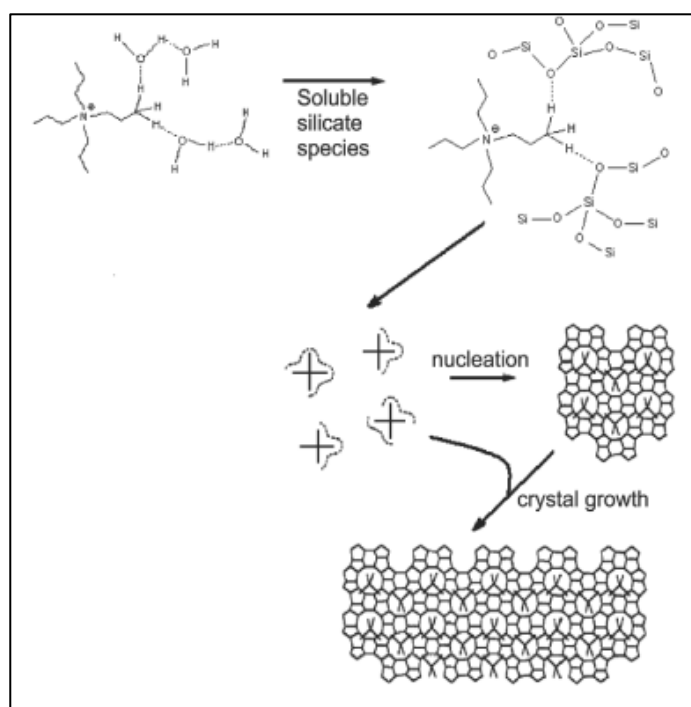


**Figure 2.10** The formation of zeolite ZSM-5 according to the idea by which it is the interaction of organics ion and silicate.

In the aqueous solution of quaternary ammonium ions, tetrapropylammonium in this case, water molecules are associated with the ions through van de Waals interaction. The addition of silicate species causes the displacement of water and establishes a network of properly organized silicate species, in a high pH solution, that are spatially organized and ready to condense, forming the first nucleus which, and upon further condensation, leads to the formation of the zeolite framework. Therefore, short distance interaction is the major component in the direct synthesis of molecular sieves in general, the structure directing agent has not only the role of filling the voids of the porous structure but also the function of interacting with the framework and stabilizing it, most of the time aided by water and other ions [35]. The calcination or extraction of the surfactant produced arrays of mono or three-dimensional channels in a structure that mimicked the liquid crystal one, as shown in Figure 2.11.

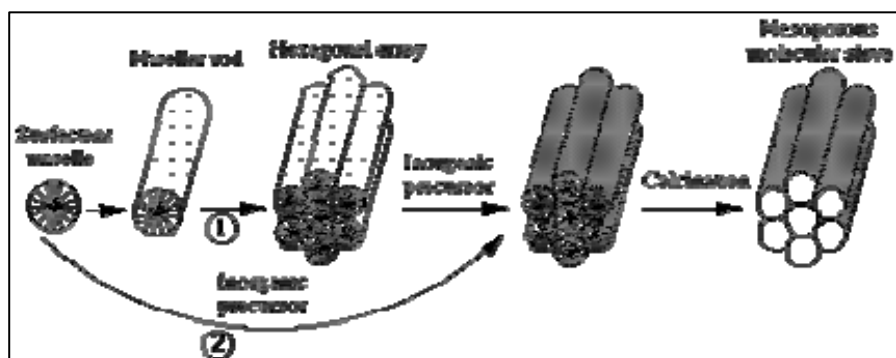


**Figure 2.11** The formation of a solid displaying a hexagonal array of pores prepared from a cationic surfactant liquid crystal arrangement and anionic inorganic precursor.

## 2.1.7 Characterization of zeolit ZSM-5

### 2.1.7.1 Powder x-ray diffraction

X-ray powder diffraction (XRD) [36] is an instrumental technique used for identification of minerals, as well as other crystalline materials. XRD is a technique in which a collimated beams of nearly monochromatic. X-rays is directed onto the flat surface of a relatively thin layer of finely ground material. XRD can provide additional information beyond basic identification. If the sample is a mixture, XRD data can be analyzed to determine the proportion of the different minerals present. Other information obtained can include the degree of crystallinity of the minerals present, possible deviations of the minerals from their ideal compositions, the structural state of the minerals and the degree of hydration for minerals that contain water in their structure. Figure 2.12 shows a monochromatic beam of X-ray incident on the surface of crystal at an angle  $\theta$ . The scattered intensity can be measured as a function of scattering angle  $2\theta$ . The resulting XRD pattern efficiently determines the different phases present in the sample.



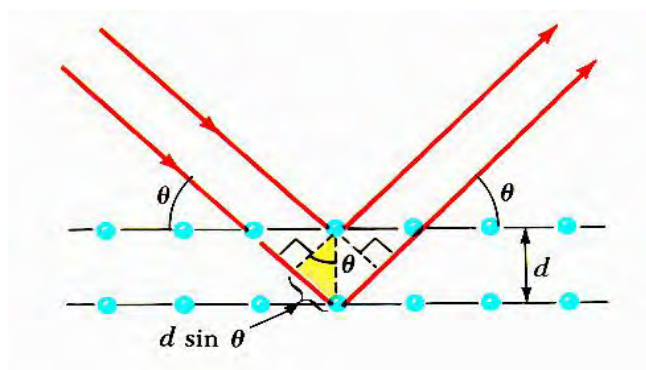


**Figure 2.12** Diffraction of X-ray by regular planes of atoms [37].

Using this method, Bragg's law is able to determine the interplanar spacing of the samples, from diffraction peak according to Bragg angle.

$$n\lambda = 2d \sin\theta$$

where the integer  $n$  is the order of the diffracted beam,  $\lambda$  is the wavelength;  $d$  is the distance between adjacent planes of atoms (the  $d$ -spacings) and  $\theta$  is the angle between the incident beam and these planes.

### 2.1.7.2 Scanning electron microscopy (SEM)

The scanning electron microscope (SEM) [38] has unique capabilities for analyzing surfaces and morphology of materials. It is analogous to the optical microscope, although different radiation sources serve to produce the required illumination. Whereas the optical microscope forms an image from light reflected from a sample surface, the SEM uses electrons for image formation. The different wavelength of these radiation sources results in different resolution levels: electrons have much shorter wavelength than light photons, and shorter wavelength is capable of generating higher resolution information. Enhanced resolution in turn permits higher magnification without loss of detail. The maximum magnification of the light microscope is about 2,000 times; beyond this level is "empty magnification", or the point where increased magnification does not provide additional information. This upper magnification limit is a function of the wavelength of visible light, 2000 Å, which equal the theoretical maximum resolution of conventional light microscope. In comparison, the wavelength of electron is less than 0.5 Å, and theoretically the maximum magnification of electron beam instrument is beyond 800,000 times.

Because of instrumental parameters, practical magnification and resolution limits are about 75,000 times and 40 Å in a conventional SEM. The SEM consists basically of four systems:

1. The *illuminating/imaging system* produces the electron beam and directs it onto the sample.
2. The *information system* includes the data released by the sample during electron bombardment and detectors which discriminate among these information signals.
3. The *display system* consists of one or two cathode-ray tubes for observing and photographing the surface of interest.
4. The *vacuum system* removes gases from the microscope column which increases the mean free path of electron, hence the better image quality.

The morphology of ZSM-5 can be easily observed in a SEM as shown in Figure 2.13.

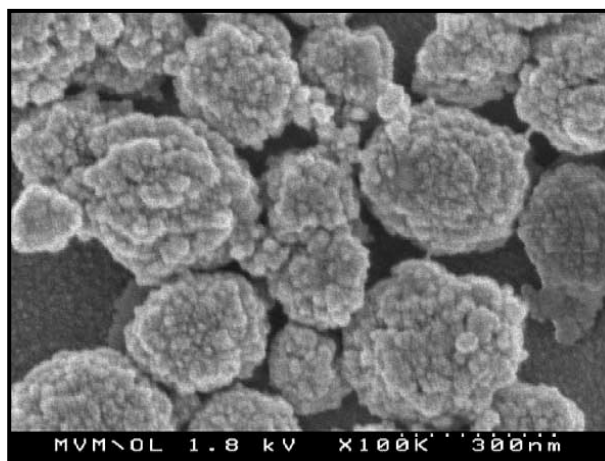


**Figure 2.13** Scanning electron micrograph of a ZSM-5 sample [39].

### 2.1.7.3 Nitrogen adsorption-desorption technique

The N<sub>2</sub> adsorption technique is used for determination of physical properties of mesoporous molecular sieves, such as the surface area, pore volume, pore diameter and pore-size distribution of solid catalysts. Adsorption of gas by a porous material is described by an adsorption isotherm, the amount of adsorbed gas by the material at a fixed temperature as a function of pressure. Porous materials are frequently characterized in terms of pore sizes derived from gas sorption data. IUPAC conventions have been proposed for classifying pore sizes and gas sorption isotherms

that reflect the relationship between porosity and sorption. The IUPAC classification of adsorption isotherms is illustrated in Figure 2.14. Six types of isotherms are characteristic of adsorbents that are microporous (type I), nonporous or macroporous (types II, III, and VI) or mesoporous (types IV and V).

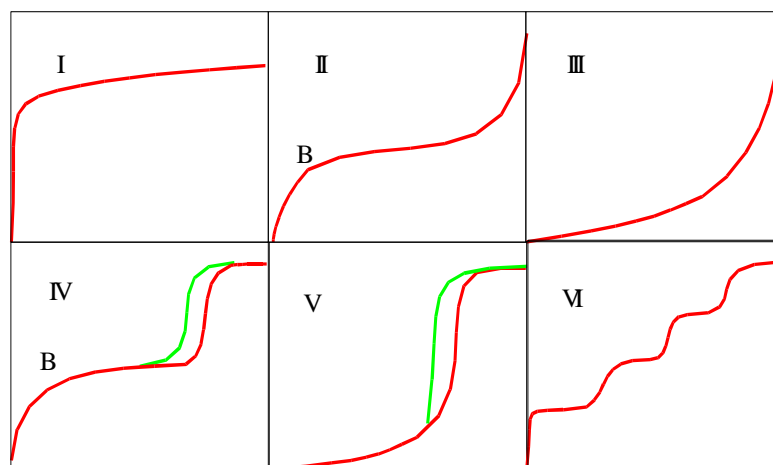


**Figure 2.14** The IUPAC classification of adsorption isotherm [40].

Adsorption isotherms are described as shown in Table 2.3 based on the strength of the interaction between the sample surface and gas adsorbate, and the existence or absence of pores. Pore types are classified as shown in Table 2.4.

Pore size distribution is measured by the use of nitrogen adsorption/desorption isotherm at liquid nitrogen temperature and relative pressures ( $P/P_0$ ) ranging from 0.05-0.1. The large uptake of nitrogen at low  $P/P_0$  indicates filling of the micropores ( $<20 \text{ \AA}$ ) in the adsorbent. The linear portion of the curve represents multilayer adsorption of nitrogen on the surface of the sample, and the concave upward portion of the curve represents filling of mesopores and macropores.

**Table 2.3** Features of adsorption isotherms [41]

Type	Features	
	Interaction between sample surface and gas adsorbate	Porosity
I	Relatively strong	Micropores
II	Relatively strong	Nonporous
III	Weak	Nonporous
IV	Relatively strong	Mesopore
V	Weak	Micropores or Mesopore
VI	Relatively strong	Nonporous

**Table 2.4** IUPAC classification of pores [42]

Pore Type	Pore diameter / nm
Micropore	Up to 2
Mesopore	2 to 50
Macropore	more than 50

The multipoint Brunauer, Emmett and Teller (BET) [43] method is commonly used in the measurement of total surface area.

$$\frac{1}{W[(P_o/P)-1]} = \frac{1}{W_m C} + \frac{C-1}{W_m C} (P/P_o)$$

Where W is the weight of nitrogen adsorbed at a given P/P<sub>o</sub>, and W<sub>m</sub> is the weight of gas to give monolayer coverage, and C is a constant that is related to the heat of adsorption. A linear relationship between 1/W [(P<sub>o</sub>/P)-1] and P/P<sub>o</sub> is required to obtain the quantity of nitrogen adsorbed. This linear portion of the curve is restricted to a limited portion of the isotherm, generally between 0.05-0.30. The slope and intercept are used for determination of the quantity of nitrogen adsorbed in the monolayer and calculate the surface area. For a single point method, the intercept is taken as zero or a small positive value, and the slope from the BET plot is used for

calculation of the surface area. The surface area reported depends upon the method used, as well as the partial pressures at which the data are collected.

#### **2.1.7.4 Temperature-programmed desorption of ammonia**

Temperature-programmed desorption (TPD) [44] is one of the most widely used and flexible techniques for characterizing the acid sites on oxide surfaces. Determination of the quantity and strength of the acid sites on alumina, amorphous silica-alumina, and zeolites is crucial to understanding and predicting the performance of a catalyst. For several significant commercial reactions (such as n-hexane cracking, xylene isomerization, propylene polymerization, methanol-to-olefins reaction, toluene disproportionation, and cumene cracking), all reaction rates increase linearly with Al content (acid sites) in H-ZSM-5. The activity depends on many factors, but the Brønsted-acid site density is usually one of the most crucial parameters.

##### Sample preparation

Samples are degassed at 100 °C for one hour in flowing helium to remove water vapor and to avoid pore damage from steaming which may alter the structure of zeolites. The samples are then temperature programmed to 500 °C at a ramp rate of 10 °C/minute and held at that temperature for two hours to remove strongly bound species and activate the sample. Finally the sample is cooled to 120 °C in a stream of flowing helium.

##### Adsorption

The sample is then saturated with the gaseous basic probe at 120°C; this temperature is used for minimizing physisorption of ammonia or organic amines. For ammonia, two techniques are available to saturate the sample: pulsing the ammonia using the loop or continuously flowing ammonia. Pulsing the ammonia allows the user to compare the quantity of ammonia adsorbed (via pulse adsorption) to the quantity desorbed for the subsequent TPD. After saturation with ammonia, pyridine, or propyl amine, the sample is purged for a minimum of one hour under a flow of helium to remove any of the physisorbed gases.

### Desorption

The temperature-programmed desorption is easily performed by ramping the sample temperature at 10°C/minute to 500°C. It is a good rule of thumb that the end temperature during the TPD not exceed the maximum temperature used in the preparation of the sample. Exceeding the maximum preparation temperature may liberate additional species from the solid unrelated to the probe molecule and cause spurious results.

During the TPD of ammonia or the non-reactive probes (pyridine or t-butyl amine), the built-in thermal conductivity detector (TCD) will monitor the concentration of the desorbed species. For the reactive probes (propyl amines), a mass spectrometer is required to quantify the density of acid sites. For these probes, several species may be desorbed simultaneously: amine, propylene, and ammonia.

#### **2.1.7.5 <sup>27</sup>Al-MAS-NMR [45]**

Another important characterization technique for mesoporous materials is solid state NMR. <sup>27</sup>Al-MAS-NMR spectroscopy has been employed to distinguish between tetrahedrally and octahedrally coordinated aluminum in the framework at approximately 50 and 0 ppm, respectively. Hence, the amount of framework aluminum can be determined and corresponds to the acidity of the solid sample.

## **2.2 The Refining Process [46, 47]**

Every refinery begins with the separation of crude oil into different fractions by distillation (Figure 2.15). The fractions are further treated to convert them into mixtures of more useful saleable products by various methods such as cracking, reforming, alkylation, polymerization and isomerisation. These mixtures of new compounds are then separated using methods such as fractionation and solvent extraction. Impurities are removed by various methods, e.g. dehydration, desalting, sulphur removal and hydrotreating.

Refinery processes have been developed in response to change market demands for certain products. With the advent of the internal combustion engine the main task of refineries became the production of petrol. The quantity of petrol available from distillation alone was insufficient to satisfy consumer demand.

Refineries began to look for ways to produce more and better quality petrol. Two types of processes have been developed:

- Breaking down large, heavy hydrocarbon molecules
- Reshaping or rebuilding hydrocarbon molecules.

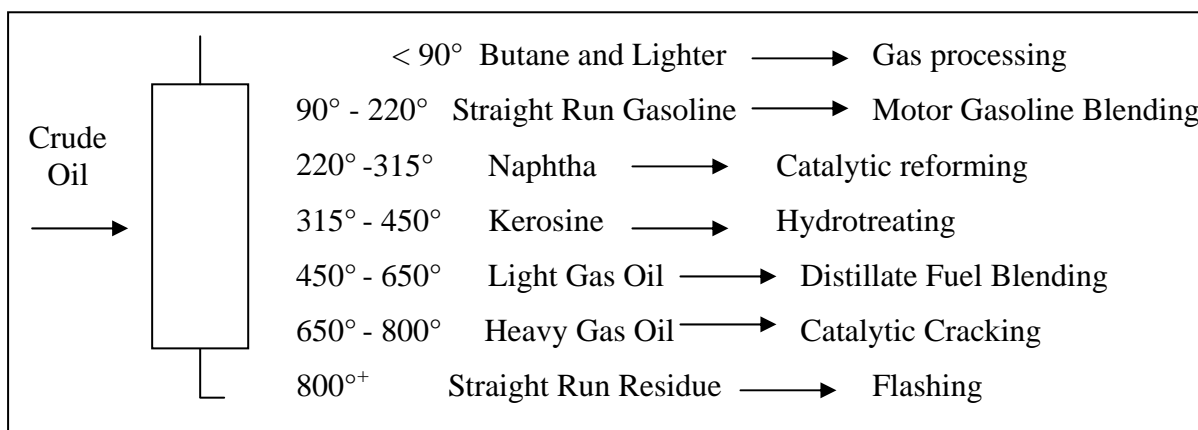


**Figure 2.15** Distilling crude and product disposition.

Cracking processes break down heavier hydrocarbon molecules (high boiling point oils) into lighter products such as petrol and diesel. These processes include catalytic cracking, thermal cracking and hydrocracking.

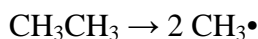
- **Catalytic cracking** [48] is used to convert heavy hydrocarbon fractions obtained by vacuum distillation into a mixture of more useful products such as petrol and light fuel oil. In this process, the feedstock undergoes a chemical breakdown, under controlled heat (450°C-500°C) and pressure. Small pellets of silica-alumina have proved to be the most effective catalysts. The cracking reaction yield petrol, LPG, unsaturated olefin compounds, cracked gas oils, a liquid residue called cycle oil, light gasses and a solid coke residue. Cycle oil is recycled to cause further breakdown and the coke, which forms a layer on the catalyst, is removed by burning. The other products are passed through fractionators to be separated and separately processed.

### - Thermal cracking [49]

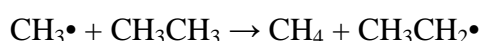
In thermal cracking elevated temperatures (~800°C) and pressures (~700kPa) are used. An overall process of disproportionation can be observed, where "light", hydrogen-rich products are formed at the expense of heavier molecules which condense and are depleted of hydrogen. The actual reaction is known as homolytic fission and produces alkenes, which are the basis for the economically important production of polymers.

A large number of chemical reactions take place during steam cracking, most of them based on free radicals. Computer simulations aimed at modeling what takes place during steam cracking have included hundreds or even thousands of reactions in their models. The main reactions that take place include:

1. Initiation reactions, where a single molecule breaks apart into two free radicals. Only a small fraction of the feed molecules actually undergo initiation, but these reactions are necessary to produce the free radicals that drive the rest of the reactions. In steam cracking, initiation usually involves breaking a chemical bond between two carbon atoms, rather than the bond between a carbon and a hydrogen atom.



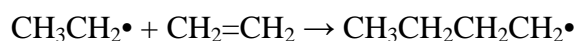
2. Hydrogen abstraction, where a free radical removes a hydrogen atom from another molecule, turning the second molecule into a free radical.



3. Radical decomposition, where a free radical breaks apart into two molecules, one an alkene, the other a free radical. This is the process that results in the alkene products of steam cracking.

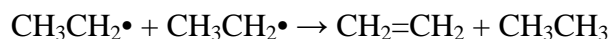
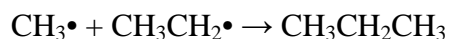


4. Radical addition, the reverse of radical decomposition, in which a radical reacts with an alkene to form a single, larger free radical. These processes are involved in forming the aromatic products that result when heavier feedstocks are used.





5. Termination reactions, which happen when two free radicals react with each other to produce products that are not free radicals. Two common forms of termination are *recombination*, where the two radicals combine to form one larger molecule, and *disproportionation*, where one radical transfers a hydrogen atom to the other, giving an alkene and an alkane.



- **Hydrocracking** can increase the yield of petrol components, as well as being used for producing light distillates. It produces no residues, only light oils. Hydrocracking is catalytic cracking in the presence of hydrogen. The extra hydrogen saturates, or hydrogenates the chemical bonds of the cracked hydrocarbons and creates isomers with the desired characteristics. Hydrocracking is also a treating process, because the hydrogen combines with contaminants such as sulphur and nitrogen, allowing them to be removed.

## 2.3 Catalytic Cracking Mechanisms

### 2.3.1 General Cracking Mechanisms [50]

In general, for components with equal carbon numbers, the rate of cracking decreases in the order: i-olefins > n-olefins > i-paraffins  $\approx$  naphthenes > n-paraffins > aromatics. The cracking mechanism can be a chain mechanism that involves the intermediate formation of carbocations, positively charged hydrocarbon species. Carbocations include both carbenium ions such as  $\text{R}_1\text{-CH}_2\text{-C}^+\text{H-R}_2$ ,  $\text{R}_1\text{-CH=C}^+\text{-R}_2$  and carbonium ions such as  $\text{R}_1\text{-CH}_2\text{-C}^+\text{H}_3\text{-R}_2$ ,  $\text{R}_1\text{-CH=C}^+\text{H}_2\text{-R}_2$ . In carbenium ions, the charge carrying carbon atom can be di- or tri-coordinated, while in carbonium ions, the charge carrying carbon atom is tetra- or pentacoordinated. The stability of the carbocations decreases in the order: tertiary > secondary > primary [51]. Cracking of hydrocarbons is primarily a reaction that proceeds through adsorbed carbenium ion intermediates.

### 2.3.2 Reactions of Olefins

The formation of carbenium ions from olefins can easily proceed by addition of the proton from a Brønsted acid site of the catalyst to the carbon–carbon double bond. Cracking of the adsorbed carbenium ion proceeds through the  $\beta$ -scission mechanism [52, 53] or through the protonated cyclopropane mechanism [54]. An illustration is given in Figure 2.16. Adsorption at a Brønsted acid site leads to formation of an adsorbed carbenium ion that can be cracked. Both the  $\beta$ -scission mechanism [52, 53] and the protonated cyclopropane mechanism [54] are shown.

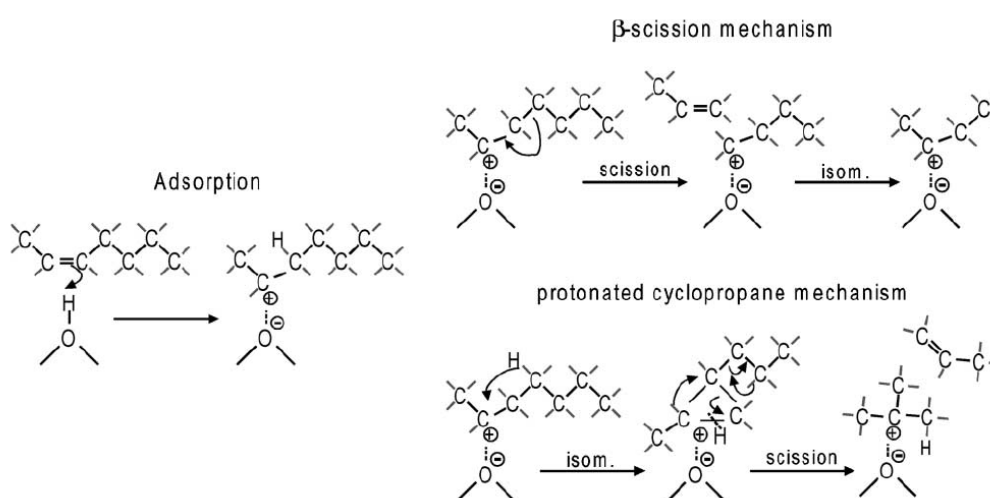
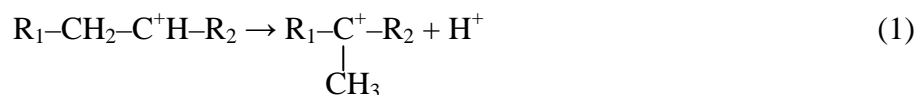


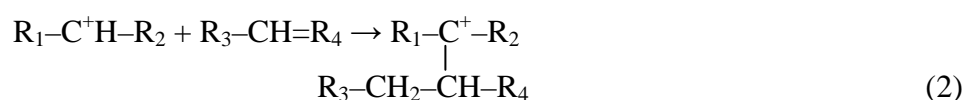
**Figure 2.16** Cracking mechanisms illustrated by the reaction of n-heptene.

Other reactions of the adsorbed carbenium ion are [55, 56]:

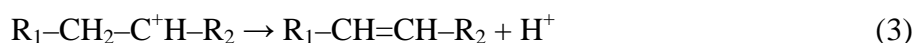
1. Isomerization to a more stable carbenium ion, for example, through a methyl shift:



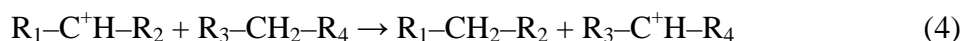
2. Oligomerization with olefin in a bimolecular reaction to form a larger adsorbed carbenium ion:



3. Desorption with deprotonation to form an olefin (the opposite of adsorption):



4. Desorption with hydride abstraction from a paraffin to form new paraffin from the carbenium ion and new carbenium ion from the paraffin (H-transfer reaction):



5. Desorption with hydride abstraction from (cyclic) olefins or coke (precursors) to form paraffin and a more aromatic compound (H-transfer reaction):



The bimolecular reactions (2), (4) and (5) can occur if the pore size of the catalyst is large enough to accommodate the reactive intermediates, or they should occur on the outer surface of the zeolite particles. If the pores are too small, as in the case of ZSM-5 (0.54 nm × 0.56 nm), these reactions cannot take place with the larger (gasoline) components, although oligomerization or dimerization of small (C<sub>2</sub>–C<sub>4</sub>) olefins could be possible. For example, in the Mobil olefins to gasoline and distillates process (MOGD) coupling of light hydrocarbons is catalyzed by ZSM-5.

With ZSM-5, cracking through dimeric intermediates has only been reported in the reactions of relatively small *n*-olefins (C<sub>4</sub>–C<sub>6</sub>). Abbot and Wojciechowski [57] have studied cracking of *n*-olefins ranging from C<sub>5</sub> to C<sub>9</sub> at 678 K with ZSM-5 and found that cracking of pentene solely took place through a dimeric/disproportionation mechanism. Cracking of heptene and larger molecules proceeded mainly through monomolecular cracking and at 678 K; hexene represented the transition case of the two mechanisms and was cracked by both monomolecular cracking and through dimeric intermediates.

With Y-type zeolites, the dimeric mechanism is a more important reaction route; for example, it has been found that cracking of C<sub>7</sub> took place for 25% via a dimeric disproportionation reaction at 473°C and for 32% at 400°C.

### 2.3.3 Proposed Cracking Mechanisms of Polymer [58]

For ZSM-5 the cracking reactions of larger  $C_7^+$  olefins are restricted to simple  $\beta$ -scission reactions. The relatively straight chains (or parts of it) can enter the pores of ZSM-5, are adsorbed, split-off small olefins, and the products are desorbed. For example, the reaction of n-heptene over ZSM-5 (for simplicity only the  $\beta$ -scission mechanism) is shown in Figure 2.17. The adsorbed  $C_7$ -carbenium ion is cracked to propene and  $C_4$ -carbenium ion. Then  $C_4$ -carbenium ion isomerizes to butene or is cracked to two ethene molecules.

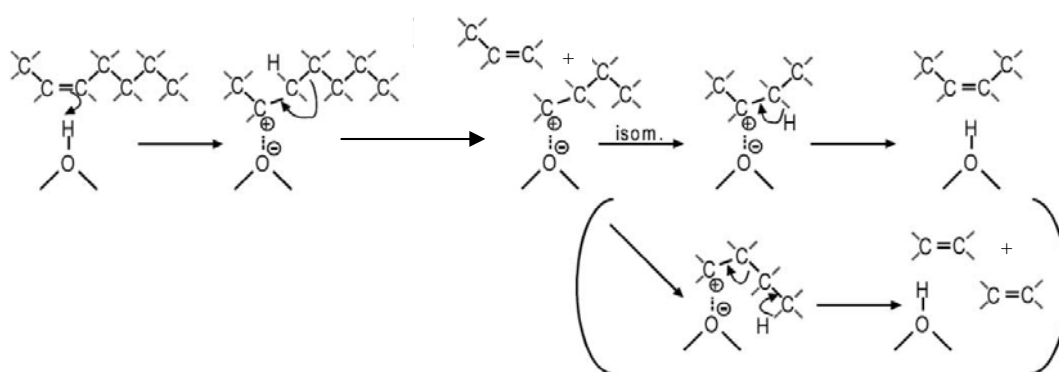


**Figure 2.17** Monomolecular cracking mechanisms (only mechanism possible with ZSM-5).

Generally, the second reaction, formation of ethene, is energetically less favorable because it involves the formation of two primary carbenium ions. However, due to the small pores of ZSM-5, the electrical field in the pores is larger and a relatively large interaction between the catalyst and the adsorbed carbenium ions shall exist. It is believed that the oxygen atoms of a zeolite structure play a role in solvating carbocations, delocalizing the positive charge into the framework. The smaller the size of the pores of the zeolite, the closer the different oxygen atoms are to the adsorbed reaction intermediates and the higher the possible interaction. So possibly, as a result of increased stabilization of the intermediates, the formation of ethene is enhanced when small pore-zeolites such as ZSM-5 are involved.

On the base catalyst, with zeolite Y as active species (pore size of 0.74 nm) adsorbed  $C_4$ -carbenium species and new heptene molecule to form an adsorbed  $C_{11}$ -carbenium ion. The  $C_{11}$  carbenium ion is cracked to hexane and  $C_5$ -carbenium ion. This bimolecular cracking mechanism proposed by Williams *et al.* [55] is

illustrated in Figure 2.18. Also, the adsorbed heptene carbenium ion could oligomerize before cracking.

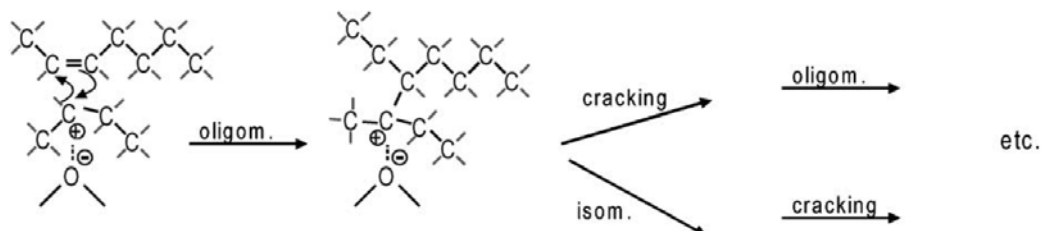


**Figure 2.18** Bimolecular cracking mechanism that can occur on zeolite Y in addition to the monomolecular mechanism.

Because of the larger adsorption strength of larger hydrocarbons, the bimolecular mechanism have an important contribution in the cracking mechanism of the heavier gasoline-range olefins, provided that the catalyst pore size is large enough to accommodate the reaction intermediates. Aromatics and highly branched components, therefore, are too large to react through bimolecular mechanisms. Linear components are the most likely ones to react through this mechanism.

According to this proposed mechanism, the active site of ZSM-5 is the acid site itself, while the active site in zeolite Y can be represented by the adsorbed carbenium ion. The reaction intermediates with ZSM-5 contain the number of carbon atoms (C<sub>5</sub>–C<sub>11</sub>), while the (surface) intermediates with the base catalyst can be much larger. As a result, the cracking products from ZSM-5 will be mainly C<sub>3</sub>, C<sub>4</sub>, and to some extent also C<sub>2</sub> olefins, while with the zeolite Y base catalyst larger fragments can be formed.

This agrees with the results that can be found in literature; the main products from *n*-olefins and *i*-olefins cracking on ZSM-5 are light olefins with a high selectivity for propene, *i*-butene, and in some cases the increased yields of ethene are reported.

### 2.3.4 Reactions of paraffins

Compared to olefins, paraffins have a lower reactivity towards cracking due to a more difficult formation of carbenium ions. Direct formation of a carbenium ion requires the abstraction of a hydride ion. This may proceed at Lewis acid sites or adsorbed carbenium ions can react with paraffins in a bimolecular-type of mechanism. The latter mechanism requires the presence of the adsorbed carbenium ions and can take place if the pore size of the catalyst is large enough to accommodate the necessary transition state (as is the case in zeolite Y but not in ZSM-5).

Indirect formation of carbenium ions is proposed to proceed through the formation of carbonium ions; paraffin reacts with a proton from a Brønsted acid site and the resulting adsorbed carbonium ion is cracked to an adsorbed carbenium ion and hydrogen or a small olefin. The formation of a carbonium ion requires an energetically unfavorable transition state and has high activation energy. This mechanism for activation of paraffins will only be significant in the absence of olefins and is favored by high temperatures, low hydrocarbon partial pressures and low conversions of the paraffins. The occurrence is not expected to be significant when cracking a gasoline mixture that contains olefins. The olefin can easily form carbenium ions and cause cracking of paraffins through the bimolecular cracking mechanisms as discussed above.

## CHAPTER III

### EXPERIMENTS

#### 3.1 Instruments and apparatus

##### Ovens and furnaces

During the zeolite synthesis course, the starting mixture was heated in a Memmert UM-500 oven. Calcination of the solid catalysts at 600°C was achieved in a Carbolite RHF 1600 muffle furnace with programmable heating rate of 1°C/min.

##### Sonicator

The mixture of starting materials for the synthesis of ZSM-5 was homogenized using a 500 W 20 Hz SONICS VC505 sonicator. The probe tip of circular shape was made of titanium with 13 mm diameter. The operation was set in pulse mode at 40% amplitude for 30 min at ambient atmosphere.

##### X-ray powder diffractometer (XRD)

The structure of synthesized microporous materials was identified by using a Rigaku, Dmax 2200/ultima plus X-ray powder diffractometer with a monochromater and Cu K<sub>α</sub> radiation (40 kV, 30 mA). The 2-theta angles were ranged from 5 to 50 degree with a scan speed of 5 degree/min and a scan step of 0.02 degree. The scattering slit, divergent slit and receiving slit were fixed at 0.5 degree, 0.5 degree, and 0.3 mm, respectively.

##### ICP-AES spectrometer

Aluminum content in the catalysts was measured at a wavelength of 396.1 nm using the Perkin Elmer Plasma-1000 inductively coupled plasma-atomic emission spectrometer (ICP-AES). A linear calibration curve was constructed using the standard concentration in the range from 0 to 30 ppm.

### **Scanning electron microscope (SEM)**

A JEOL JSM-6480LV scanning electron microscope was used to examine the morphology and particle size of ZSM-5. All samples were coated with sputtering gold under vacuum.

### **Nitrogen adsorptometer**

Characterization of catalyst for nitrogen adsorption-desorption isotherms, BET specific surface area, and pore size distribution was carried out using a BELSORP-II instrument. The sample was near 40 mg weighed exactly and the pretreatment was performed under vacuum at 400°C for 3h before each measurement.

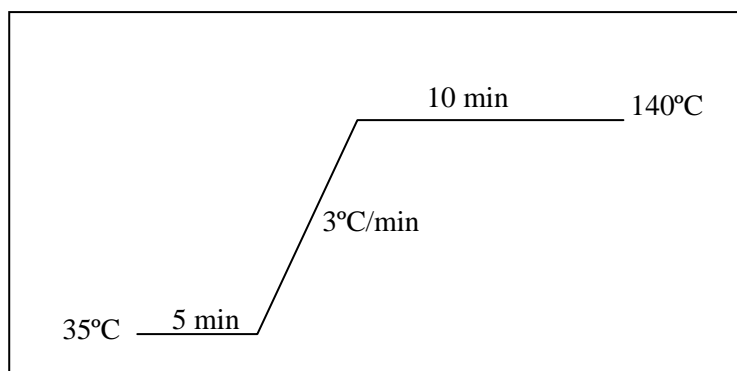
### **NH<sub>3</sub> TPD machine**

Acid strength of catalysts was determined using a BEL-CAT Japan instrument. The sample was near 200 mg weighted exactly and pretreatment at 400°C 20 min before each measurement.

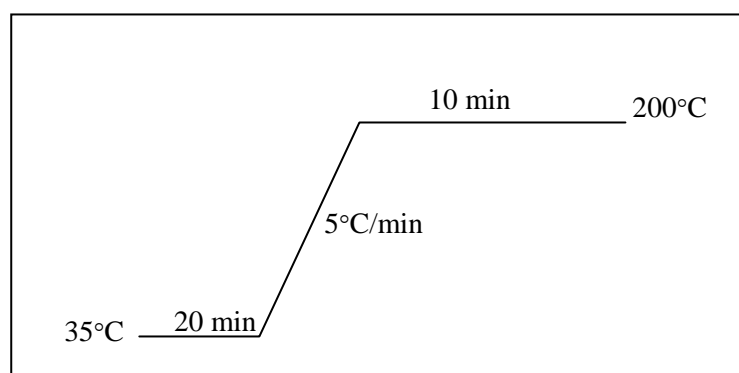
### **Gas chromatograph**

Hydrocarbon gases were analyzed using a Varian CP-3800 gas chromatograph equipped a 50-m long and 0.53-mm inner diameter Alumina-KCl PLOT column and flame ionization detectors (FID). Liquid samples were analyzed using a Varian CP-3800 gas chromatograph equipped with a 30-m long and 0.25-mm inner diameter CP-sil 5 (0.25 μm film thickness) column and flame ionization detectors (FID). The heating programs for the GC columns are shown in Schemes 3.1 and 3.2, respectively. The sample volumes for each measurement are 3.00 mL for liquid and 1.00 mL for gas, respectively.





**Scheme 3.1** The heating program for the GC column used in gas analysis.



**Scheme 3.2** The heating program for the GC column used in liquid analysis.

### 3.2 Chemicals and gases

1. Sodium metasilicate pentahydrate,  $\text{Na}_2\text{SiO}_3 \cdot 5\text{H}_2\text{O}$  (Fluka, reagent grade)
2. Tetraethyl orthosilicate, TEOS (Aldrich, 98% wt)
3. Tetrapropylammonium bromide, TPABr (Fluka, reagent grade)
4. Tetrapropylammonium hydroxide, TPAOH (Aldrich, reagent grade)
5. Aluminium isopropoxide, AIP (Aldrich)
6. Sodium aluminate,  $\text{NaAlO}_2$  (Riedel-de Haën, reagent grade)
7. Ammonium chloride,  $\text{NH}_4\text{Cl}$  (Fluka, reagent grade)
8. Hydrochloric acid, HCl (Fluka, 37% wt)
9. Sulfuric acid,  $\text{H}_2\text{SO}_4$  (Merk, reagent grade)
10. Standard gas mixture and liquid mixture for GC analysis (kindly obtained from PTT Chemical Public Company Limited)

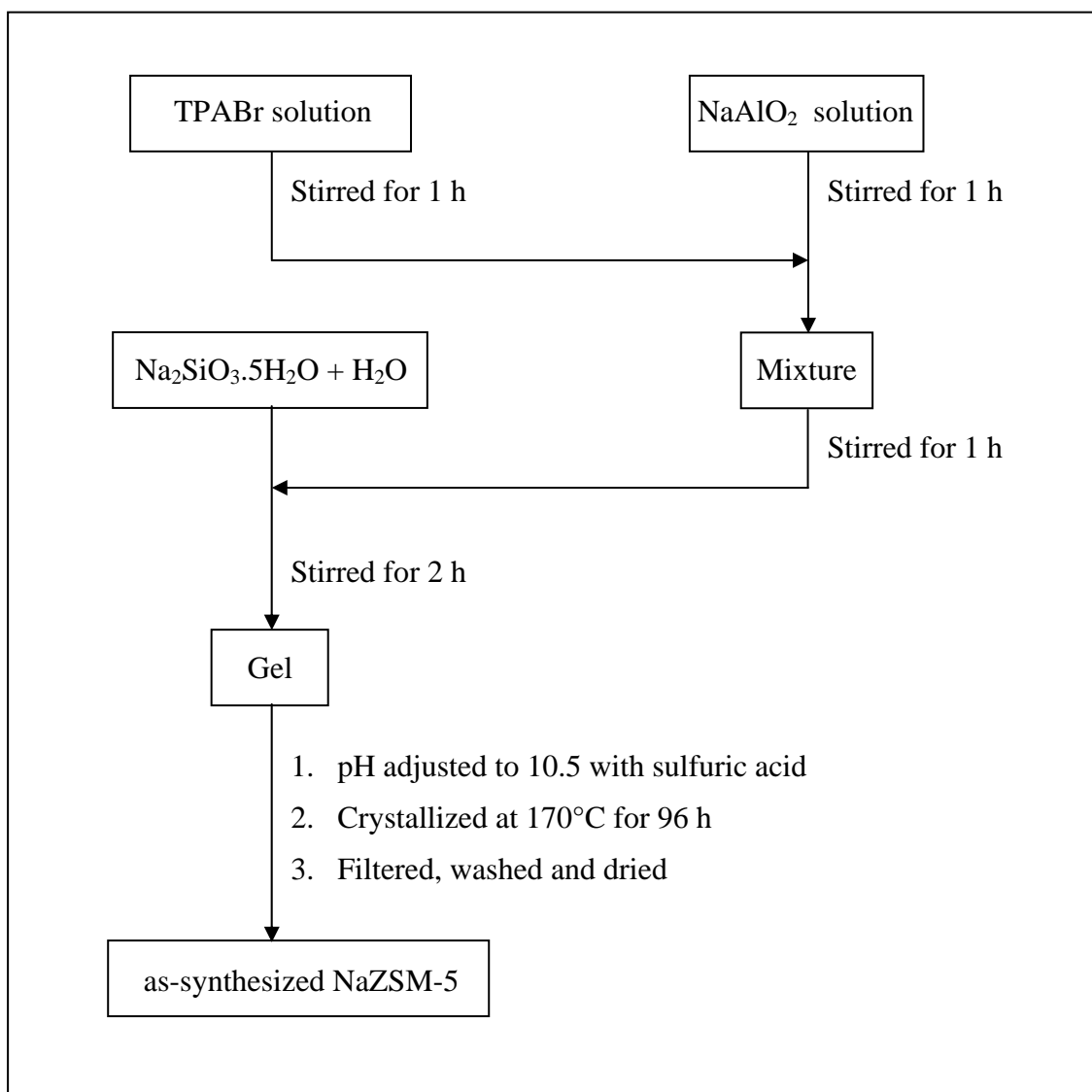
11. Nitrogen gas,  $N_2$  (Thai Industrial Gases (TIG), highly pure grade )
12. Ammonia gas,  $NH_3$  (Linde Gas Thailand, highly pure grade)

### 3.3 Synthesis of ZSM-5 by hydrothermal method

The synthesis of ZSM-5 by hydrothermal method was modified from the method reported by Szostak and Thomas [59]. The gel composition was the same but the starting materials were different. Another difference was the synthesis in a basic media instead of an acidic media. Schematic diagram for NaZSM-5 preparation is shown in Scheme 3.3. A solution of TPABr (10.06 g of TPABr in 103.60 g of water) was added dropwise into a solution of  $NaAlO_2$  (1.56 g of in 103.60 g of water). The mixture was stirred additionally for one hour before it was added dropwise into a 4-neck round bottom flask containing a solution of 80.59 g of  $Na_2SiO_3 \cdot 5H_2O$  in 80.59 g of water. The resulting gel with molar composition of  $SiO_2 : 1.025Na_2O : 0.025Al_2O_3 : 0.1TPABr : 47.131H_2O$  was mechanically stirred for 2 hours at 350 rpm. Apparatus for gel preparation is shown in Figure 3.1. After that, pH of the gel was adjusted to 10.5 with concentrated  $H_2SO_4$ . The gel was transferred into a Teflon lined stainless-steel autoclave and it was either sonicated or unsonicated in comparison before crystallized at  $170^\circ C$  for a required period during 3-96 h. The solid product was separated from the solution by centrifugation and washed with deionized water until alkali free. The solid product was dried in an oven at  $100^\circ C$  overnight. The white solid samples were denoted as HTBr. The NaZSM-5 samples were characterized using XRD, ICP-AES, SEM,  $NH_3$ -TPD, and nitrogen adsorption-desorption instruments.

### 3.4 Synthesis of ZSM-5 by xerogel method

An alternate method namely the xerogel method was used for the synthesis of TPAZSM-5 via a silica xerogel formation and a wetness impregnation procedure reported in the literature [60]. This xerogel was prepared by two step sol-gel method. In the first step 40 g of tetraethyl orthosilicate (TEOS) was hydrolyzed with 14 g of 0.05 M aqueous HCl and 17.28 g of deionized water in ice water bath for 1 h. Once the initially two-phase system became monophasic, 2.8 g of 20 wt% TPAOH aqueous solution was dropwise added to the previous mixture until the gel point and the hydrous gel obtained was dried at  $110^\circ C$  overnight. In the second step, the mixture of



**Scheme 3.3** Schematic diagram for the synthesis of ZSM-5 by hydrothermal method.

0.6536 g aluminium isopropoxide and 46 g of 20 wt% aqueous TPAOH solution was added dropwise to a 500 cm<sup>3</sup> 4-necked round bottom flask containing the silica xerogel from the first step with stirring under nitrogen atmosphere. Then the mixture with the molar ratio of SiO<sub>2</sub> : 0.0083Al<sub>2</sub>O<sub>3</sub> : 0.2500TPAOH : 15.6479H<sub>2</sub>O was aged by stirring under nitrogen atmosphere for 12 h. The gel was transferred into a Teflon lined stainless-steel autoclave and it was sonicated for 30 min under the ambient atmosphere without cooling, before crystallized at 170°C for a required period during 3-96 h. The solid product was separated by centrifugation, washed with deionized

water, dried at 100°C overnight. The white solid samples were denoted as XGOH. The TPAZSM-5 samples were characterized using XRD, ICP-AES, SEM and nitrogen adsorption-desorption instruments. The schematic diagram of this procedure is shown in Scheme 3.4.

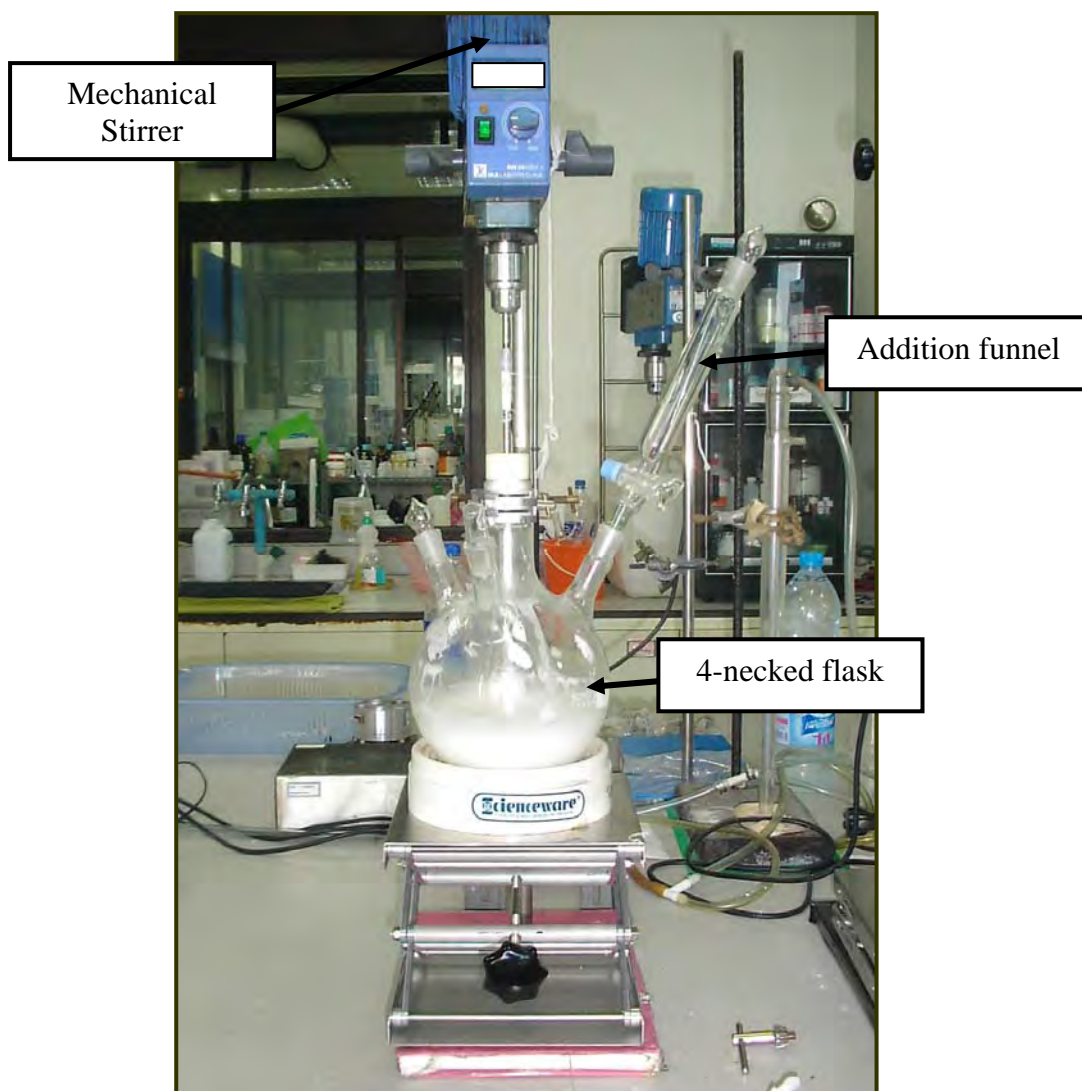


**Figure 3.1** Apparatus for synthesis of ZSM-5.

### 3.5 Preparation of ZSM-5 with two different types of template

The ZSM-5 samples with two different types of template *i. e.* TPABr and TPAOH, by the hydrothermal method as described in Section 3.3. The samples are denoted as HTBr and HTOH (sample HTBr prepared by using TPABr as template, sample HTOH prepared by using TPAOH as template). The samples were characterized using XRD, SEM, and nitrogen adsorption-desorption instruments.

### 3.6 Preparation of ZSM-5 at various pH values

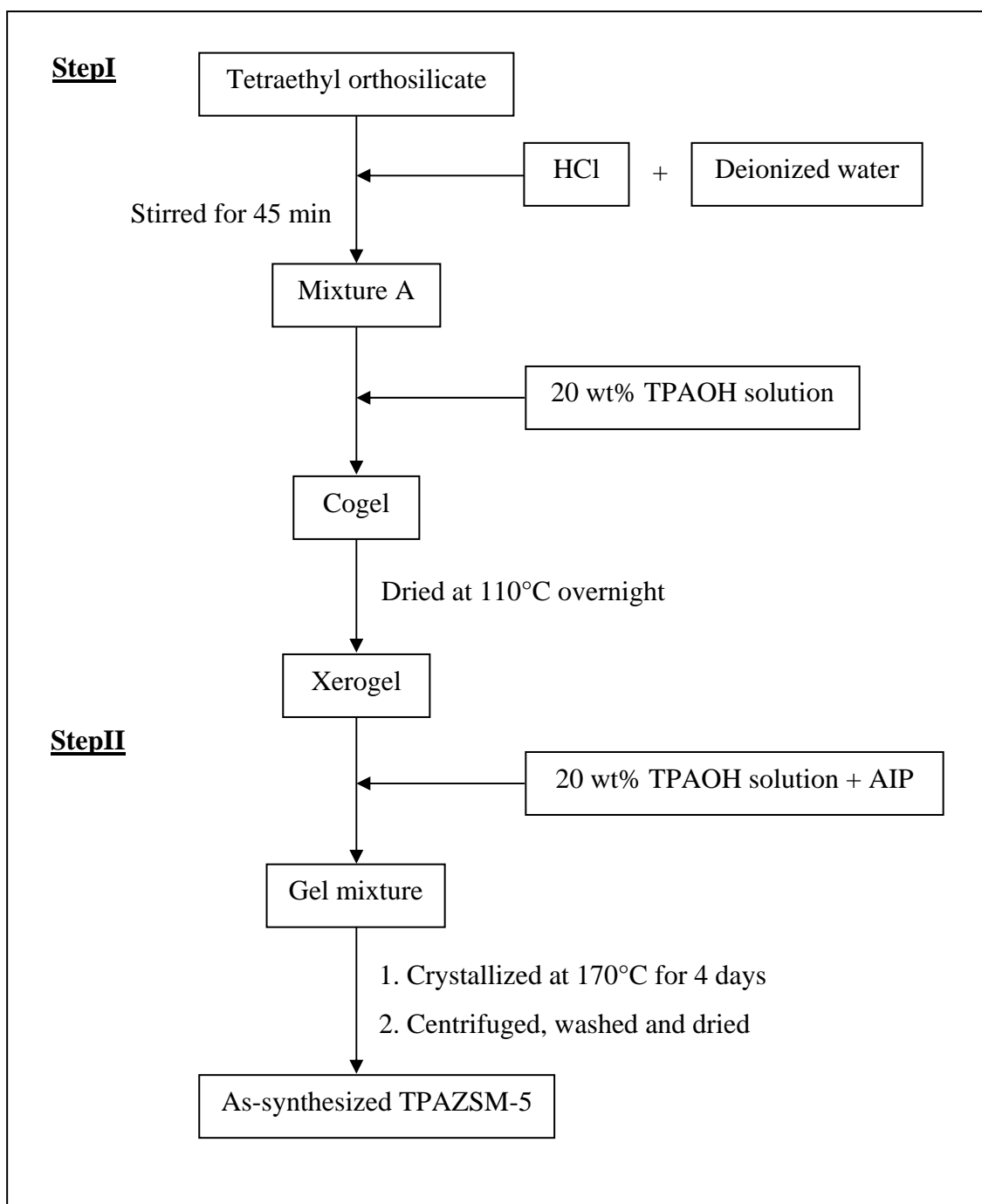
By the hydrothermal method, ZSM-5 samples were synthesized using TPAOH as template at the pH of 9.0, 9.5, 10.0 and 10.5. The pH was adjusted with sulfuric acid to a required value. The samples are denoted as HTOH-x, where x is the pH of gel. The crystallization was carried out at 170°C for 4 days. The samples were characterized using XRD, SEM, and nitrogen adsorption-desorption instruments.

### 3.7 Preparation of ZSM-5 with various template/SiO<sub>2</sub> mole ratios

By the hydrothermal method, ZSM-5 samples were synthesized using TPAOH as template, the pH of 10.5 and the various template/SiO<sub>2</sub> mole ratios of 0.1, 0.2 and 0.5 as denoted by y in the sample notation of HTOH-10.5-y. The samples were characterized using XRD, SEM and nitrogen adsorption-desorption instruments.

### 3.8 Preparation of ZSM-5 with and without sonication

By the hydrothermal method, ZSM-5 samples were synthesized using TPAOH/SiO<sub>2</sub> mole ratios of 0.1. After the pH of gel was adjusted to 10.5 with sulfuric acid, the gel was divided into two portions equally and introduced in two autoclaves. The gel in one autoclave was sonicated with ultrasound for 30 min while the other was not. Then both autoclaves were heated in an oven at 170°C for 4 days. The samples are denoted as HTOH-10.5-0.1so (with sonication) and HTOH-10.5-0.1ns (without sonication). The samples were characterized using XRD, SEM and nitrogen adsorption-desorption instruments.



**Scheme 3.4** Schematic diagram for the synthesis of ZSM-5 by xerogel method.

### 3.9 Preparation of ZSM-5 with various crystallization times

In order to study effect of crystallization time on formation of zeolite ZSM-5, both HTOH-10.5-0.1so and XGOH samples were synthesized in same way as described in Section 3.3 and 3.4, respectively with various crystallization times of 24, 48, 72 and 96 h for HTOH-10.5-0.1so and 2, 6, 12, 18, 24, 48, 72 and 96 h for XGOH. Sample notation is HTOH-10.5-0.1so-zh and XGOH-zh, when z is the crystallization time.

### 3.10 Preparation of ZSM-5 with various Si/Al mole ratios

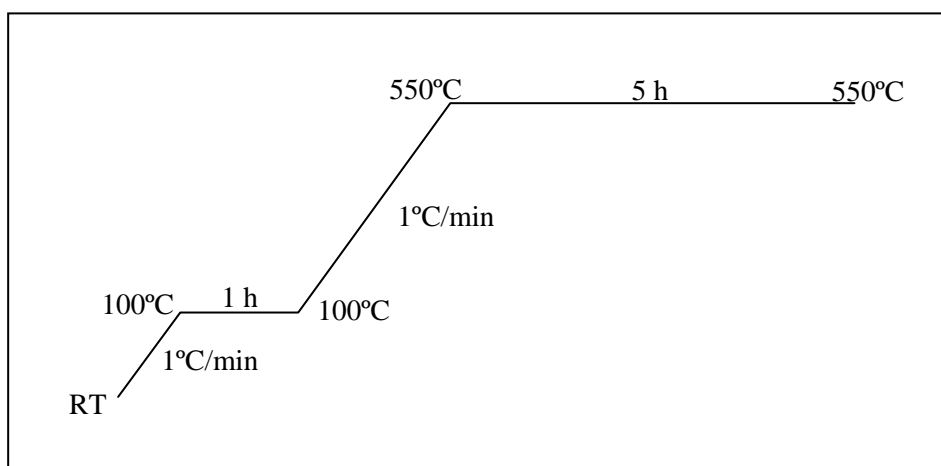
In a series of HTOH-10.5-0.1so-24h samples, various Si/Al mole ratios in gel of 20, 40 and 60 using the similar method to that described in Section 3.3. Different amounts of aluminum required for each sample were used as indicated in Table 3.1. The samples were characterized using XRD, SEM, NH<sub>3</sub>-TPD, and nitrogen adsorption-desorption instruments.

**Table 3.1** Required amounts of sodium aluminate in the preparation of ZSM-5 samples with various Si/Al mole ratios in gel

Sample	Si/Al molar ratio in gel	NaAlO <sub>2</sub> dissolved in 10.00 g H <sub>2</sub> O (g)
HTOH-10.5-0.1so-24h-20	20	0.148
HTOH-10.5-0.1so-24h-40	40	0.075
HTOH-10.5-0.1so-24h-60	60	0.050

### 3.11 Removal of organic template from the ZSM-5 catalysts

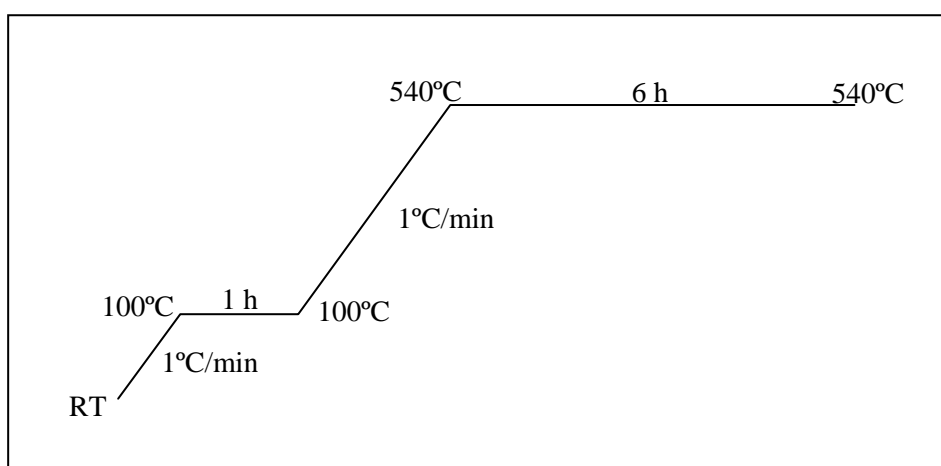
To remove an the organic templates from the pores of ZSM-5, the as-synthesized samples were calcined in a muffle furnace at 550°C for 5 h using a heating gram as shown in Scheme 3.5.



**Scheme 3.5** A heating program for removal of the organic templates from the pores of ZSM-5.

### 3.12 Ammonium ion exchange of zeolite samples

Into an Erlenmeyer flask, 1 g of calcined NaZSM-5 with the HTBr notation was dispersed in 50 ml of an aqueous solution of  $\text{NH}_4\text{Cl}$  and boil under a reflux condition for 3 h. The zeolite was then separated from the mother liquor by centrifugation, and washed with deionized water until free of  $\text{Cl}^-$  which was able to be detected by precipitation with a silver nitrate solution. The ammonium exchanged zeolite was air-dried overnight. The resulted acidic HZSM-5 catalyst was obtained via the removal of ammonia gas upon calcinations at in a muffle furnace at  $540^\circ\text{C}$  for 5 h. The heating program used is shown in Scheme 3.6.



**Scheme 3.6** The heating program for ammonia removal from ZSM-5.



### 3.13 Sample preparation for ICP-AES analysis

In a 100 cm<sup>3</sup> Teflon beaker, 0.0400 g of a calcined catalyst was soaked with 10 cm<sup>3</sup> of 6 M HCl and 10 cm<sup>3</sup> of 48% hydrofluoric acid as added subsequently to get rid of silica in the form of volatile SiF<sub>4</sub>. Then the sample was carefully heated to dryness, but not boiled, on a hot plate. The HF treatment was repeated twice more. An amount of 10 cm<sup>3</sup> mixture of 6 M HCl : 6 M HNO<sub>3</sub> at a volume ratio of 1:3 was added and further heated to dryness. An amount of 10 cm<sup>3</sup> deionized water was added to the beaker and warmed for 5 minutes to complete dissolution. The solution was transferred to a 50 cm<sup>3</sup> polypropylene volumetric flask and made to the volume by adding deionized water. The flask was capped and shaken thoroughly. The solution was transferred into a plastic bottle with a treaded cap lined with a polyethylene seal.

### 3.14 Activities of HZSM-5 catalysts in HDPE cracking

#### 3.14.1 Catalytic cracking of HDPE

Catalytic cracking of plastic polymer over HZSM-5 was carried out in glass reactor (4.4 cm. i.d. and 37 cm. length) by batch operation as shown in Figure 3.2 and Scheme 3.7. The reactor was purged with nitrogen gas to remove of air before use. A mixture of 0.5 g catalyst and 5.0 g of HDPE was loaded into the reactor. After purging with nitrogen flow rate of 20 ml/min to remove air, the temperature of the reactor was increased to 400°C (20°C/min) using a split-tube furnace equipped with a programmable temperature controller and a K-type thermocouple. The temperature was maintained constant at the reaction temperature for 40 min. The liquid fraction of products was withdrawn from the reactor automatically with the nitrogen stream and condensed to a 10-cm<sup>3</sup> graduated cylinder connected between the reactor and the bottom of the cooling condenser of 5°C. The gas fraction of products was passed through a cooling condenser and collected in a Tedlar gas sampling bag connected to the top of the condenser. The Tedlar bag was connected to the catalytic line since the start of heating. After completion of the reaction, the split tube furnace was opened and the reactor containing the used catalyst and residue was cooled down to room temperature and weighed. The values of %conversion and %yield were calculated based on the equations as follows:

$$\% \text{ Conversion} = \frac{\text{mass of liquid fraction} + \text{mass of gas fraction} \times 100}{\text{mass of plastic}}$$

mass of gas fraction = mass of the reactor with plastic and catalyst before reaction –  
 mass of the reactor with residue and used catalyst after reaction  
 – mass of liquid products

$$\% \text{ Yield of gas fraction} = \frac{\text{mass of gas fraction} \times 100}{\text{mass of plastic}}$$

$$\% \text{ Yield of liquid fraction} = \frac{\text{mass of liquid fraction} \times 100}{\text{mass of plastic}}$$

The degradation products were classified into three groups that are gas fraction, liquid fraction and residue. The gas products were analyzed by a gas chromatography. The liquid fraction was separated into two portions, light oil and heavy oil, by reduced pressure distillation as shown in Figure 3.3. The distilled oil was analyzed by GC. The values of retention time of components in the distillate oil in the GC column were compared to those of n-paraffins having the same boiling point range. The GC standard gasoline was purchased from Supelco. The GC peaks appeared between  $C_n$  and  $C_{n+1}$  have presumably the same boiling point range as  $C_{n+1}$  n-paraffin. The value of %coke formed was determined by the weight loss upon calcination of the used catalyst after leaching out of waxes by n-hexane.

### 3.14.2 Effect of crystallization time

Effect of crystallization time on HDPE catalytic cracking was investigated using the procedure as described in 3.13.1 but crystallization time was varied for 6, 12, 48 and 96 hours.

### 3.14.3 Effect of preparation of ZSM-5 and temperature

The degradation of HDPE waste was carried out using XGOH-12h and HTOH-10.5-0.1so-24h-60 catalysts at various reaction temperatures. The reaction was performed in similar way to what described in Section 3.13.1 and the experiments

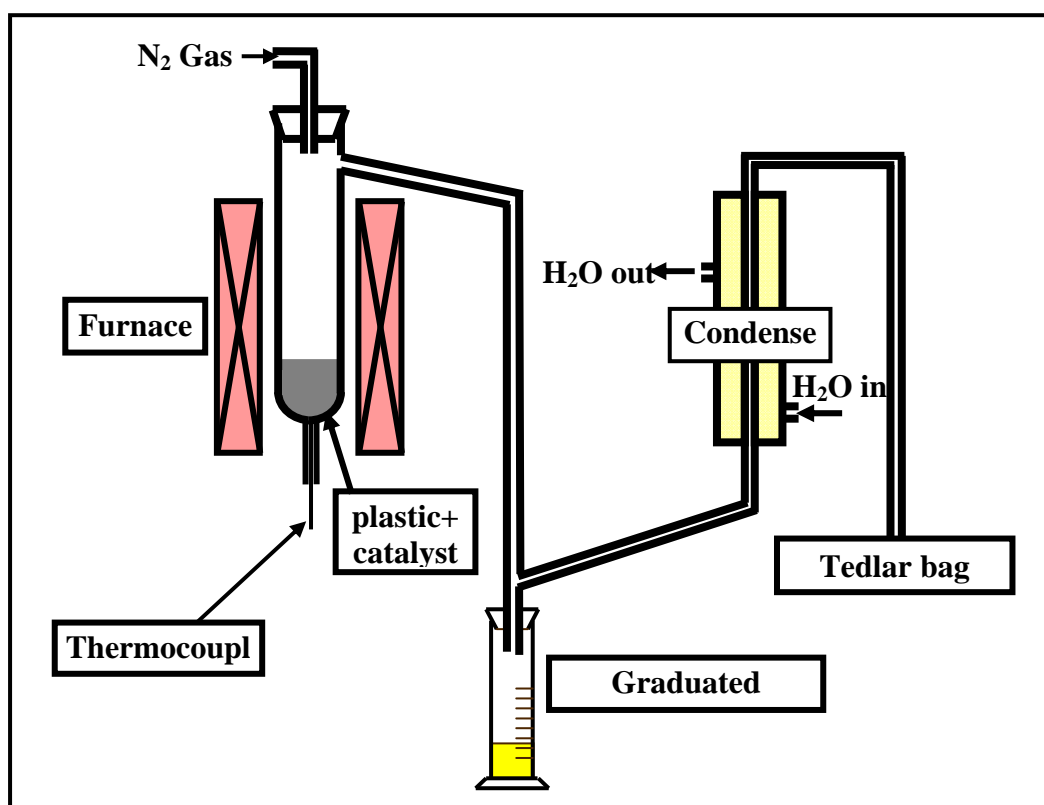
were carried out at two different reaction temperatures of 380°C and 400°C comparison.

#### 3.14.4 Effect of Si/Al mole ratios

The catalytic cracking reaction was carried out using HTOH-10.5-0.1so-24h samples with the Si/Al mole ratios in gel of 20, 40 and 60 as catalysts. The reaction was performed in similar way to Section 3.13.1. The experiments were carried out at two different reaction temperatures of 380°C and 400°C.

#### 3.15 Catalyst regeneration

The spent catalysts after a single loop use were subjected to regeneration. They were regenerated by calcination in air at 550°C for 5 h. The regenerated catalysts were characterized by XRD, SEM and test activity by catalytic cracking of HDPE at reaction temperature 400°C. The reaction was performed in similar way to what described in Section 3.13.1.



Scheme 3.7 Apparatus for catalytic cracking.

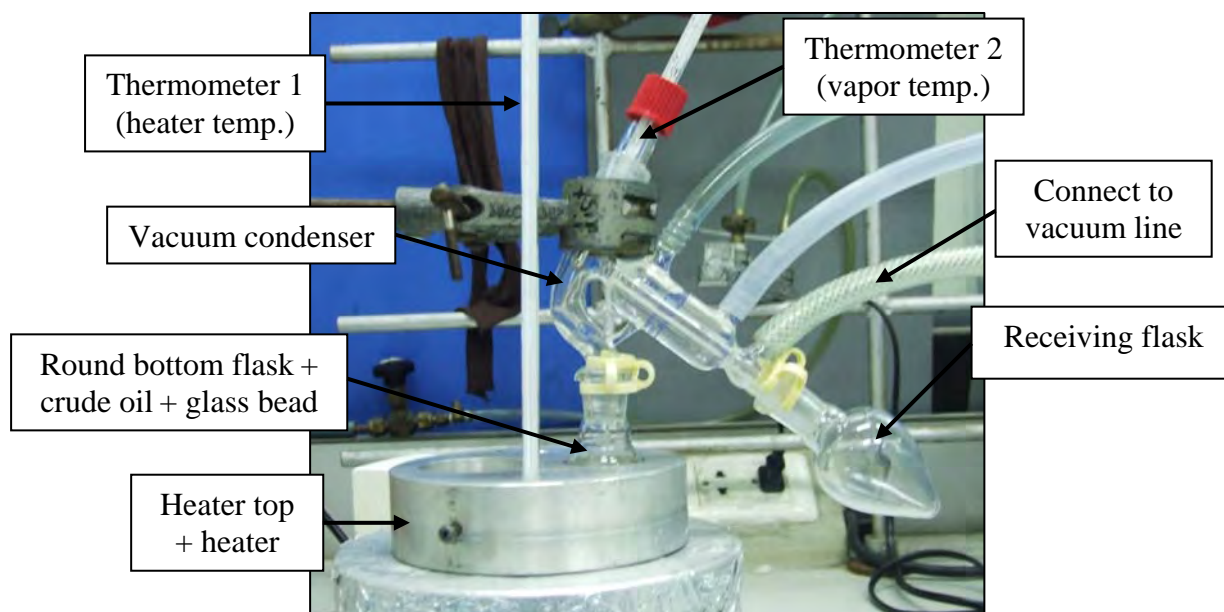
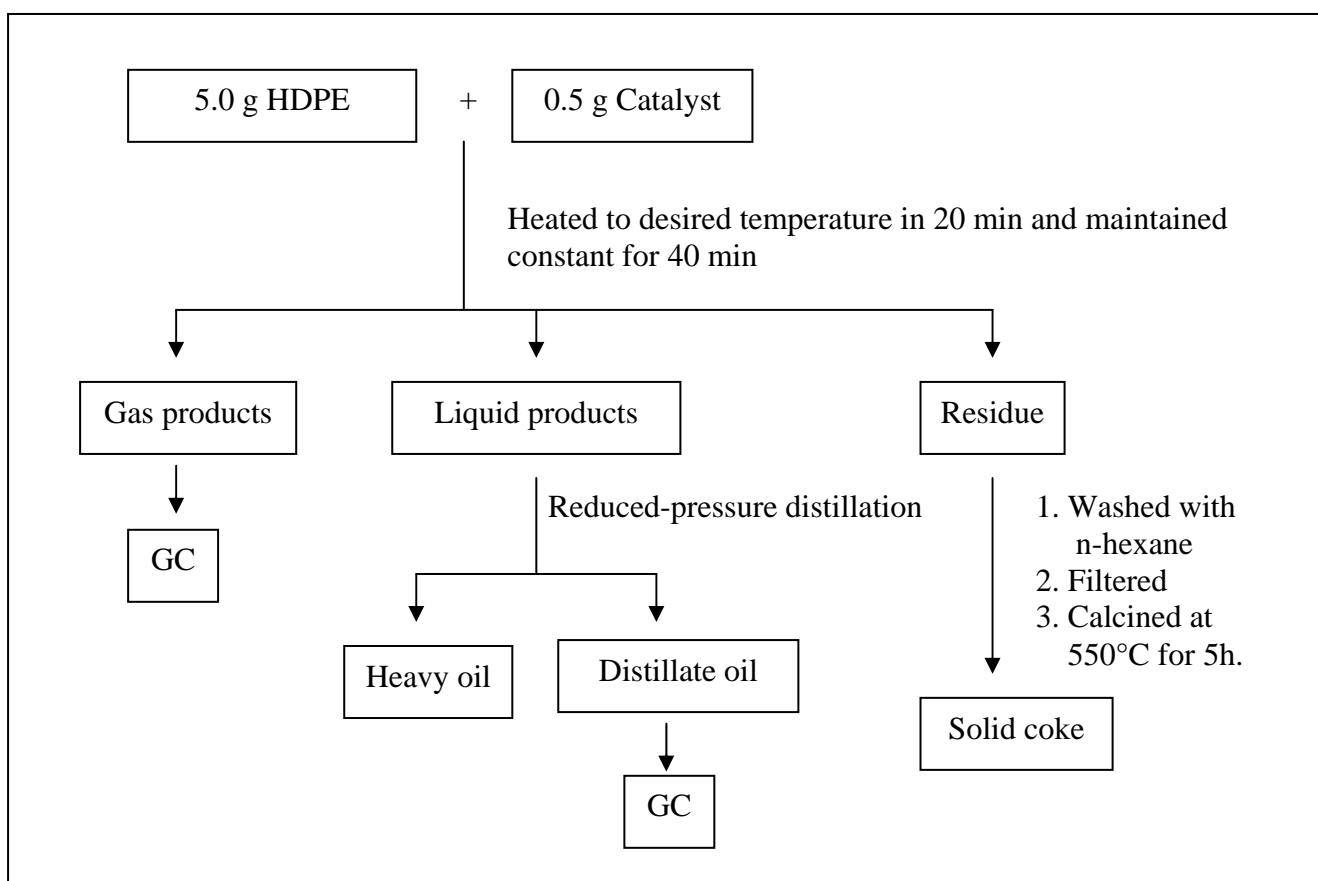


**Figure 3.2** Apparatus for reduce pressure distillation.



**Scheme 3.8** Catalytic cracking of HDPE using HZSM-5 as catalyst.

## CHAPTER IV

### RESULTS AND DISCUSSION

#### 4.1 Parameters affecting formation of ZSM-5 synthesized by hydrothermal method

##### 4.1.1 Effect of template type on formation of ZSM-5

###### 4.1.1.1 XRD results

Tetrapropylammonium bromide (TPABr) and tetrapropylammonium hydroxide (TPAOH) were used as templates in preparing ZSM-5 at the same ratio of Si/Al in gel of 20 and the same pH of 10.5. The hydrothermal synthesis was performed without sonication. The XRD patterns of both samples are shown in Figure 4.1. Both samples show the typical characteristic pattern of MFI structure [61] with 20% different crystallinity. Using tetrapropylammonium hydroxide as template, the crystallinity of ZSM-5 is 80% of that using tetrapropylammonium bromide. It indicates that TPAOH gives the structure of ZSM-5 with higher crystallinity than TPABr does.

###### 4.1.1.2 SEM images

SEM images show no effect of template type on morphology of the zeolite samples but the significant decrease in particle (crystal aggregate) size from 4.0  $\mu\text{m}$  to 2.0  $\mu\text{m}$  upon changing the template from TPABr to TPAOH (Figure 4.2(a) and (b)). This effect is due to the small molecular size of TPAOH than TPABr.

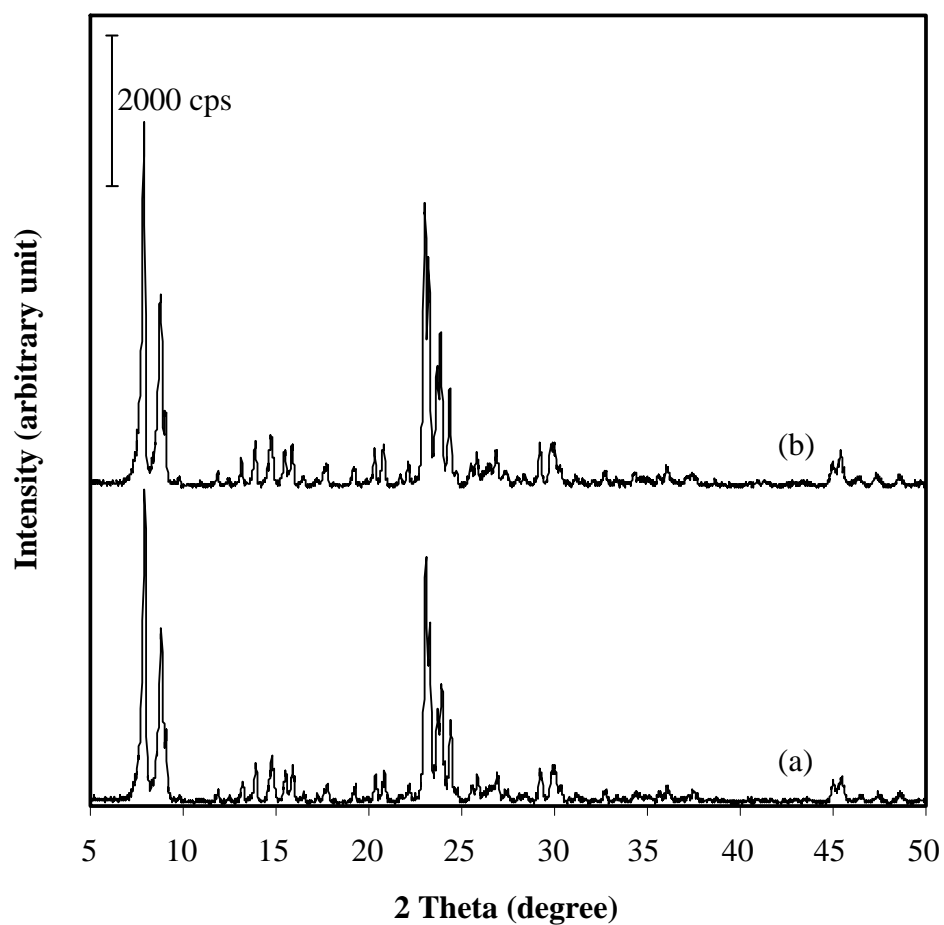


**Figure 4.1** XRD patterns of the calcined ZSM-5 prepared from different templates : (a) TPABr and (b) TPAOH.

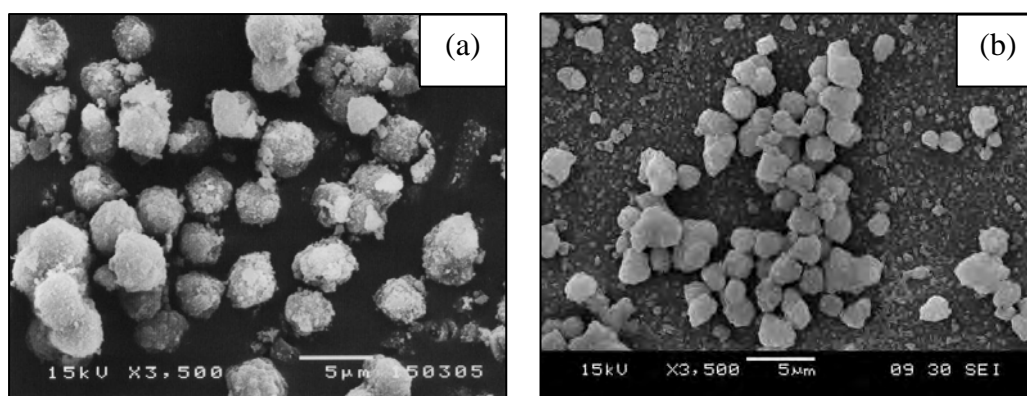


**Figure 4.2** SEM images of the calcined ZSM-5 prepared from different templates: (a) TPABr and (b) TPAOH.

### 4.1.1.3 Nitrogen adsorption

The  $N_2$  adsorption-desorption isotherms for the calcined Samples HTBr and HTOH are shown in Figure 4.3. The samples exhibit a type I isotherm, characteristic of microporous materials [62]. Both of isotherm exhibit three different adsorption zones [62]. The first zone observed at very low partial pressures, corresponds to the nitrogen-adsorption in the ZSM-5 micropore system. The second zone at medium partial pressures is the saturation indicating the completion of pore filling with  $N_2$  molecules. The third zone at high relative pressures ( $P/P_0 > 0.8$ ), is the adsorption on the external surface [62]. The textural properties of both samples are listed in Table 4.1. Sample HTOH has particle size than Sample HTBr, thus the BET surface area and external surface area of the former are slightly higher. This agrees with Serrano *et al.* [62], the smaller crystal size shows the higher external surface area. Both samples show the same pore size of 0.6 nm which is the average size for the structure of ZSM-5.

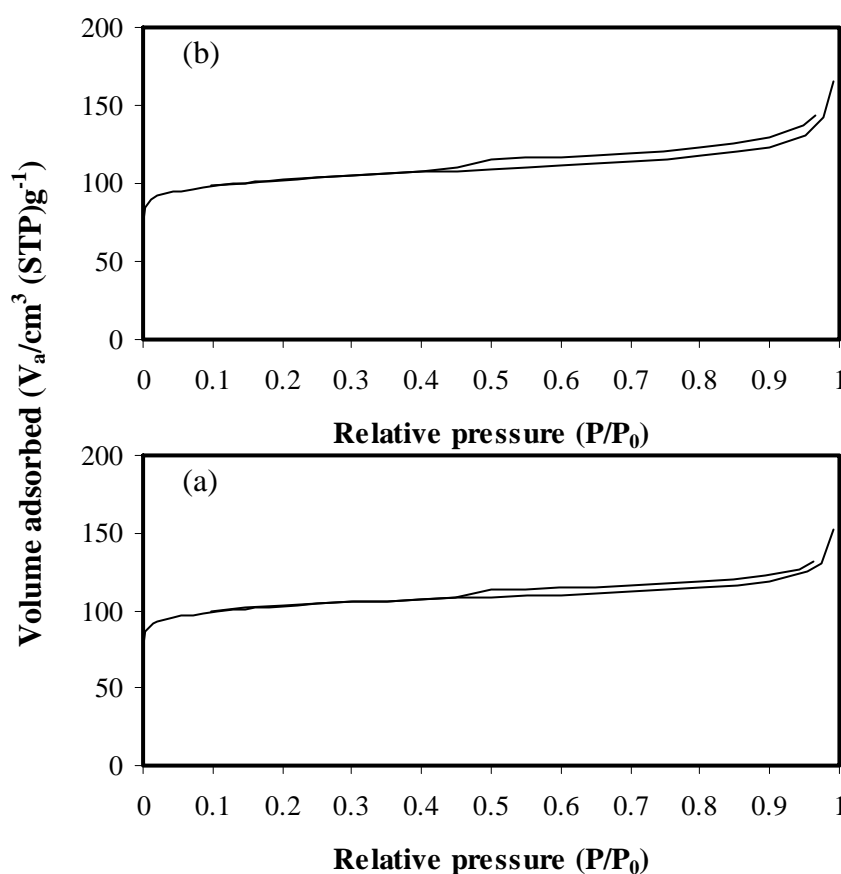


**Figure 4.3**  $N_2$  adsorption-desorption isotherms of (a) Sample HTBr and (b) Sample HTOH.

**Table 4.1** Textural properties of Sample HTBr compared with Sample HTOH

Sample	Particle size <sup>a</sup> ( $\mu\text{m}$ )	$S_{\text{BET}}$ <sup>b</sup> ( $\text{m}^2/\text{g}$ )	$S_{\text{ext}}$ <sup>c</sup> ( $\text{m}^2/\text{g}$ )	$d_p$ <sup>d</sup> (nm)
HTBr	4.0	380	30	0.6
HTOH	2.0	401	54	0.6

<sup>a</sup> Particle size determined by SEM images

<sup>b</sup> Specific surface area determined by BET-plot method

<sup>c</sup> External surface area determined by t-plot method

<sup>d</sup> Pore size distribution determined by MP-plot method

#### 4.1.2 Effect of pH of gel on formation of ZSM-5

##### 4.1.2.1 XRD results

XRD patterns of calcined Samples HTOH (the Si/Al ratio in gel of 20) prepared at various pH of 9.0, 9.5, 10.0, 10.5 and 11.0 are shown in Figure 4.3. All XRD patterns in Figure 4.4 show characteristic peaks of the MFI structure without any other phase. With increasing the pH of gel in the range from 9.0 to 11.0, the crystallinity of ZSM-5 decreases. This indicates that the crystallinity of ZSM-5 is strongly affected by the pH of gel and the formation of ZSM-5 crystals prefers low pH about 9.0-9.5. However, the aim of this work is the preparation of nanoparticle ZSM-5. Thus the particle size must be considered along with the XRD results.

##### 4.1.2.2 SEM images

SEM images of calcined Samples HTOH (the Si/Al ratio in gel of 20) prepared at different pH of 9.0, 9.5, 10.0, 10.5 and 11.0 are shown in Figure 4.5. The zeolite particle size and morphology are strongly affected by pH. The particles with cauliflower shape were formed at the pH range of 9.0-10.5. The reason is that more nucleation centers were formed at higher alkalinities [63]. The particles of sample prepared at the pH of 11.0 have hexagonal-like shape which is totally different from the shape of the samples at low pH. With increasing the pH from 9.00 to 11.0, the particle size of ZSM-5 decreases. At high magnification, it can be observed that each particle, no matter at any pH, is the aggregate of tiny crystals of



which the sizes are 750 nm at low pH (9.0-10.0) and 145 nm at high pH (10.5-11.0). The particle sizes and morphology of Samples HTOH are summarized in Table 4.2.

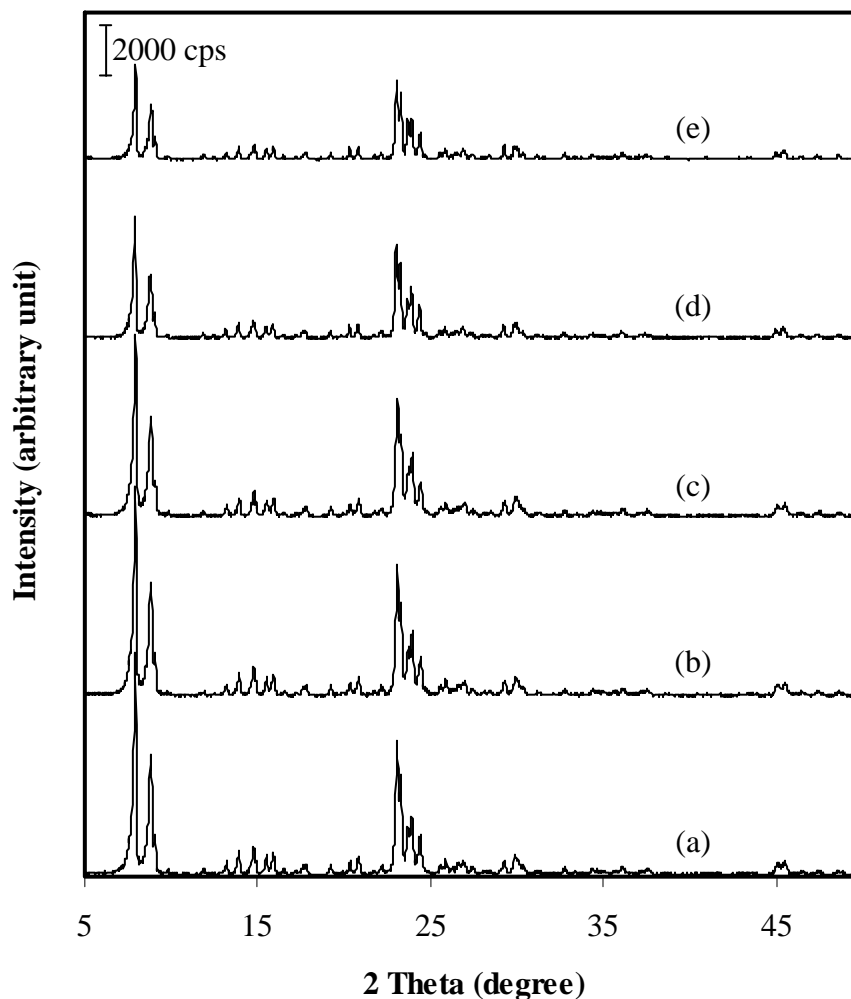


**Figure 4.4** XRD patterns of calcined Samples HTOH (the Si/Al ratio in gel of 20) prepared at various pH gel values: (a) 9.0, (b) 9.5, (c) 10.0, (d) 10.5 and (e) 11.0.

#### 4.1.2.3 Nitrogen adsorption

Figure 4.6 illustrates the nitrogen adsorption-desorption isotherms of calcined Samples HTOH prepared of various pH. All samples exhibits a type I isotherm which is typical for microporous materials. The increase in pH values from 9.0 to 10.5 does not make the specific surface area different but at the pH value of 11.0, the sample shows the lowest BET and external surface areas due to the smooth surface of the particles as shown in Figure 4.5 (h). Sample HTOH-10.5 shows

the highest external surface area as shown in Table 4.3 owing to the smallest particle size. From Table 4.3, all samples show distribution of micropore with the same pore size about 0.6 nm.

**Table 4.2** Particle size and morphology of calcined Samples HTOH with the Si/Al in gel of 20 prepared at various pH values

pH of gel	Particle size <sup>a</sup> ( $\mu\text{m}$ )	Morphology
9.0	16.0	cauliflower-like shape
9.5	9.9	cauliflower-like shape
10.0	3.5	cauliflower-like shape
10.5	2.0	cauliflower-like shape
11.0	1.6 x 1.4	hexagonal shape

<sup>a</sup> Particle size determined by SEM images

**Table 4.3** BET specific surface area and external surface area of calcined Samples HTOH prepared at various pH values

Sample	$S_{\text{BET}}^{\text{a}}$ ( $\text{m}^2/\text{g}$ )	$S_{\text{ext}}^{\text{b}}$ ( $\text{m}^2/\text{g}$ )	$d_p^{\text{c}}$ (nm)
HTOH-9.0	398	30	0.6
HTOH-9.5	399	34	0.6
HTOH-10.0	394	39	0.6
HTOH-10.5	401	54	0.6
HTOH-11.0	377	13	0.6

<sup>a</sup> Specific surface area determined by BET-plot method

<sup>b</sup> External surface area determined by t-plot method

<sup>c</sup> Pore size distribution determined by MP-plot method

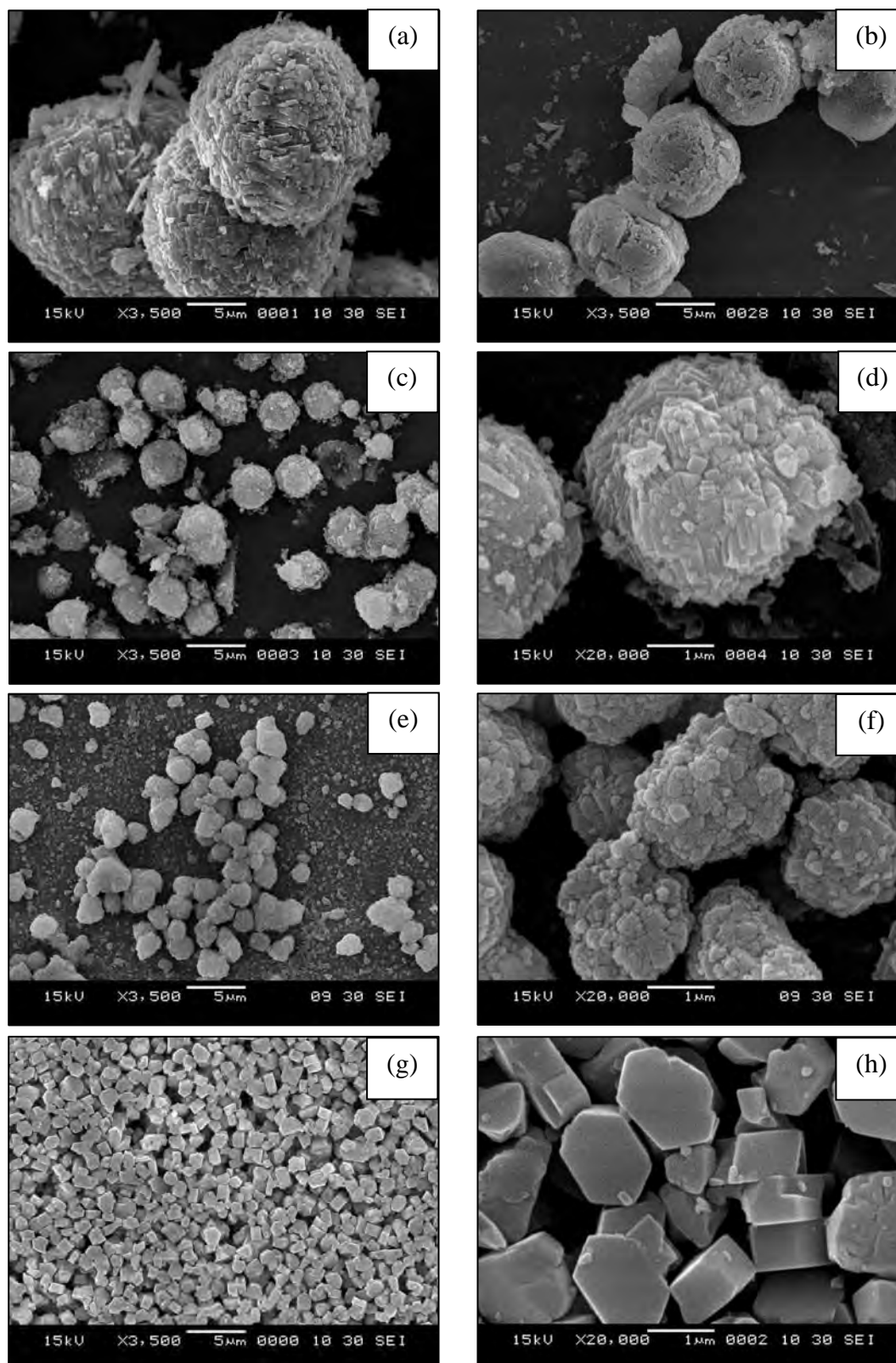


**Figure 4.5** SEM images of calcined Samples HTOH with different pH: (a) pH = 9.0 (3500x), (b) pH = 9.5 (3500x), (c) pH = 10.0 (3500x), (d) pH = 10.0 (20000x), (e) pH = 10.5 (3500x), (f) pH = 10.5 (20000x), (g) pH = 11.0 (3500x) and (h) pH = 11.0 (20000x).

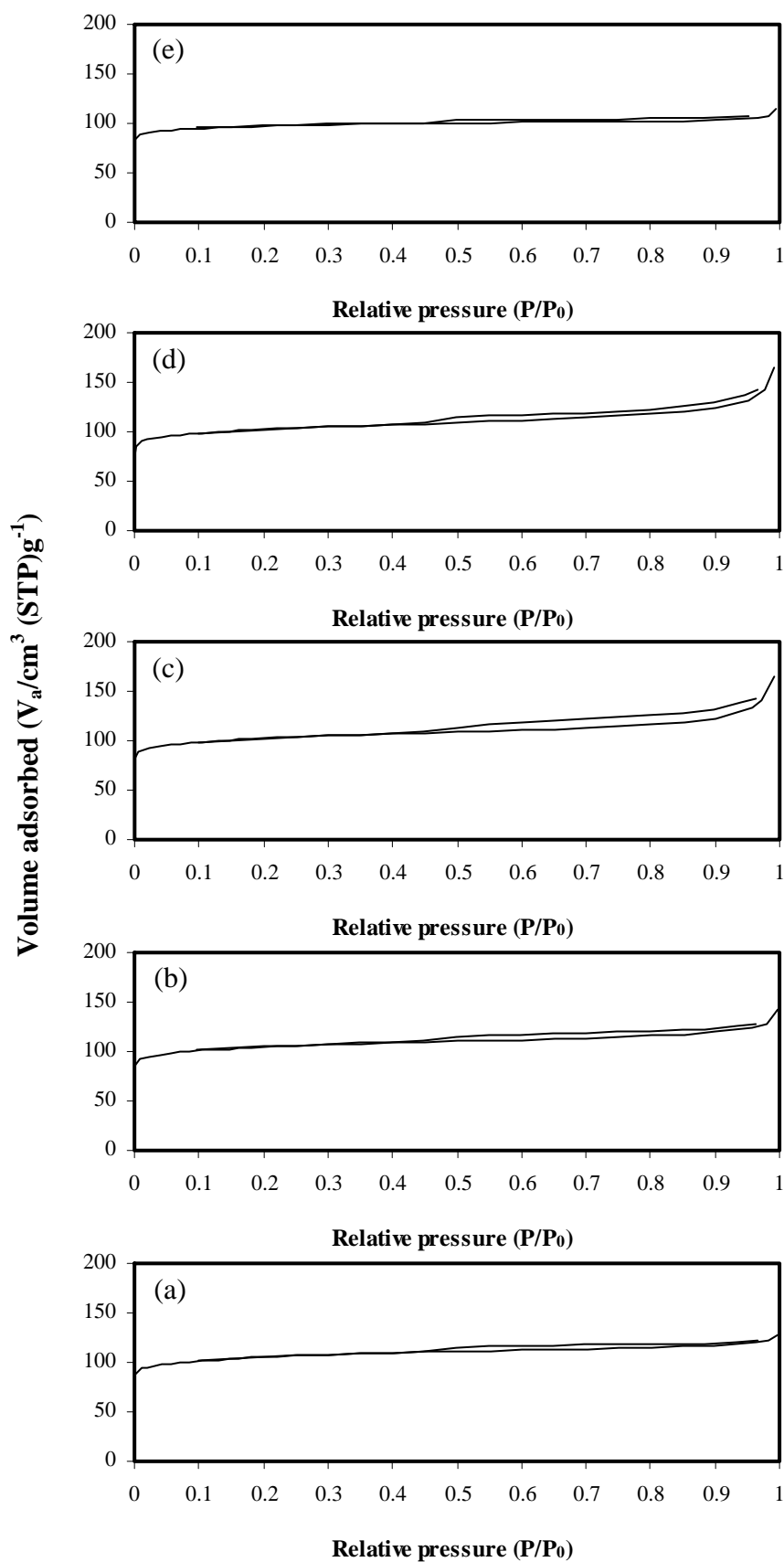


**Figure 4.6**  $N_2$  adsorption-desorption isotherms of calcined HTOH samples prepared at different pH values of (a) 9.0, (b) 9.5, (c) 10.0, (d) 10.5 and (e) 11.0.

### 4.1.3 Effect of template/SiO<sub>2</sub> ratios on formation of ZSM-5

#### 4.1.3.1 XRD results

The effect of TPAOH/SiO<sub>2</sub> ratios was investigated for Samples HTOH-10.5 with the Si/Al ratio in gel of 20 using crystallization time of 4 days. XRD patterns of samples are shown in Figure 4.7. All samples show the characteristic peaks of ZSM-5. There is no difference in crystallinity when using TPAOH/SiO<sub>2</sub> ratio of 0.1 or 0.2. With increasing the TPAOH/SiO<sub>2</sub> ratio up to 0.5, the crystallinity of the zeolite decreases obviously due to ions cannot coverage template through out.

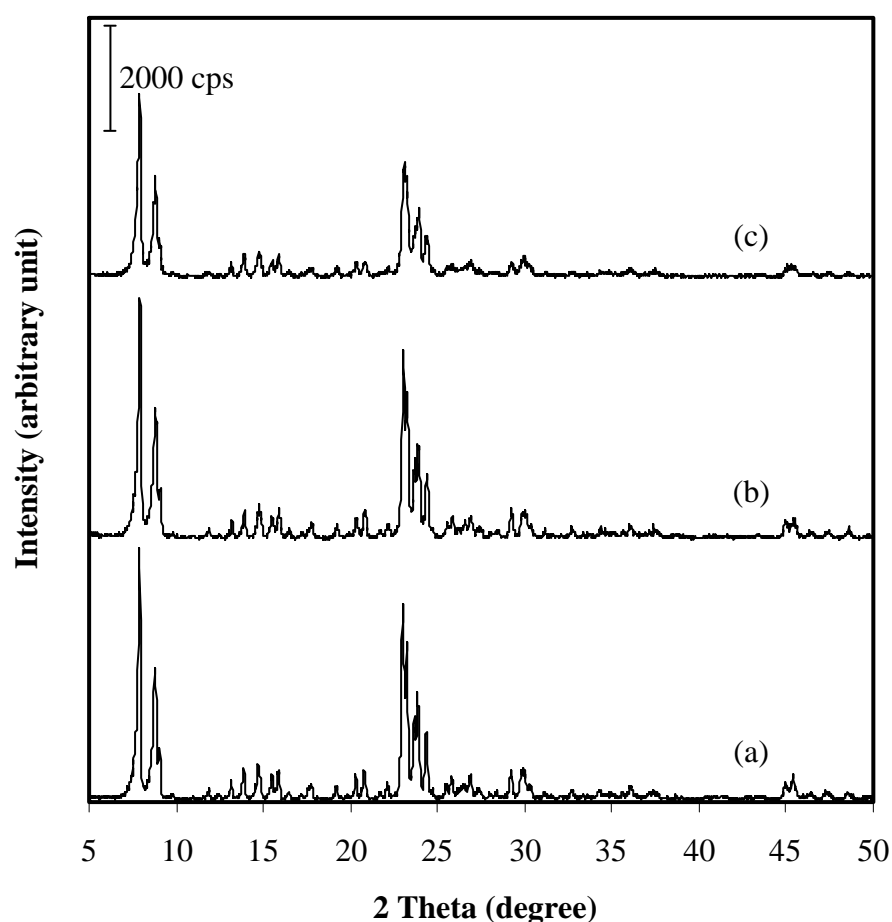


**Figure 4.7** XRD patterns of calcined Samples HTOH-10.5 prepared from various TPAOH/SiO<sub>2</sub> mole ratios: (a) 0.1, (b) 0.2 and (c) 0.5.

#### 4.1.3.2 SEM images

SEM images of calcined Samples HTOH-10.5 with various template/SiO<sub>2</sub> ratios are shown in Figure 4.8. Cauliflower-like shape was observed for all samples. It can be concluded that the particle size and morphology of these samples are not significantly affected by the ratios of template/SiO<sub>2</sub> range from 0.1-0.5.

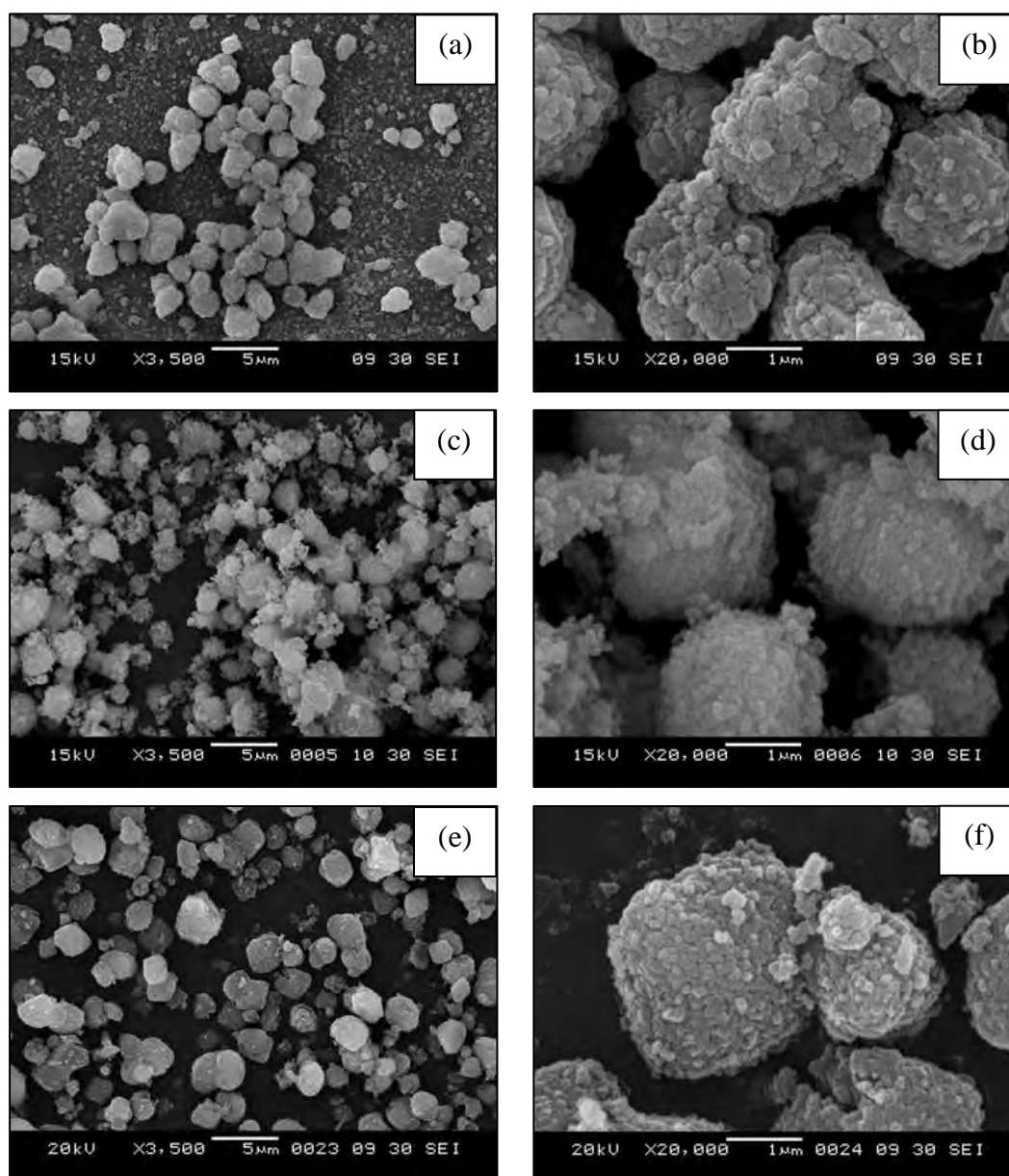


**Figure 4.8** SEM images of calcined Samples HTOH-10.5 (the Si/Al ratio in gel of 20) with various ratios of TPAOH/SiO<sub>2</sub>: (a) 0.1 (3500x), (b) 0.1 (20000x), (c) 0.2 (3500x), (d) 0.2 (20000x), (e) 0.5 (3500x) and (f) 0.5 (20000x).

#### 4.1.3.3 Nitrogen adsorption

Figure 4.9 shows the nitrogen adsorption-desorption isotherms of calcined Samples HTOH-10.5 which were prepared by using different template/SiO<sub>2</sub> mole ratio from 0.1 to 0.5. The samples exhibit a type I isotherm, characteristic of microporous materials. Table 4.4 shows the BET specific surface area, external surface area and pore volume of HTOH-10.5 samples prepared by using different template/SiO<sub>2</sub> mole ratios. These parameters were not significantly affected by the template/SiO<sub>2</sub> ratios.

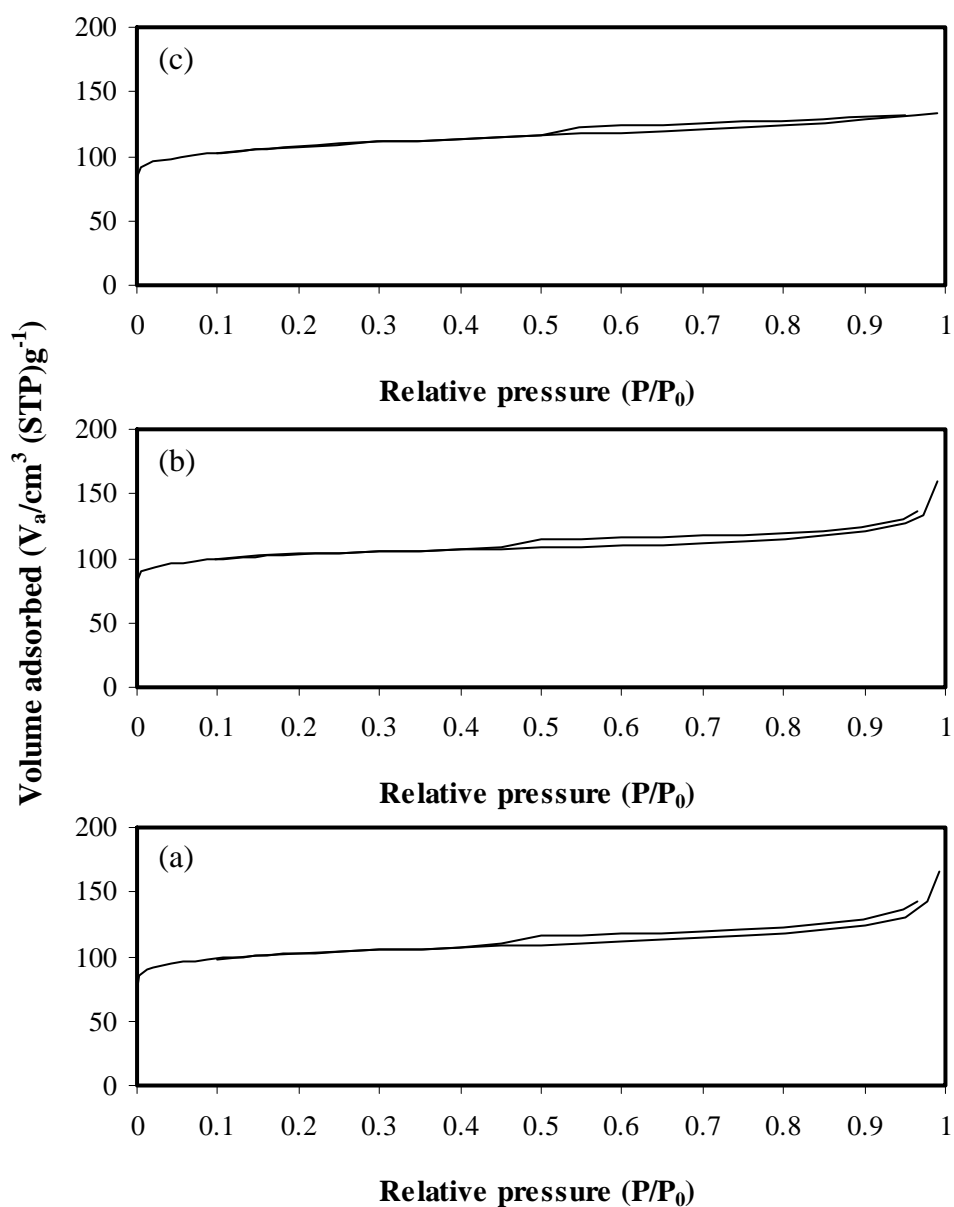


**Figure 4.9** N<sub>2</sub> adsorption-desorption isotherms of Samples HTOH-10.5 with different TPAOH/SiO<sub>2</sub> mole ratios: (a) 0.1, (b) 0.2 and (c) 0.5.

**Table 4.4** BET specific surface area, external surface area and pore size of Samples HTOH-10.5 with various template/SiO<sub>2</sub> mole ratios

Sample	S <sub>BET</sub> <sup>a</sup> (m <sup>2</sup> /g)	S <sub>ext</sub> <sup>b</sup> (m <sup>2</sup> /g)	d <sub>p</sub> <sup>c</sup> (nm)
HTOH-10.5-0.1	401	54	0.6
HTOH-10.5-0.2	397	43	0.6
HTOH-10.5-0.5	407	45	0.6

<sup>a</sup> Specific surface area determined by application of BET-plot method

<sup>b</sup> External surface area determined by application of t-plot method

<sup>c</sup> Pore size distribution determined by application of MP-plot method

#### 4.1.3.4 NH<sub>3</sub>-TPD profiles

From NH<sub>3</sub>-TPD experiment, the total desorbed amount of ammonia is related to the number of acid sites whereas the temperature of maximum desorption provides the acid strength of the samples. Figure 4.10 shows NH<sub>3</sub>-TPD profiles of Samples HTOH-10.5 with various ratios of template/SiO<sub>2</sub>. There are two peaks, one is located at low temperature (about 180°C, peak I) corresponding to desorption of the adsorbed NH<sub>3</sub> on weaker acid sites and the other is at high temperature (about 460°C, peak II) corresponding to the desorption of the adsorbed NH<sub>3</sub> on stronger acid sites [64]. A number of acid sites from NH<sub>3</sub>-TPD analysis of the samples are shown in Table 4.5. The results indicate that the number of acid sites in Sample HTOH-10.5-0.1 is higher than in Sample HTOH-10.5-0.5 and Sample HTOH-10.5-0.2, respectively.



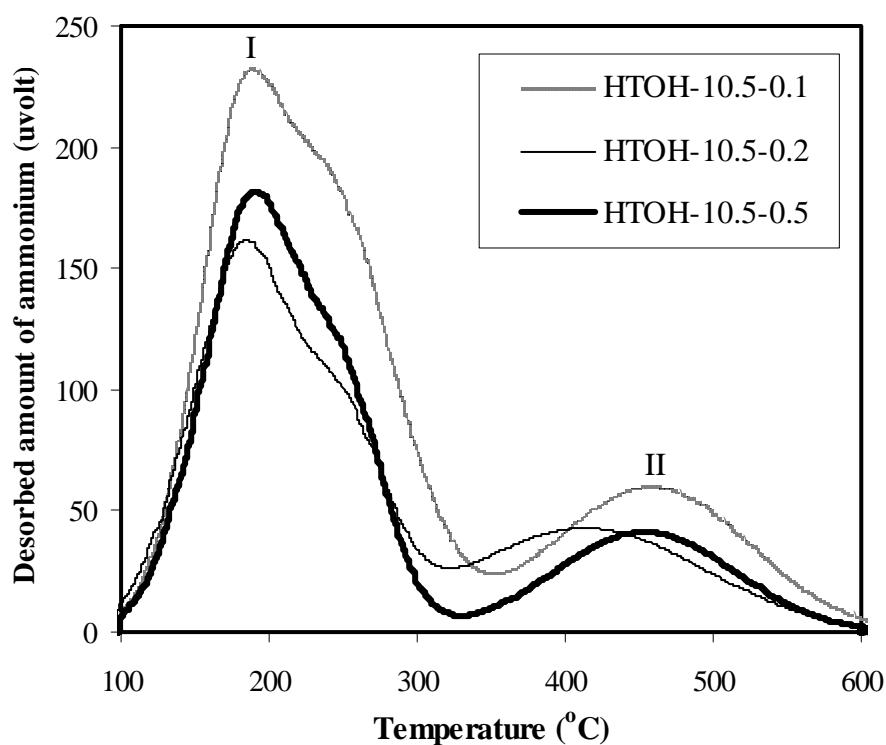


**Figure 4.10**  $\text{NH}_3$ -TPD profiles of Samples HTOH-10.5 with various template/ $\text{SiO}_2$  ratios in gel.

**Table 4.5** Number of acid sites from  $\text{NH}_3$ -TPD analysis of the calcined Samples HTOH-10.5 with various template/ $\text{SiO}_2$  ratios

Sample	No. of acid sites <sup>a</sup> (mmol/g)		
	Peak I <sup>b</sup>	Peak II <sup>c</sup>	Total <sup>d</sup>
HTOH-10.5-0.1	3.1595	0.2346	3.3941
HTOH-10.5-0.2	2.2639	0.2934	2.5573
HTOH-10.5-0.5	2.6887	0.1474	2.8361

<sup>a</sup> Desorbed amount of ammonia

<sup>b</sup> Number of acid sites at low temperature peak

<sup>c</sup> Number of acid sites at high temperature peak

<sup>d</sup> Total number of acid sites

#### 4.1.4 Effect of sonication on formation of ZSM-5

##### 4.1.4.1 XRD results

Figure 4.11 indicates XRD patterns of HTOH-10.5-0.1ns and HTOH-10.5-0.1so catalysts prepared by without sonication and using sonication, respectively, were similar. It can be concluded that applying sonication for 30 min during the gel formation step does not affect the structure and the crystallinity of zeolite ZSM-5. The results are similar to that report by Kumar *et al* [65].

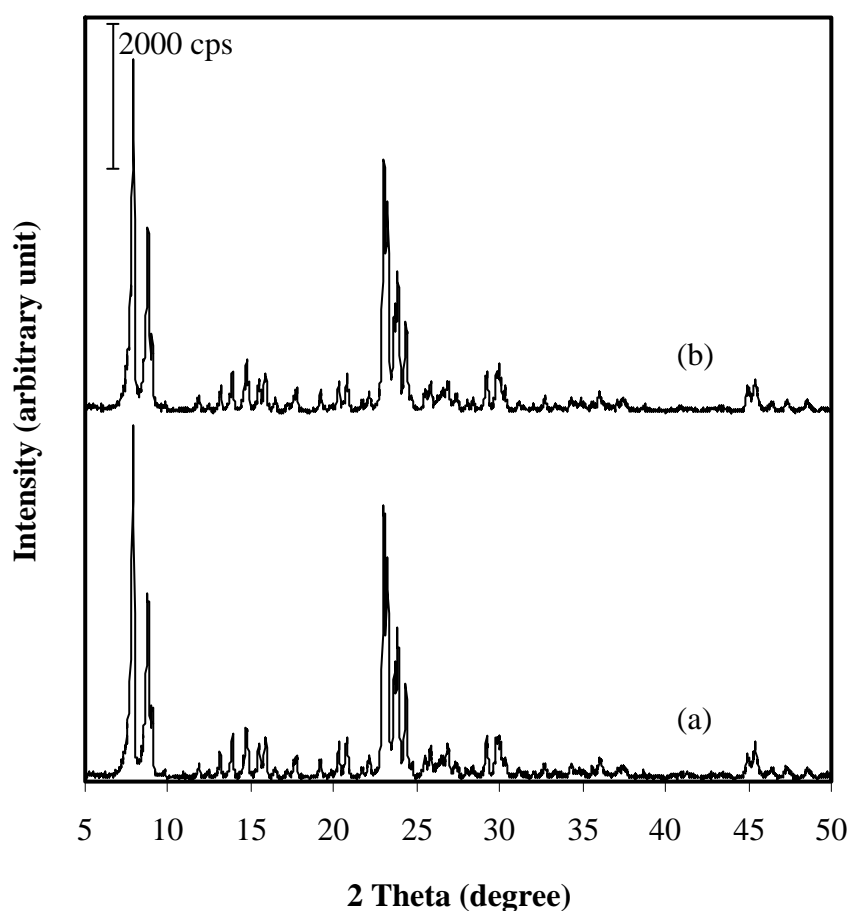


**Figure 4.11** XRD patterns of calcined Samples HTOH-10.5-0.1 prepared (a) without sonication and (b) with sonication.

#### 4.1.4.2 SEM images

Figure 4.12 shows SEM images of Sample HTOH-10.5-0.1ns and Sample HTOH-10.5-0.1so. The samples show similar surface appearance and particle shape. The morphology is not affected by sonication but particle size is affected by sonication. The Sample HTOH-10.5-0.1so shows relatively larger particle size, averagely about 2.7  $\mu\text{m}$  while Sample HTOH-10.5-0.1ns has the size about 2  $\mu\text{m}$ . The synthesis ZSM-5 with sonication has been demonstrated to offer the possibilities of increasing the nucleation and crystallization rate and improving the yield (Table 4.6) [66].

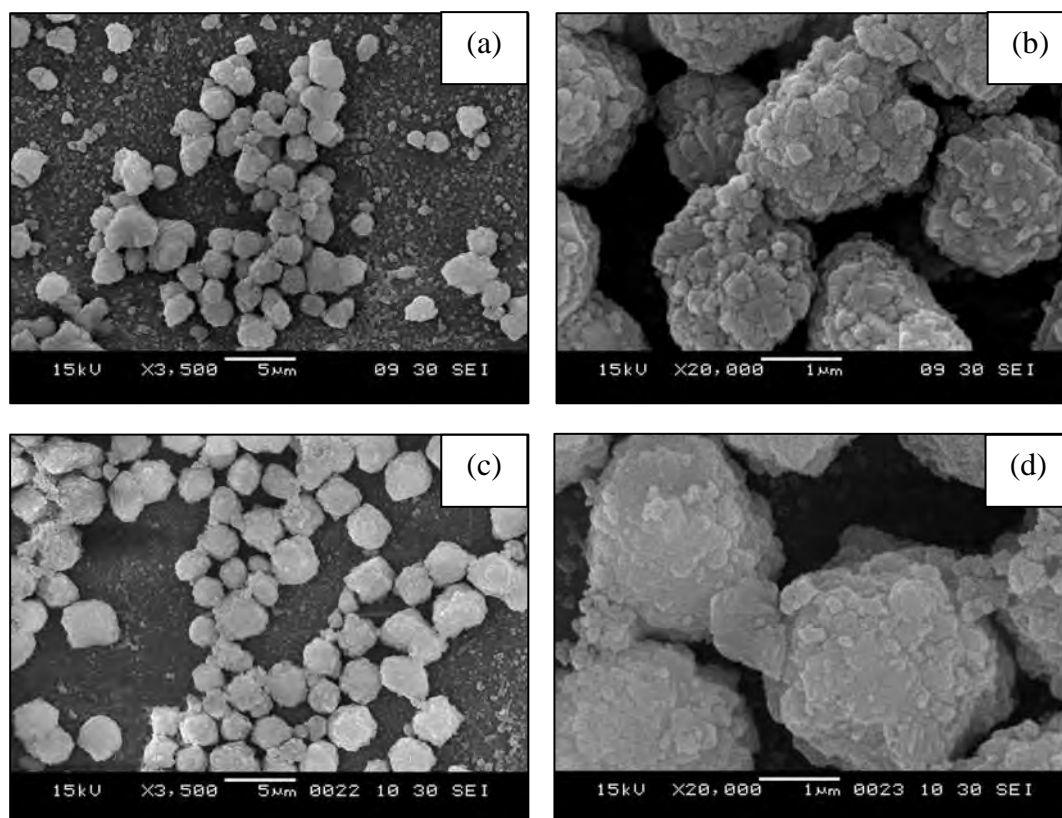


**Figure 4.12** SEM images of the calcined Samples HTOH-10.5-0.1 prepared (a) without sonication (3500x), (b) without sonication (20000x), (c) with sonication (3500x) and (d) with sonication (20000x).

#### 4.1.4.3 Nitrogen adsorption

The nitrogen adsorption-desorption isotherm of sample HTOH-10.5-0.1ns and HTOH-10.5-0.1so in Figure 4.13 exhibit a type I isotherm which is the typical of microporous solid. The textural properties of sample HTOH-10.5-0.1ns and sample HTOH-10.5-0.1so are shown in Table 4.8. Sample HTOH-10.5-0.1ns and sample HTOH-10.5-0.1so show similar specific surface area and external surface area. Sample HTOH-10.5-0.1so shows higher yield than HTOH-10.5-0.1ns. It can also be illustrated that application of sonication accelerated nucleation, crystallization rate and improving the yield [66]. Therefore, the synthesis ZSM-5 with sonication was chosen to study effect of crystallization time on formation of zeolite ZSM-5.

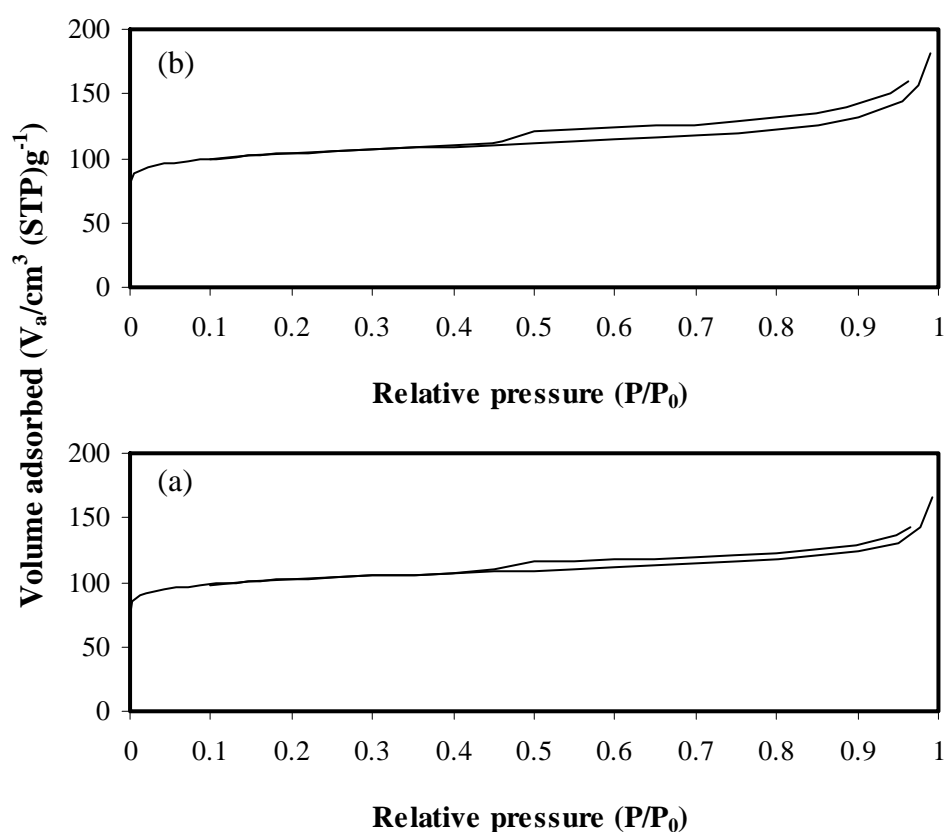


**Figure 4.13** N<sub>2</sub> adsorption-desorption isotherms of the the calcined HTOH-10.5-0.1 prepared (a) without sonication and (b) with sonication.

**Table 4.6** Textural properties of Sample HTOH-10.5-0.1ns and Sample HTOH-10.5-0.1so

Sample	Particle size <sup>a</sup> ( $\mu\text{m}$ )	Yield <sup>b</sup> (%)	$S_{\text{BET}}$ <sup>c</sup> ( $\text{m}^2/\text{g}$ )	$S_{\text{ext}}$ <sup>d</sup> ( $\text{m}^2/\text{g}$ )	$d_p$ <sup>e</sup> (nm)
HTOH-10.5-0.1ns	2.0	70	401	54	0.6
HTOH-10.5-0.1so	3.0	85	397	46	0.6

<sup>a</sup> Particle size determined by SEM images

<sup>b</sup> % Yield based on  $\text{SiO}_2$

<sup>c</sup> Specific surface area determined by application of BET-plot method

<sup>d</sup> External surface area determined by application of t-plot method

<sup>e</sup> Pore size distribution determined by application of MP-plot method

#### 4.1.5 Effect of crystallization time on formation of ZSM-5

##### 4.1.5.1 XRD results

Figure 4.14 shows the XRD patterns of Samples HTOH-10.5-0.1so prepared by varying crystallization time from 24-96 hours at the temperature of  $170^\circ\text{C}$ . All patterns of samples confirmed that ZSM-5 zeolite phase was formed. All samples show similar crystallinity, therefore the crystallization time has no significant effect on crystallinity of the produced zeolite.

##### 4.1.5.2 SEM images

The SEM images of the four samples are shown in Figure 4.15. The particle shape, particle size and surface appearance of all samples are very similar. The particles of all samples have a cauliflower-like morphology. The samples have particle size about  $3 \mu\text{m}$ .

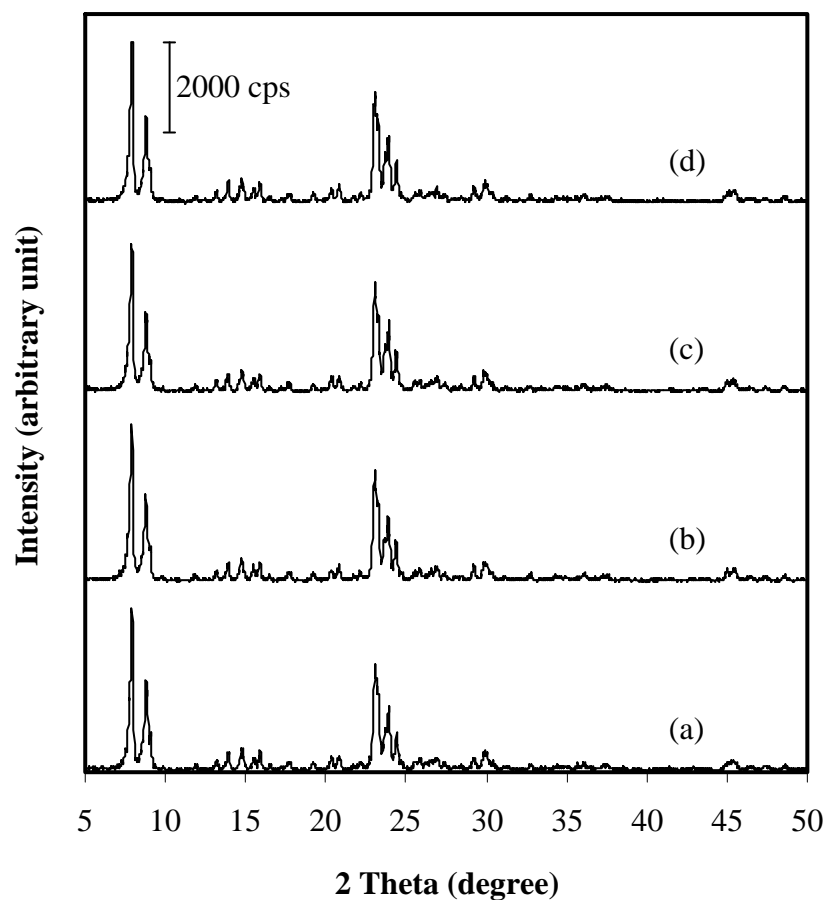


**Figure 4.14** XRD patterns of calcined Samples HTOH-10.5-0.1so crystallized for various periods: (a) 24 h, (b) 48 h, (c) 72 h and (d) 96 h.

#### 4.1.5.3 Nitrogen adsorption

The N<sub>2</sub> adsorption-desorption isotherms for the calcined sample OH-0.1-so with various crystallization time are shown in Figure 4.16. The samples exhibit a type I isotherm, the characteristic pattern of microporous materials. The specific surface area and external surface area are listed in Table 4.7. All samples show similar values of specific surface area. Sample HTOH-10.5-0.1so-24h is selected for further studies in other section due to its shortest crystallization time.

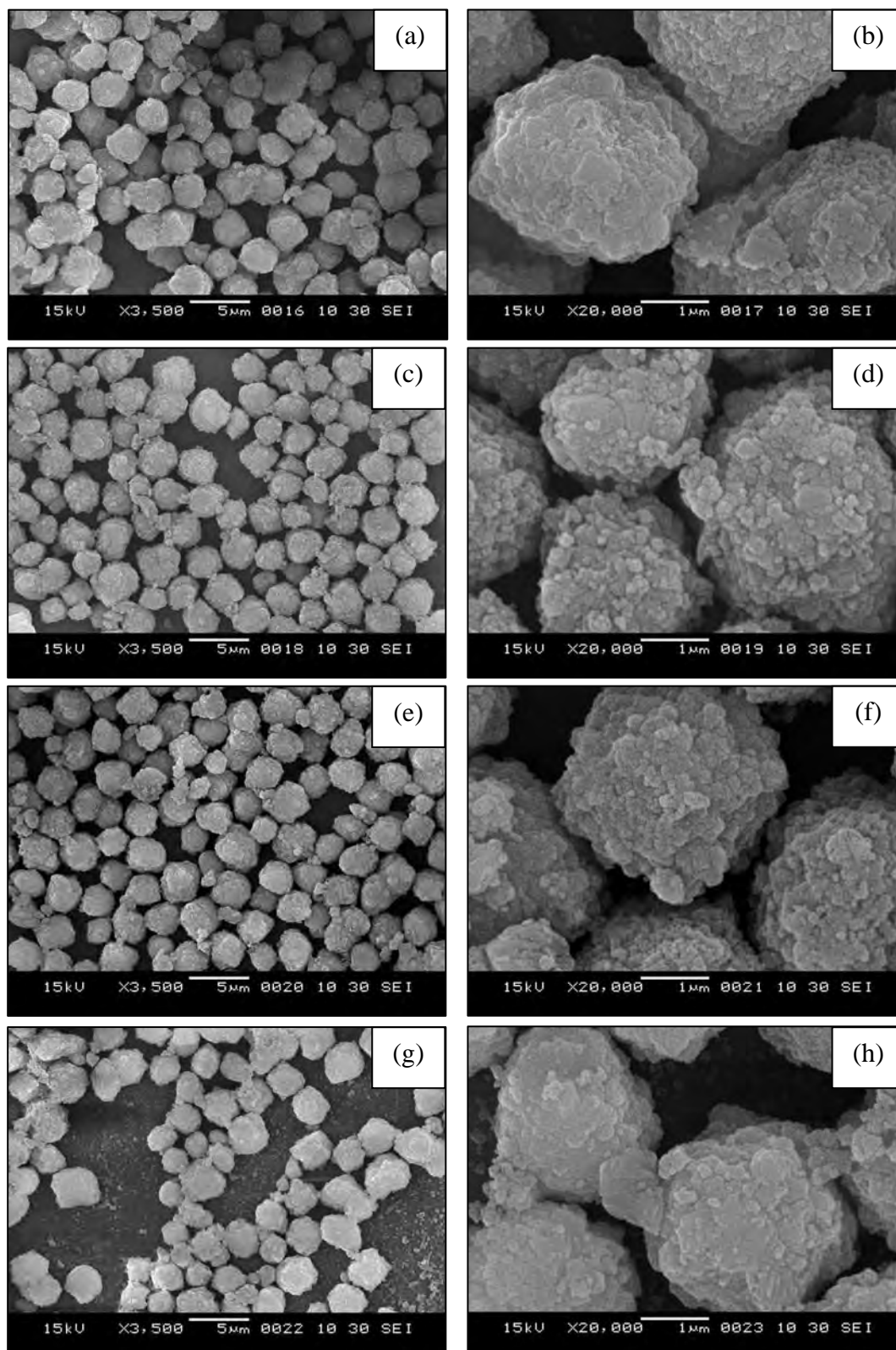


**Figure 4.15** SEM images of calcined Samples HTOH-10.5-0.1so with different crystallization periods: (a), (b) 24 h, (c), (d) 48 h, (e), (f) 72 h and (g), (h) 96 h. The right images are correspondent to the left one at high magnification.

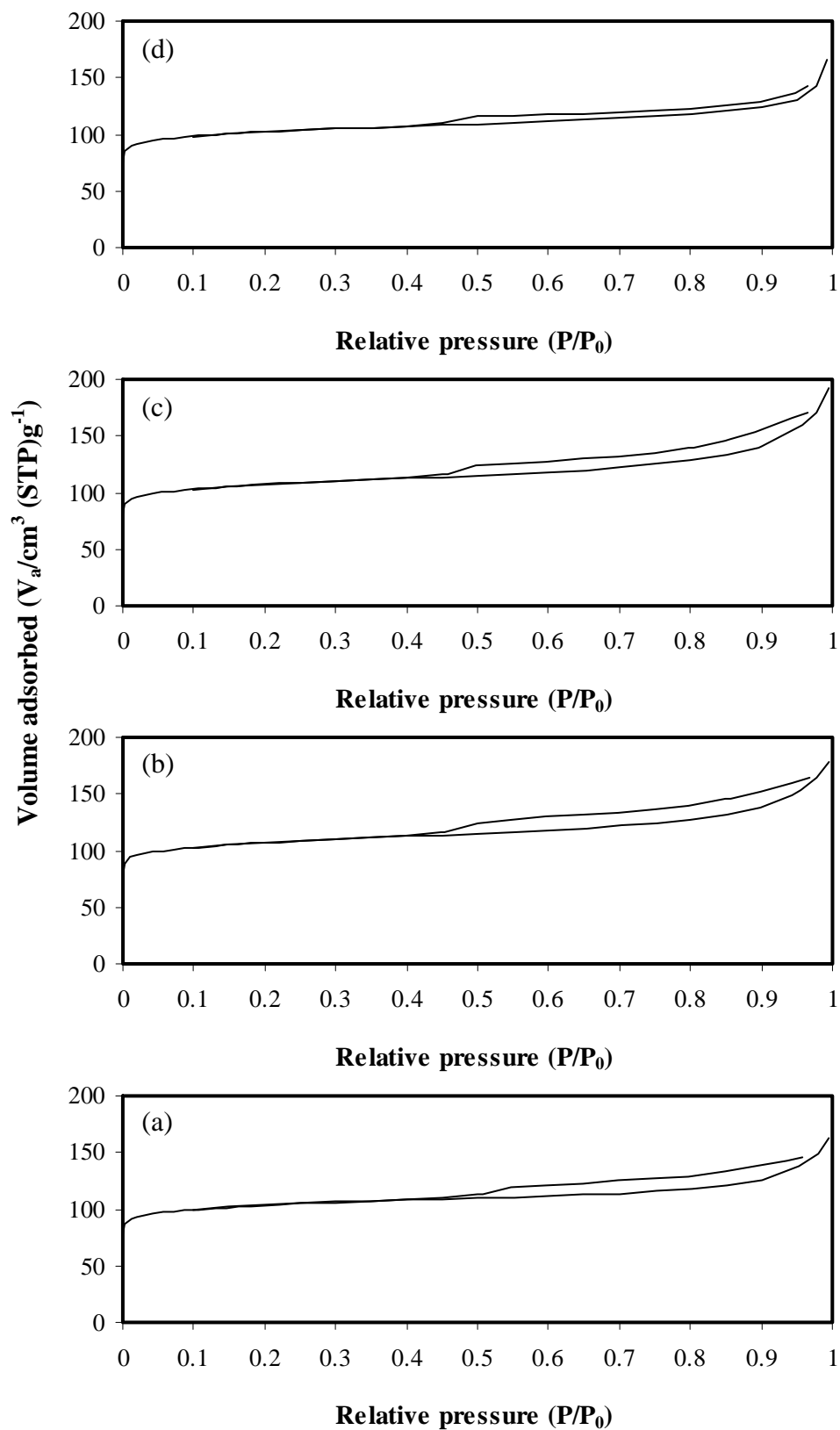


**Figure 4.16**  $\text{N}_2$  adsorption-desorption isotherms of Samples HTOH-10.5-0.1so with different crystallization time: (a) 24 h, (b) 48 h, (c) 72 h and (d) 96 h.



**Table 4.7** BET specific surface area, external surface area and pore size distribution of calcined Samples HTOH-10.5-0.1so with various crystallization time

Sample	$S_{\text{BET}}^{\text{a}}$ (m <sup>2</sup> /g)	$S_{\text{ext}}^{\text{b}}$ (m <sup>2</sup> /g)	$d_{\text{p}}^{\text{c}}$ (nm)
HTOH-10.5-0.1so-24h	398	40	0.6
HTOH-10.5-0.1so-48h	408	53	0.6
HTOH-10.5-0.1so-72h	404	57	0.6
HTOH-10.5-0.1so-96h	397	46	0.6

<sup>a</sup> Specific surface area determined by application of BET-plot method

<sup>b</sup> External surface area determined by application of t-plot method

<sup>c</sup> Pore size distribution determined by application of MP-plot method

#### 4.1.6 Effect of the Si/Al ratios on formation of ZSM-5

##### 4.1.6.1 Elemental analysis

The Si/Al ratios in gel and in catalyst of Samples HTOH-10.5-0.1so-24h are compared in Table 4.8. The result of nearly the same Si/Al ratios for each sample suggests that the catalysts obtained really contain aluminum. However, data from only ICP-AES technique can not exhibit the position of aluminum atoms, whether they are located at the tetrahedral framework or octahedral non-framework, therefore data from <sup>27</sup>Al-NMR is needed for completion.

**Table 4.8** Si/Al molar ratios in gel and in catalyst of calcined Samples HTOH-10.5-0.1so-24h with different Si/Al ratios

Sample	Si/Al molar ratio in gel <sup>a</sup>	Si/Al molar ratio in catalyst <sup>b</sup>
HTOH-10.5-0.1so-24h-20	20	20.0
HTOH-10.5-0.1so-24h-40	40	41.7
HTOH-10.5-0.1so-24h-60	60	61.2

<sup>a</sup> Calculated from reagent quantities.

<sup>b</sup> Aluminum (Al) was determined by ICP-AES and Si was calculated from the deduction of AlO<sub>2</sub> and equivalent Na amounts from the sample weight.

#### 4.1.6.2 XRD results

Figure 4.17 shows XRD patterns of Samples HTOH-10.5-0.1so-24h with different Si/Al ratios of 20, 40 and 60. The crystallinity increases when the Si/Al ratio in gel is increased. The greater amount of Al incorporated into the zeolite structure, the less ordered structure resulting in the decrease of XRD peak intensities at low angles ranging from  $8^{\circ}$ - $10^{\circ}$ . This effect is known for XRD patterns of zeolites.

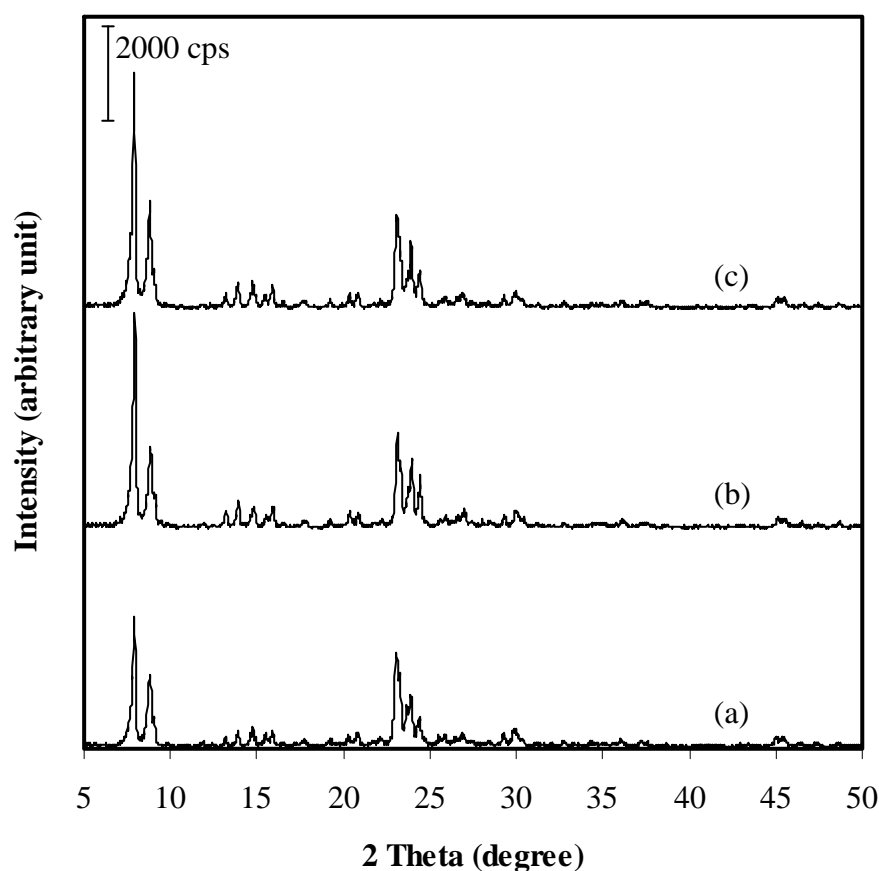


**Figure 4.17** XRD patterns of calcined Samples HTOH-10.5-0.1so-24h with different Si/Al ratios in gel (a) 20, (b) 40 and (c) 60.

#### 4.1.6.3 $^{27}\text{Al}$ -MAS-NMR spectra

Figure 4.18 shows the  $^{27}\text{Al}$ -MAS-NMR spectra of calcined Samples HTOH-10.5-0.1so-24h with various Si/Al ratios. The signal at about 50 ppm is typically assigned to tetrahedrally coordinated ( $\text{T}_d$ ) framework aluminum, and the peak at about 0 ppm is assigned to the octahedrally coordinated ( $\text{O}_h$ ) non-framework

aluminum [67]. Only the signal of aluminum atoms at the framework site was observed for all samples. The result indicates no aluminum migration from the tetrahedral site to the non-framework site after calcination at elevated temperature, i.e. high thermal stability of the ZSM-5 samples. As aluminum content increased, the signals at the framework site increased in intensity.

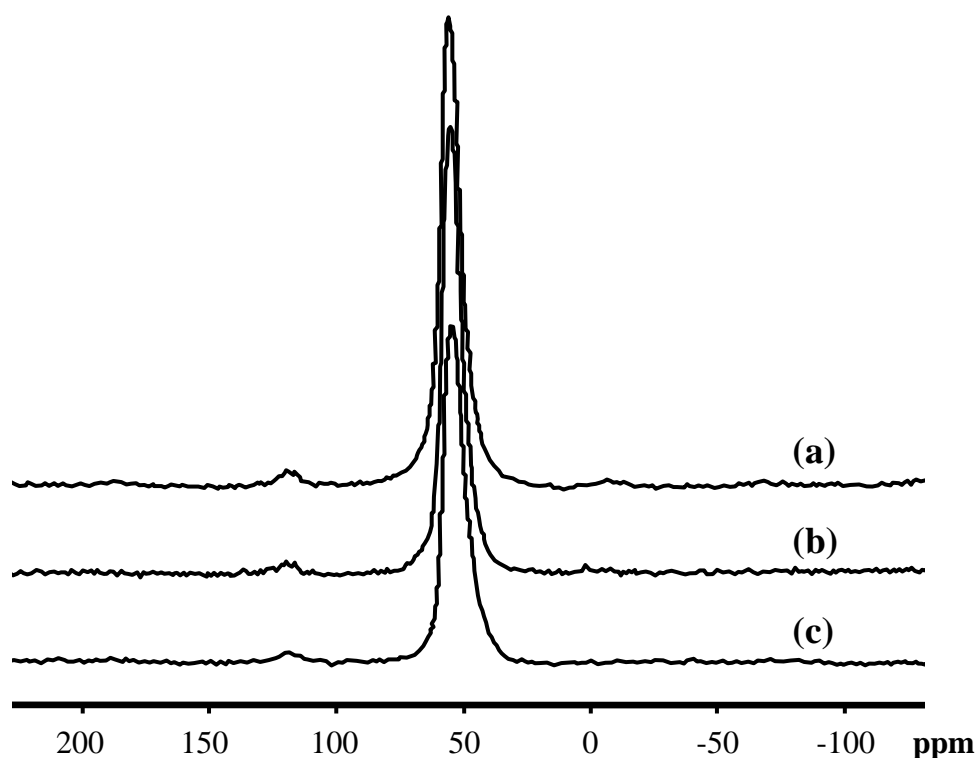


**Figure 4.18**  $^{27}\text{Al}$ -MAS-NMR spectra of calcined Samples HTOH-10.5-0.1so-24h with different Si/Al ratios in gel (a) 20, (b) 40 and (c) 60.

#### 4.1.6.4 SEM images

Figure 4.19 shows SEM image of Samples HTOH-10.5-0.1so-24h prepared with various Si/Al ratios. The results show that all samples have cauliflower-like morphology. The decrease of Si/Al ratio from 60 to 20 led to a slightly change of particle size but the larger particle size was formed when the Si/Al ratio was reduced to 20. Particle sizes of all samples are shown in Table 4.9.

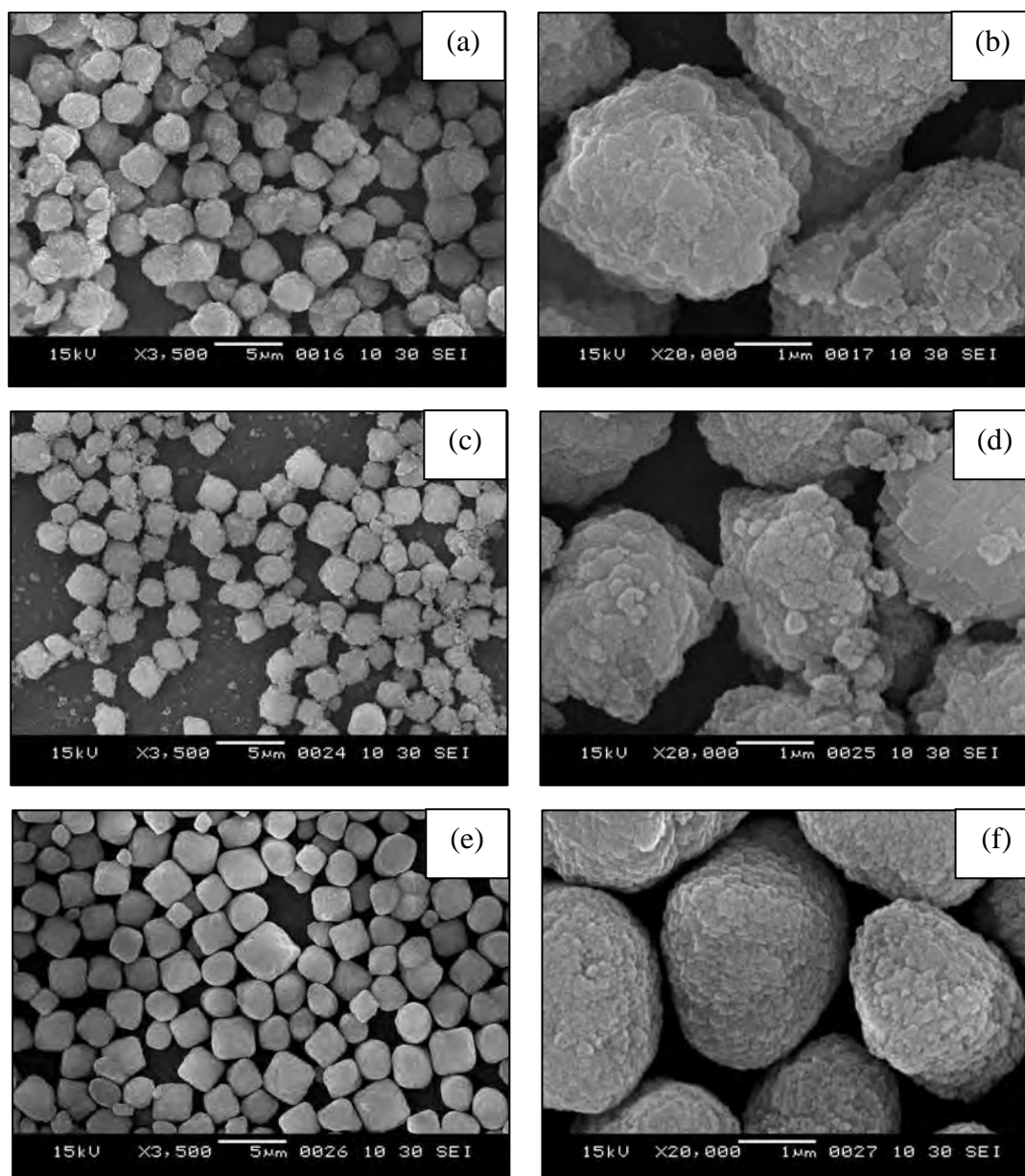


**Figure 4.19** SEM images of calcined Samples HTOH-10.5-0.1so-24h with various Si/Al ratios in gel of (a) 20 (3500x), (b) 20 (20000x), (c) 40 (3500x), (d) 40 (20000x), (e) 60 (3500x) and (f) 60 (20000x).

**Table 4.9** Textural properties of Samples HTOH-10.5-0.1so-24h with various Si/Al ratios in gel

Sample	Particle size ( $\mu\text{m}$ )	$S_{\text{BET}}^{\text{a}}$ ( $\text{m}^2/\text{g}$ )	$S_{\text{ext}}^{\text{b}}$ ( $\text{m}^2/\text{g}$ )	$d_{\text{p}}^{\text{c}}$ (nm)
HTOH-10.5-0.1so-24h-20	3.1	398	40	0.6
HTOH-10.5-0.1so-24h-40	2.5	441	75	0.6
HTOH-10.5-0.1so-24h-60	2.7	439	60	0.6

<sup>a</sup> Specific surface area determined by application of BET-plot method

<sup>b</sup> External surface area determined by application of t-plot method

<sup>c</sup> Pore size distribution determined by application of MP-plot method

#### 4.1.6.5 Nitrogen adsorption

Figure 4.20 shows the  $\text{N}_2$  adsorption-desorption isotherm of Samples HTOH-10.5-0.1so-24h with various Si/Al ratios. The samples exhibit a type I isotherm, typical for microporous materials. The textural properties of HTOH-10.5-0.1so-24h with various Si/Al ratios are summarized in Table 4.9. Samples HTOH-10.5-0.1so-24h-40 and HTOH-10.5-0.1so-24h-60 show similar specific surface area but higher than that of sample HTOH-10.5-0.1so-24h-20 due to their smaller particle size. Sample HTOH-10.5-0.1so-24h-40 shows relatively the highest external surface area.

#### 4.1.6.6 $\text{NH}_3$ -TPD profiles

Figure 4.21 shows  $\text{NH}_3$ -TPD profiles of calcined HTOH-10.5-0.1so-24h with different Si/Al ratios. The  $\text{NH}_3$ -TPD profiles of all samples exhibit two  $\text{NH}_3$  desorption peaks corresponding to different types of acid sites as discussed previously. The high temperature peak is due to the stronger acid sites and the low temperature peak is related to the weaker acid sites. The data from  $\text{NH}_3$ -TPD analysis are shown in Table 4.10. The number of weaker acid sites decreases obviously when the Si/Al ratio increases due to the decrease in aluminum content in catalyst.

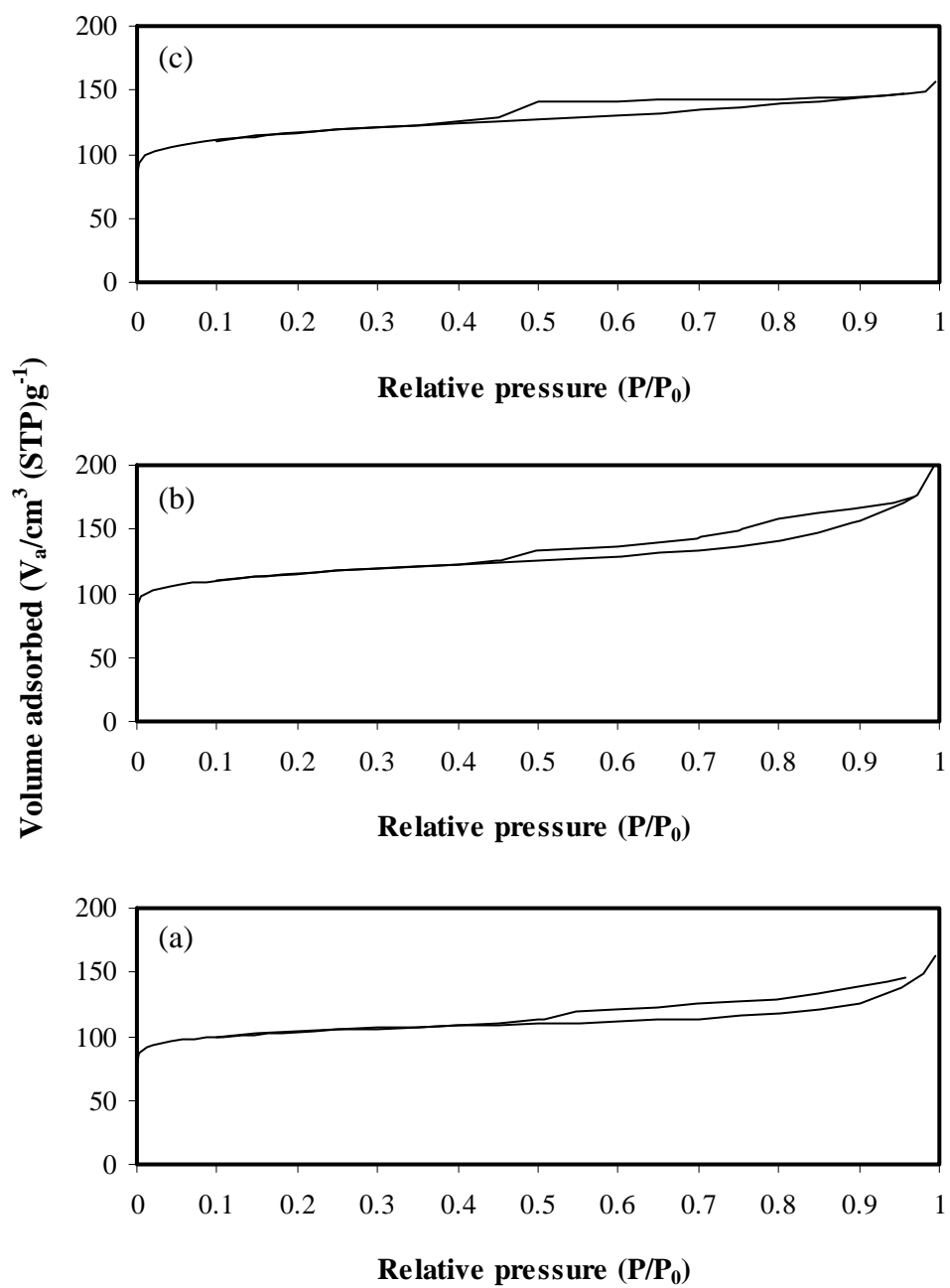


**Figure 4.20**  $\text{N}_2$  adsorption-desorption isotherms of calcined Samples HTOH-10.5-0.1so-24h with various Si/Al mole ratios: (a) 20, (b) 40 and (c) 60.

**Table 4.10** Number of acid sites from NH<sub>3</sub>-TPD analysis of calcined Samples HTOH-10.5-0.1so-24h with various Si/Al ratios

Sample	No. of acid sites <sup>a</sup> (mmol/g)		
	Peak I <sup>b</sup>	Peak II <sup>c</sup>	Total <sup>d</sup>
HTOH-10.5-0.1so-24h-20	3.7167	0.1239	3.8406
HTOH-10.5-0.1so-24h-40	3.0906	0.1558	3.2464
HTOH-10.5-0.1so-24h-60	2.3023	0.0630	2.3653

<sup>a</sup> Desorbed amount of ammonia

<sup>b</sup> Number of acid sites at low temperature peak

<sup>c</sup> Number of acid sites at high temperature peak

<sup>d</sup> Total number of acid sites

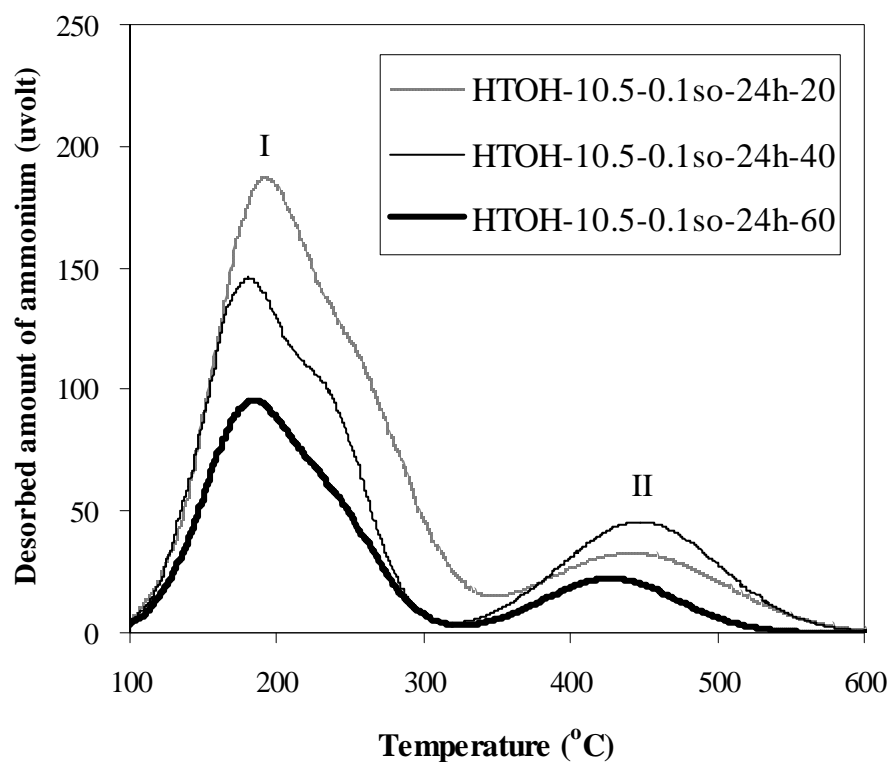


**Figure 4.21** NH<sub>3</sub>-TPD profiles of Samples HTOH-10.5-0.1so-24h with various Si/Al ratios in gel (a) 20, (b) 40 and (c) 60.

## **4.2 Parameters affecting formation of ZSM-5 synthesized by xerogel method**

### **4.2.1 Effect of crystallization time on formation of ZSM-5**

#### **4.2.1.1 XRD results**

The effect of crystallization time ranging from 2 to 96 h on formation of zeolite ZSM-5 (Si/Al = 60) was studied for xerogel method with employing the sonication of gel with ultrasound wave. All XRD patterns of the as-synthesized products as shown in Figure 4.22 show the characteristic peaks of ZSM-5 without any contaminant phase except the sample crystallized for 2 h showing no reflection peak. It indicates that only amorphous product was obtained for the latter. As a result, 2 h crystallization time is not enough to form ZSM-5 crystals. Upon prolongation of crystallization time, formation of pure zeolite, ZSM-5, can be achieved at 170°C after 6 h. With increasing crystallization time from 6 h to 96 h, the intensity of characteristic peak at  $2\theta$  of 23° slightly increases. The plot of the intensity of characteristic peak at  $2\theta$  of 23° versus crystallization time is shown in Figure 4.23. When increasing the crystallization time longer than 12 h, there is no significant change of the intensity of characteristic peak at  $2\theta$  of 23°. In conclusion, the xerogel method can provide high crystallinity of ZSM-5 within only 12 h crystallization time.

#### **4.2.1.2 SEM images**

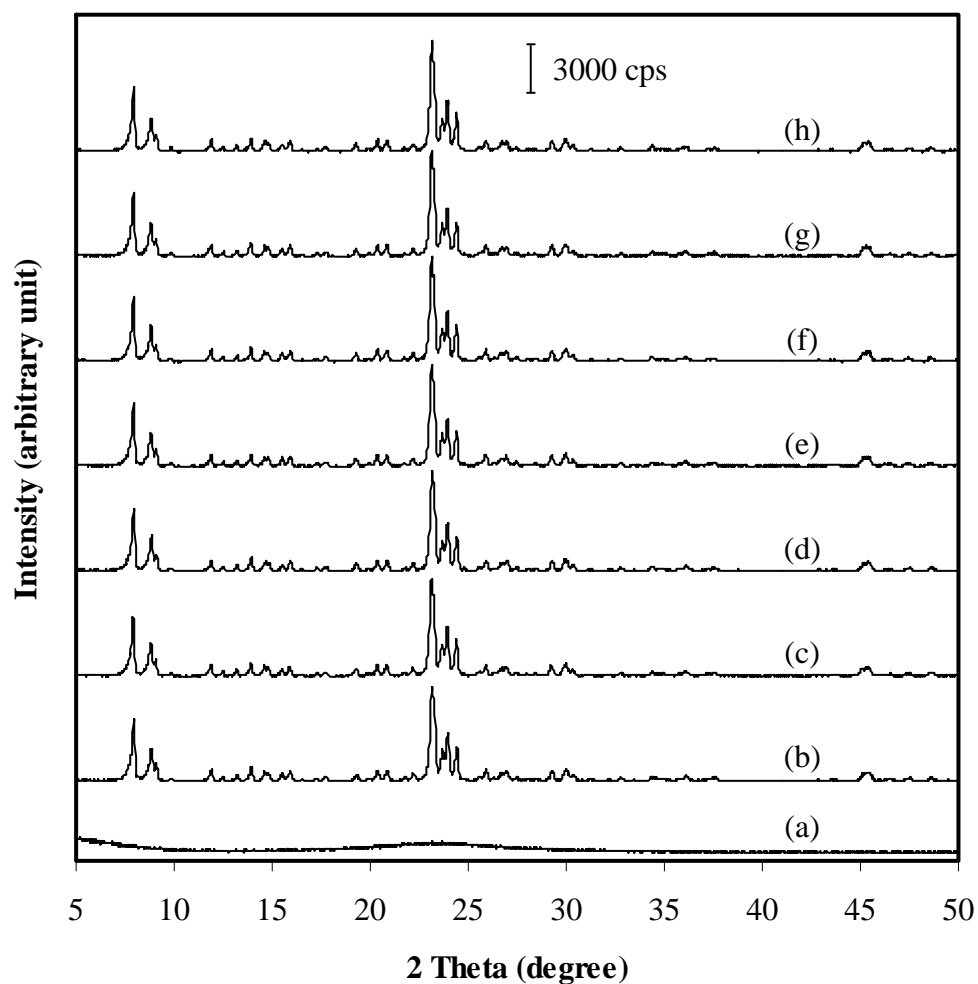
SEM images of zeolite ZSM-5 catalysts synthesized with xerogel method at various crystallization periods are shown in Figure 4.24. All samples exhibit agglomeration of small crystals to larger particles. The increase of crystallization time from 6 h to 24 h led to slightly change of particle size, but no further change after the crystallization times of 24 h. The particle size of ZSM-5 prepared with xerogel method is much smaller than ZSM-5 prepared with hydrothermal method. It can be concluded that the particle size strongly depends on the synthesis method.

#### **4.2.1.3 Nitrogen adsorption**

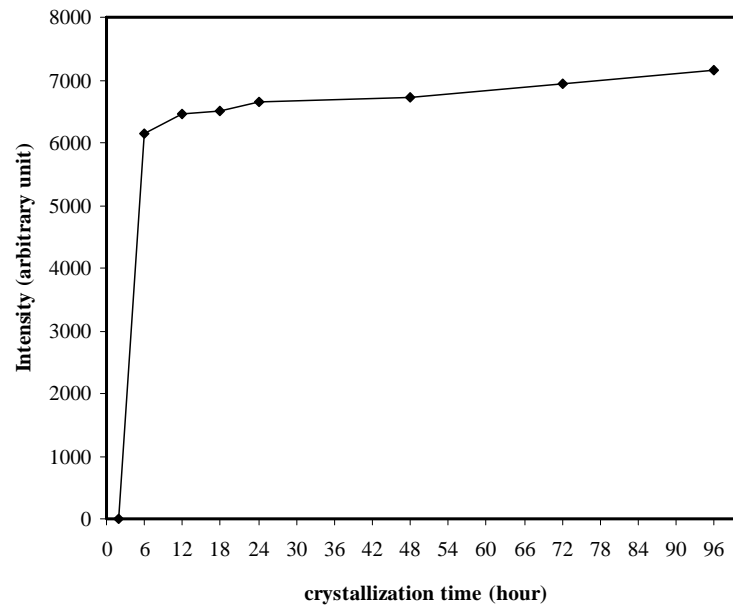
Figure 4.25 shows the adsorption-desorption isotherms of XGOH samples prepared with various crystallization periods. All samples exhibit a type I isotherm, which is the typical isotherm of microporous solid. Table 4.11 shows the textural properties of XGOH samples prepared with various crystallization



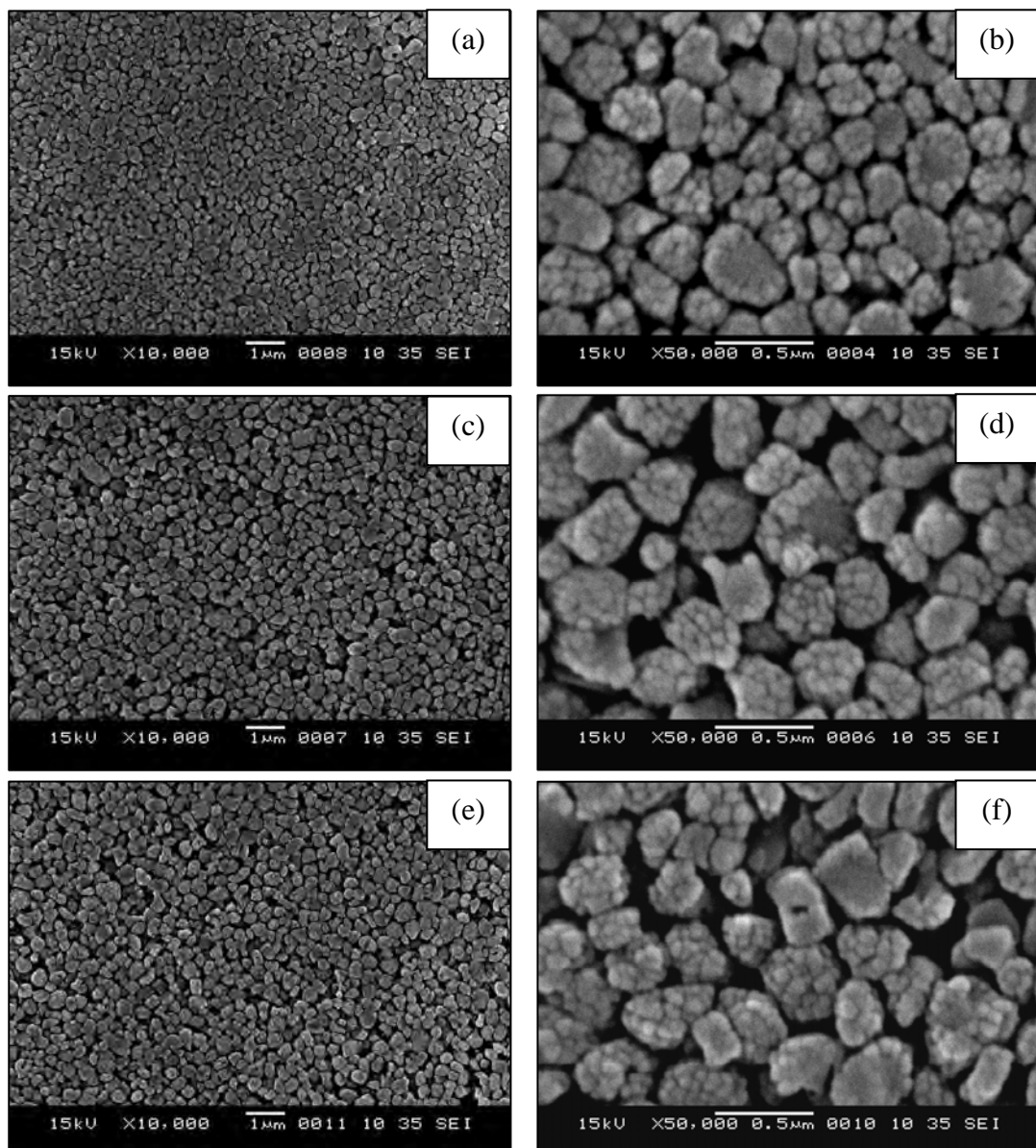
periods. The BET specific surface areas and external surface areas are not significantly different except XGOH-12h shows the highest external surface area. The pore size for all samples are 0.6 nm.

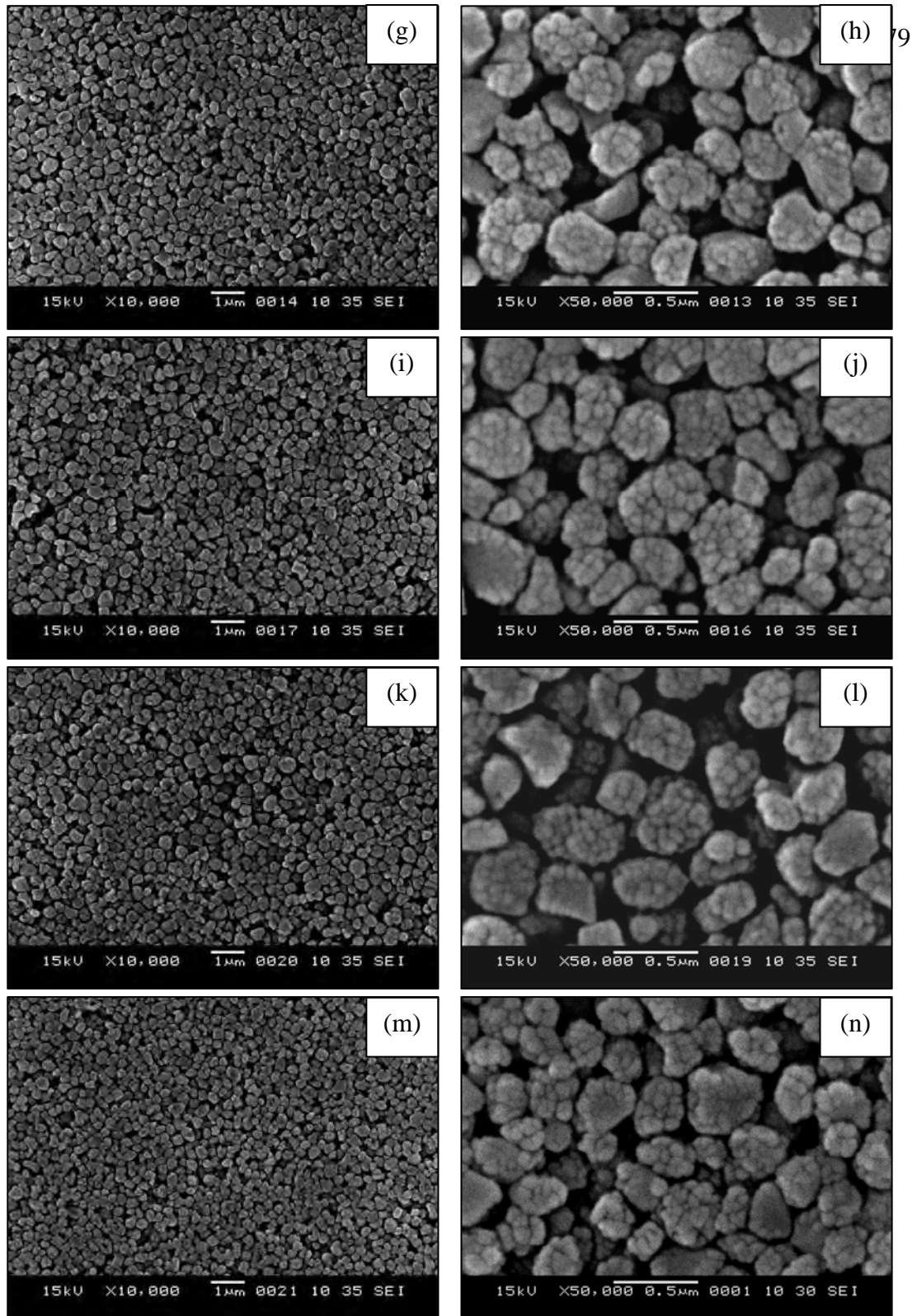


**Figure 4.22** XRD patterns of as-synthesized XGOH with ultrasound irradiation and crystallized for various periods: (a) 2 h, (b) 6 h, (c) 12 h, (d) 18 h, (e) 24 h, (f) 48 h, (g) 72 h and (h) 96 h.

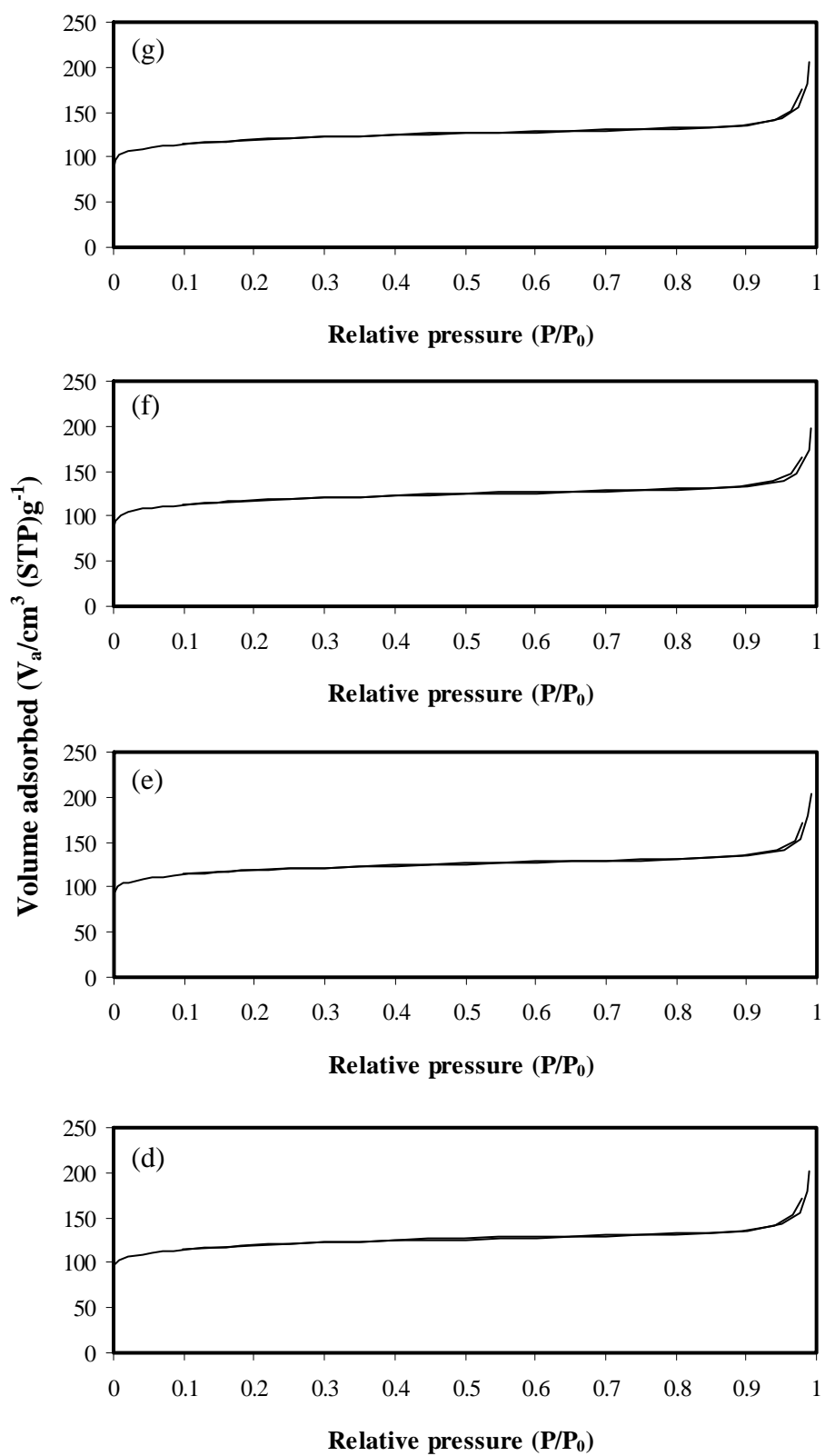


**Figure 4.23** Relationship between the intensity of characteristic peak at  $2\theta$  of  $23^\circ$  and crystallization time.





**Figure 4.24** SEM images of calcined Samples XGOH crystallized at 170°C for various periods: (a) 6 h (10000x), (b) 6 h (50000x), (c) 12 h (10000x), (d) 12 h (50000x), (e) 18 h (10000x), (f) 18 h (50000x), (g) 24 h (10000x), (h) 24 h (50000x), (i) 48 h (10000x), (j) 48 h (50000x), (k) 72 h (10000x), (l) 72 h (50000x), (m) 96 h (10000x) and (n) 96 h (50000x).



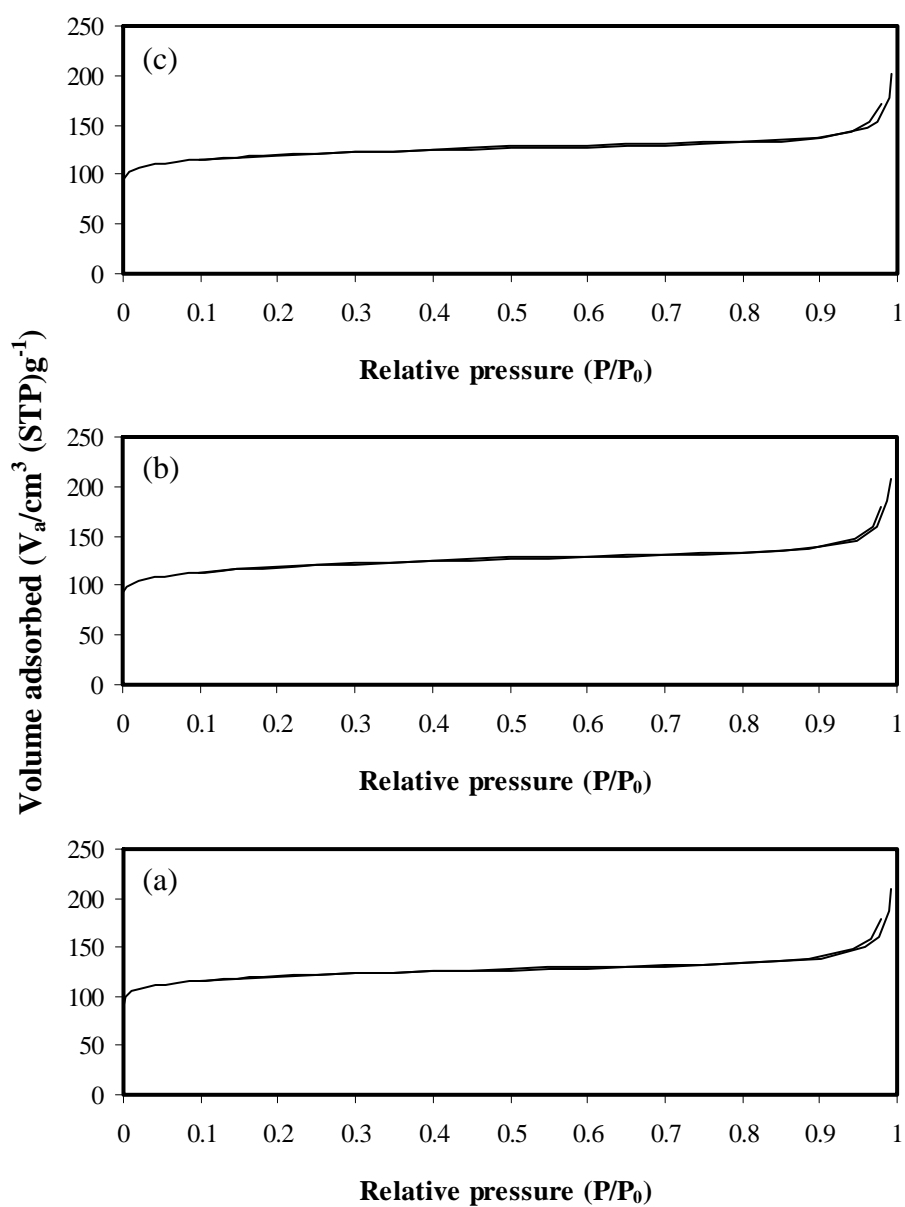


**Figure 4.25**  $\text{N}_2$  adsorption-desorption isotherms of calcined Samples XGOH crystallized at  $170^\circ\text{C}$  for various crystallization periods: (a) 6 h, (b) 12 h, (c) 18 h, (d) 24 h, (e) 48 h, (f) 72 h and (g) 96 h.

**Table 4.11** Textural properties of Samples XGOH prepared with various crystallization periods

Sample	Particle size <sup>a</sup> (nm)	S <sub>BET</sub> <sup>b</sup> (m <sup>2</sup> /g)	S <sub>ext</sub> <sup>c</sup> (m <sup>2</sup> /g)	d <sub>p</sub> <sup>d</sup> (nm)
XGOH-6h	320	463	39	0.6
XGOH-12h	340	458	47	0.6
XGOH-18h	350	453	38	0.6
XGOH-24h	370	457	37	0.6
XGOH-48h	360	456	38	0.6
XGOH-72h	360	449	36	0.6
XGOH-96h	360	455	37	0.6

<sup>a</sup> Particle size determined by SEM images

<sup>b</sup> Specific surface area determined by application of BET-plot method

<sup>c</sup> External surface area determined by application of t-plot method

<sup>d</sup> Pore size distribution determined by application of MP-plot method

#### 4.2.1.4 XRF analysis

Table 4.12 shows the Si/Al ratios in catalyst of XGOH-xh (using the gel with Si/Al ratio of 60) samples prepared with employing sonication before crystallization for various periods. It was clearly observed that the Si/Al ratios in catalyst of all samples were less than the Si/Al ratios in gel which were calculated from reagent quantities. The aluminum content determined by XRF technique is the total content of both framework and non-framework species. Only the data from XRF technique can not classify the aluminum species, whether it is located at the tetrahedral framework or octahedral non-framework species. Consequently, supportive data from <sup>27</sup>Al-MAS-NMR is needed. %Al<sub>2</sub>O<sub>3</sub> decreases with the increase of crystallization time. On the other word, the Si/Al ratio in catalyst is approaching to the ratio in the reactant gel when increasing the crystallization time of the xerogel synthesis method.

**Table 4.12** Si/Al ratios of Samples XGOH with various crystallization periods by XRF

Sample	%SiO <sub>2</sub>	%Al <sub>2</sub> O <sub>3</sub>	Si/Al
XGOH-6h	92.30	1.90	41.30
XGOH-12h	92.30	1.82	42.91
XGOH-48h	92.70	1.61	48.83
XGOH-96h	94.70	1.58	50.85

#### 4.2.1.5 <sup>27</sup>Al-MAS-NMR spectra

<sup>27</sup>Al-MAS-NMR spectra of calcined XGOH samples with various crystallization time of 6 h, 12 h 48 h and 96 h are shown in Figure 4.26. The spectra of all samples show only a signal centered at 50 ppm associated to tetrahedrally coordinated Al atoms in the framework, which gradually decreases with the increase of crystallization times. This is in agreement with the XRF data. It can be concluded that the Si/Al ratio analyzed by XRF technique is the real Si/Al value in catalyst. There is no Al atoms located on the surface or at the non-framework site.

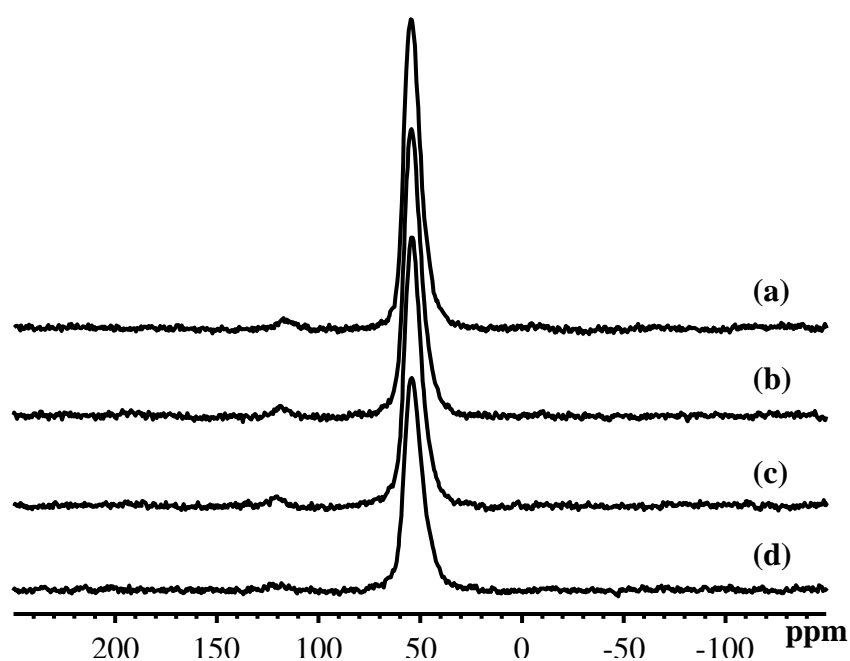


**Figure 4.26** <sup>27</sup>Al-MAS-NMR spectra of calcined Samples XGOH with different crystallization time: (a) 6 h, (b) 12 h, (c) 48 h and (d) 96 h.

### 4.3 Activity of various ZSM-5 catalysts in HDPE cracking

#### 4.3.1 Effect of crystallization time

The ZSM-5 samples prepared with xerogel method, the Si/Al ratio in gel of 60 and various crystallization time: 6 h, 12 h, 48 h and 96 h were tested for their catalytic activities in cracking of HDPE at 380°C for 40 min. The thermal cracking was performed as a blank test. The values of %conversion and product yields for thermal cracking and catalytic cracking of HDPE over XGOH catalysts with various crystallization time are compared in Table 4.13.

**Table 4.13** Values of %conversion and %yield obtained by catalytic cracking of HDPE over XGOH catalysts with various crystallization time (Condition: 10 wt% catalyst of plastic, N<sub>2</sub> flow of 20 cm<sup>3</sup>/min, 380°C and reaction time of 40 min)

	Thermal	XGOH-6h	XGOH-12h	XGOH-48h	XGOH-96h
%Conversion*	0.87	70.53	84.07	75.67	83.87
% Yield*					
1. gas fraction	0.87	44.60	48.40	44.40	48.93
2. liquid fraction	0.00	25.93	35.67	31.27	34.94
- distillate oil	-	22.29	30.63	25.40	28.91
- heavy oil	-	3.64	5.04	5.87	6.02
3. residue	99.13	29.47	15.93	24.33	16.13
- solid coke	-	0.86	0.88	0.92	1.00
Total volume of liquid fraction ( cm <sup>3</sup> )	-	1.85	2.53	2.22	2.48
Liquid fraction density (g/ cm <sup>3</sup> )	-	0.70	0.70	0.70	0.71

\*Deviation within 0.6% for conversion, 0.8% for yield of gas fraction, 0.8% for yield of liquid fraction, and 0.6% for yield of residue.

For thermal cracking of HDPE waste at 380°C, no liquid fraction was found in the graduated cylinder and %conversion is only 0.87%. The result indicates the difficulty in degradation of HDPE waste without catalyst. Therefore, the total weight loss of plastic precursor after reaction is dedicated to gas fraction. For the catalytic cracking over ZSM-5 catalysts prepared with various crystallization periods,



the plastic conversion increases to about 70-84 wt% depending on the crystallization period. Catalytic cracking of HDPE over ZSM-5 catalysts produced higher yields of gas fraction than liquid fraction and larger distilled oil than heavy oil due to its strong acidity and small pore size. For the catalytic cracking of HDPE over XGOH samples, when the crystallization time increases from 12 to 96 h, the conversion and product yields are maximized when XGOH-12h was used as catalyst. Therefore, crystallization time of 12 h is an optimum condition which was chosen for the rest of studies.

Figure 4.27 shows the accumulated volume of liquid fraction obtained by catalytic cracking of HDPE over samples XGOH catalysts with various crystallization times at 380°C. The initial rates of liquid fraction formation by XGOH-12h and XGOH-96h are much faster than those of other catalysts but the highest total volume of liquid fraction was obtained for the case of using XGOH-12h as catalyst.

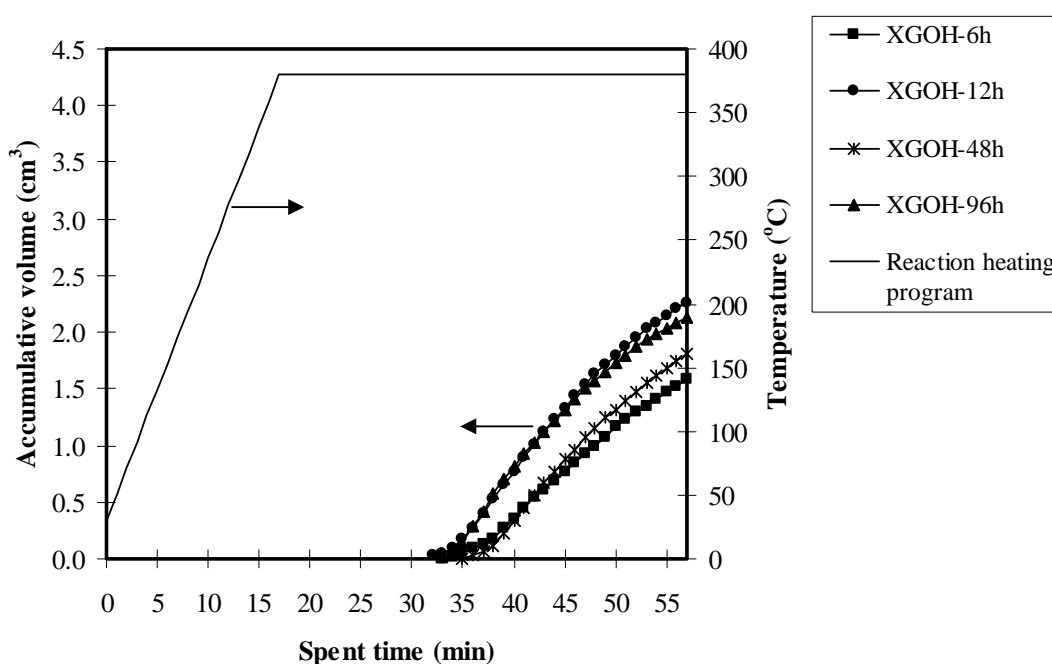


**Figure 4.27** Accumulative volume of liquid fractions obtained by catalytic cracking of HDPE over Samples XGOH with various crystallization time at 380°C (Condition: 10 wt% catalyst of plastic, N<sub>2</sub> flow of 20 cm<sup>3</sup>/min and reaction of 40 min).

Figure 4.28 shows distribution of gas fraction obtained by thermal cracking and catalytic cracking of HDPE over Sample XGOH with various

crystallization time at 380°C. The major components in gas fraction obtained by thermal cracking are ethene, propene, n-butane and C<sub>5</sub>+ whereas the major components from catalytic cracking contain propene, n-butane, i-butene and C<sub>5</sub>+. In addition, all distribution plots of HDPE waste cracking over all four catalysts exhibit similar gas product distribution, indicating that the distribution of gas products is not affected by variation of crystallization time from 6 to 96 h.

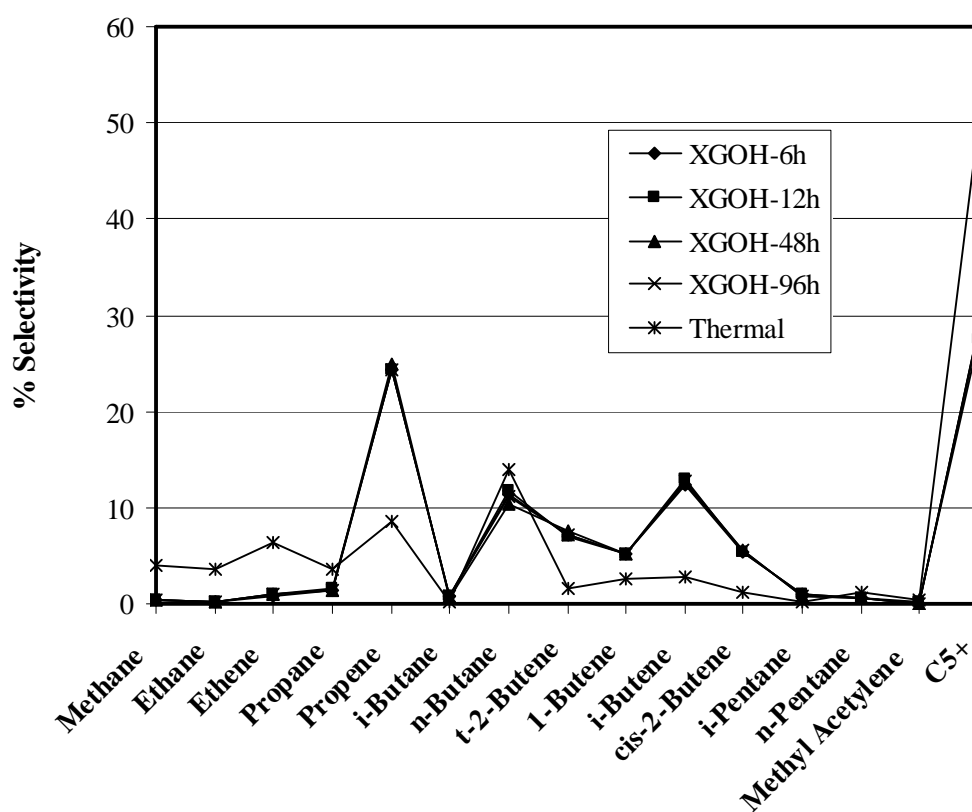


**Figure 4.28** Distribution of gas fraction obtained by thermal cracking and catalytic cracking of HDPE over Samples XGOH with various crystallization time at 380°C (Condition: 10 wt% catalyst of plastic, N<sub>2</sub> flow of 20 cm<sup>3</sup>/min and reaction of 40 min).

Figure 4.29 shows carbon number distribution of distillate oil obtained by catalytic cracking of HDPE waste using ZSM-5 catalysts prepared with xerogel method, with application of sonication and crystallized for various periods. Liquid products are investigated with the C<sub>np</sub> value which relates to the boiling point range of n-paraffins. The liquid components are mainly in the range C<sub>6</sub>-C<sub>9</sub> for all samples,

showing that ZSM-5 catalysts exhibit good catalytic activities for producing light hydrocarbon liquids. All liquid distribution plots obtained by catalytic cracking HDPE waste over XGOH catalysts crystallized for various periods are approximately similar in the range of C<sub>6</sub>-C<sub>9</sub> hydrocarbon. There is slightly difference in %selectivity compared among these catalysts. However, the difference is not significant. This result indicates that variations of crystallization time from 6 to 96 h do not affect the distribution of liquid products.

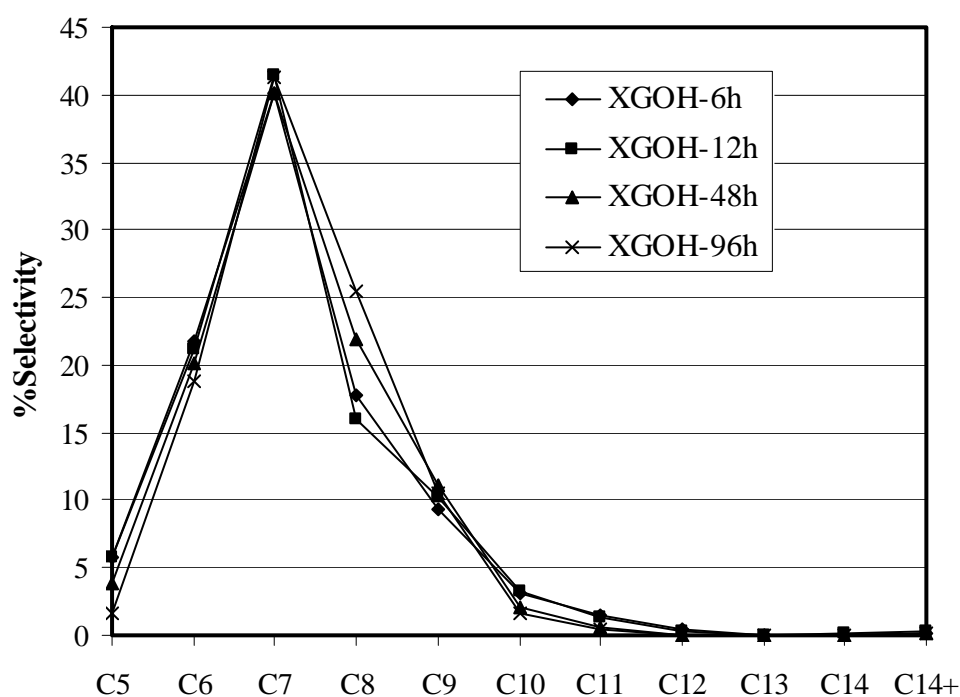


**Figure 4.29** Carbon number distribution of distillate oil obtained by catalytic cracking of HDPE over Samples XGOH with various crystallization time at 380°C (Condition: 10 wt% catalyst of plastic, N<sub>2</sub> flow of 20 cm<sup>3</sup>/min and reaction of 40 min).

### 4.3.2 Effect of preparation methods and temperature

Samples XGOH-12h and HTOH-10.5-0.1so-24h-60 were used for studying the effect of preparation: hydrothermal and xerogel methods, on their catalytic activities in cracking of HDPE waste. The values of %conversion and the product yields for the thermal cracking and catalytic cracking of HDPE over XGOH-12h and HTOH-10.5-0.1-24h-60 at 380°C and 400°C are shown in Table 4.14. XGOH-12h and HTOH-10.5-0.1-24h-60 give similar conversions but HTOH-10.5-0.1-24h-60 shows higher yields of gas fraction. Compared with XGOH-12h, HTOH-10.5-0.1-24h-60 has more external surface area. Therefore, the number of acid sites on external surface area of HTOH-10.5-0.1-24h-60 is more than XGOH-12h. On the other word, the XGOH-12h shows higher yield of liquid fraction and distillate oil than HTOH-10.5-0.1so-24h-60. From this result, we can use HTOH-10.5-0.1-24h-60 as the catalyst for cracking HDPE waste if we want gaseous product and use XGOH-12h for liquid product.

The values of %conversion and the product yields increase when reaction temperature increases from 380°C to 400°C. For thermal cracking at both reaction temperatures, no liquid fractions was found in the graduated cylinder. The result shows the difficulty in degradation of HDPE without catalyst at the temperature about 400°C or less. For the catalytic cracking, when the reaction temperature increases from 380°C to 400°C, the amount of residue decreases from 16.73 wt% to 3.53 wt% for HTOH-10.5-0.1-24h-60 and 15.93 wt% to 3.33 wt% for XGOH-12h. The result indicates that the residue decomposed into liquid and gas hydrocarbons resulting in higher yield of gas and liquid fractions than the case of thermal cracking. The liquid fractions have pale yellow color for both temperatures.

**Table 4.14** Values of %conversion and %yield obtained by thermal cracking and catalytic cracking of HDPE over Samples XGOH-12h and HTOH-10.5-0.1-24h-60 at 380°C and 400°C (Condition: 10 wt% catalyst of plastic, N<sub>2</sub> flow of 20 cm<sup>3</sup>/min and reaction of 40 min)

	Reaction temperature=380°C			Reaction temperature=400°C		
	Thermal	HTOH-10.5-0.1-24h-60	XGOH-12h	Thermal	HTOH-10.5-0.1-24h-60	XGOH-12h
a <sub>s</sub> , BET(m <sup>2</sup> /g)		439	458		439	458
a <sub>2</sub> , external surface area (m <sup>2</sup> /g)		60	47		60	47
%Conversion*	0.87	83.27	84.07	3.67	96.47	96.67
% Yield*						
1. gas fraction	0.87	57.67	48.40	3.67	66.60	52.67
2. liquid fraction	0.00	25.60	35.67	0.00	29.87	44.00
- distillate oil	-	17.28	30.63	-	21.46	37.91
- heavy oil	-	8.32	5.04	-	8.41	6.09
3. residue	99.13	16.73	15.93	96.33	3.53	3.33
- solid coke	-	0.70	0.88	-	0.69	0.69
Total volume of liquid fraction (cm <sup>3</sup> )	-	1.67	2.53	-	1.97	3.14
Liquid fraction density (g/ cm <sup>3</sup> )	-	0.77	0.70	-	0.76	0.70

\*Deviation within 0.3% for conversion, 0.5% for yield of gas fraction, 0.5% for yield of liquid fraction, and 0.3% for yield of residue.

Figure 4.30 shows the accumulative volume of liquid fractions in the graduated cylinder increased as a function of spent time. The initial rate of liquid fraction formation at 400°C is much faster than that at 380°C and the total volume of liquid fraction obtained at 400°C is greater than that at 380°C.

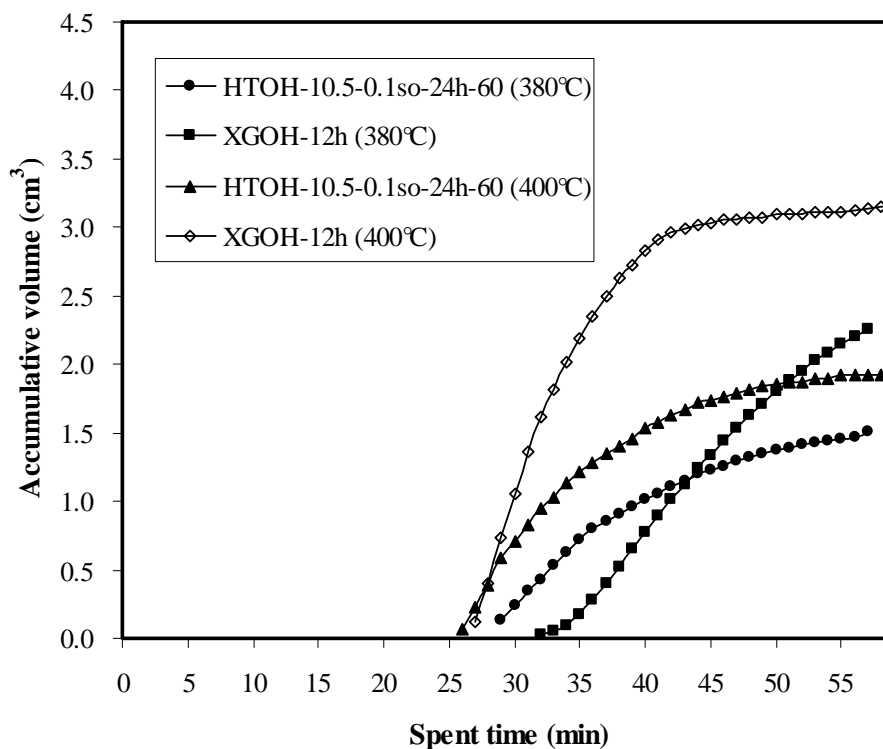


**Figure 4.30** Accumulative volume of liquid fractions obtained by catalytic cracking of HDPE over Samples XGOH-12h and HTOH-10.5-0.1-24h-60 at 380°C and 400°C (Condition: 10 wt% catalyst of plastic, N<sub>2</sub> flow of 20 cm<sup>3</sup>/min and reaction of 40 min).

Figure 4.31 and 4.32 show distribution of gas fraction obtained by thermal cracking and catalytic cracking of HDPE over XGOH-12h and HTOH-10.5-0.1-24h-60 at 380°C and 400°C, respectively. Considering only gases which are normally C<sub>1</sub> through C<sub>5</sub>, the major components for thermal cracking are propene and n-butane while that for catalytic cracking is propene for XGOH-12h and n-butane for HTOH-10.5-0.1-24h-60 independently from temperature. However, the vapor of C<sub>5</sub>+ (liquids at ambient condition) which has higher boiling point than that of C<sub>5</sub> (n-pentane) is obviously detected in large amount. For thermal cracking, the reaction temperature affects distribution of gas fraction products. When the reaction temperature increases, the gas fractions of lighter hydrocarbon (methane, ethane, ethene, propane and n-butane) increases while heavier hydrocarbon (C<sub>5</sub>+) decreases. At 380°C, C<sub>5</sub>+ remains in a great amount due to less efficiency of thermal cracking at low temperature. The temperature effect is not observed for the cracking over ZSM-5.

The explanation is the catalysts encourage the degradation of C<sub>5</sub>+ to lighter molecules even at 380°C.

Figure 4.33 shows product distribution of distillate oil obtained by catalytic cracking of HDPE over XGOH-12h and HTOH-10.5-0.1-24h-60 at 380°C and 400°C. The distillate oil components are mainly in the range of C<sub>6</sub> to C<sub>9</sub> for XGOH-12h and C<sub>7</sub> to C<sub>9</sub> for HTOH-10.5-0.1-24h-60. However, the effect of temperature on the product selectivity is not significant. According to the results of temperature effect on HDPE cracking, the temperature of 400°C is selected to be the test condition for further studies in this work due to considerably higher amount of liquid and lower amount of residue fractions were obtained.

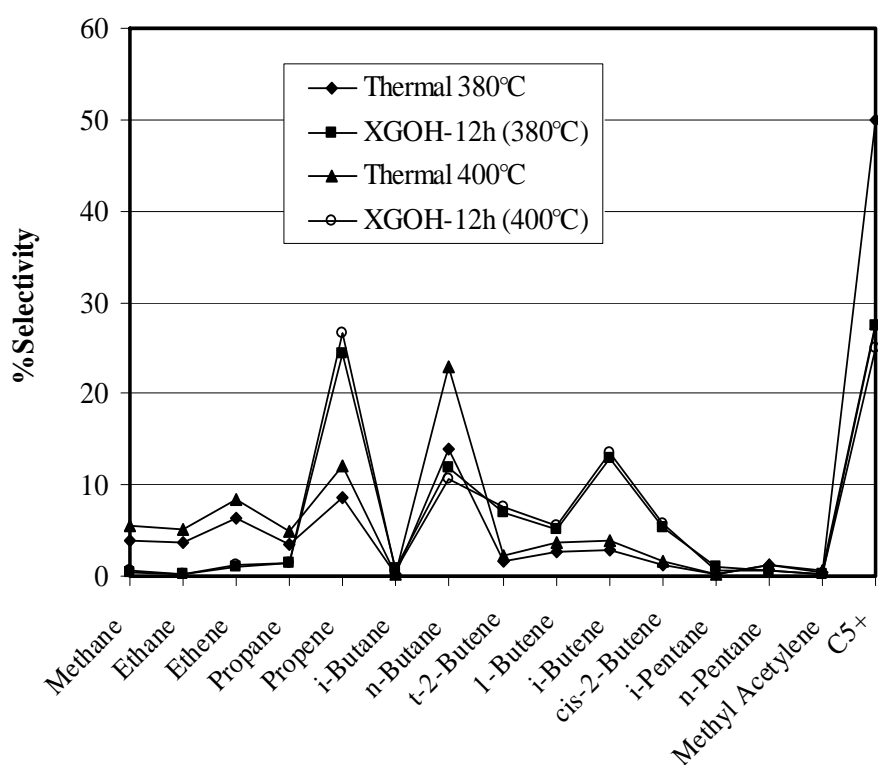


**Figure 4.31** Distribution of gas fraction obtained by the thermal cracking and catalytic cracking of HDPE over XGOH-12h at 380°C and 400°C (Condition: 10 wt% catalyst of plastic, N<sub>2</sub> flow of 20 cm<sup>3</sup>/min and reaction of 40 min).

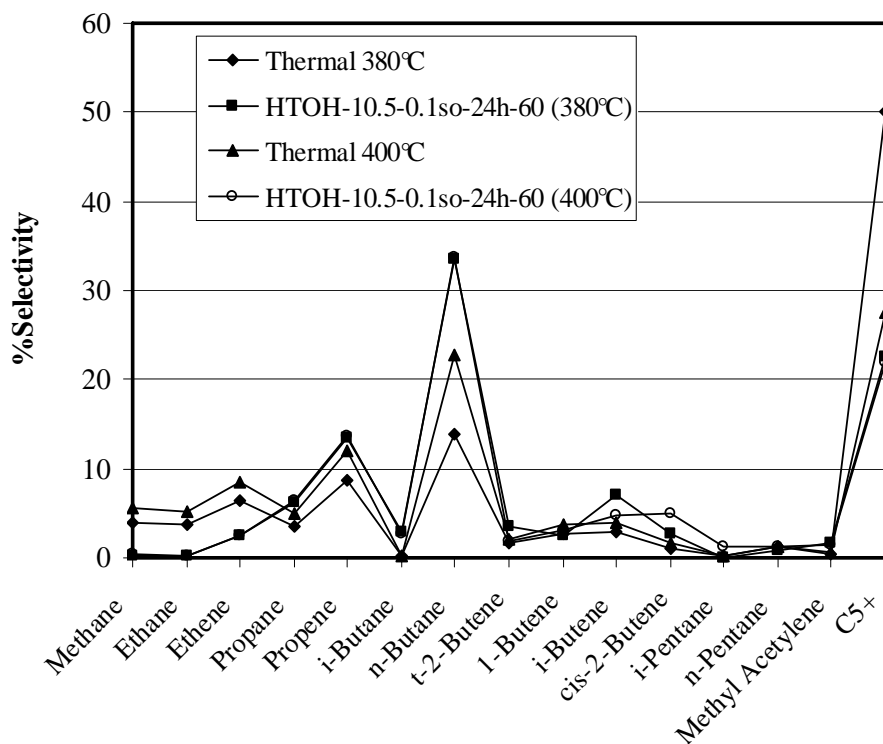


**Figure 4.32** Distribution of gas fraction obtained by the thermal cracking and catalytic cracking of HDPE over HTOH-10.5-0.1-24h-60 at 380°C and 400°C (Condition: 10 wt% catalyst of plastic, N<sub>2</sub> flow of 20 cm<sup>3</sup>/min and reaction of 40 min).

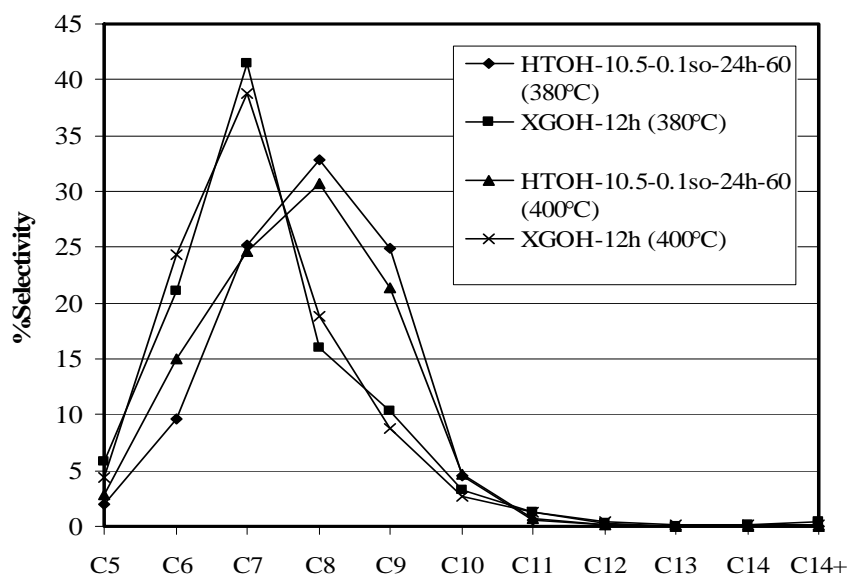


**Figure 4.33** Carbon number distribution of liquid fractions from catalytic cracking of HDPE over Samples XGOH-12h and HTOH-10.5-0.1-24h-60 at 380°C and 400°C (Condition: 10 wt% catalyst of plastic, N<sub>2</sub> flow of 20 cm<sup>3</sup>/min and reaction of 40 min).



### 4.3.3 Effect of Si/Al ratios

The value of %conversion and product yield from thermal cracking and catalytic cracking of HDPE waste over ZSM-5 catalysts prepared with hydrothermal method and with different Si/Al ratios are compared in Table 4.15. The conversion is not linearly related to the Si/Al ratios because there are more specific effects of acidity. For HTOH-10.5-0.1so-24h catalysts with the Si/Al ratios of 40 and 60 give similar conversions but HTOH-10.5-0.1so-24h-20 provides lower conversion due to HTOH-10.5-0.1so-24h-20 having the lowest BET specific surface area (See Table 4.15). For the HTOH-10.5-0.1so-24h-40, which has the highest external surface area, shows large amount of distillate oil and the lowest heavy oil. Significantly high BET specific surface area as well as external surface area is the reason why HTOH-10.5-0.1so-24h-40 exhibits the extreme activity. Both the BET specific surface area and external surface area play the key role on the activity of the catalysts. Acidity seems to be less pronounced under this condition. It could be started that the acidities of all ZSM-5 catalysts are very high due to the unique property of MFI typed structure and it is over the minimum requirement for cracking process.

Figure 4.34 shows accumulative volume of liquid fraction in the graduated cylinder. The rates of liquid fraction formation for HDPE cracking over HTOH-10.5-0.1-24h-40 and HTOH-10.5-0.1-24h-60 catalysts are not different, because both samples show very similar specific surface area. The rate of liquid fraction formation over Sample HTOH-10.5-0.1-24h-20 is the slowest owing to the lowest specific surface area.

Figure 4.35 shows distribution of gas fraction obtained by thermal cracking and catalytic cracking of HDPE over samples HTOH-10.5-0.1-24h with different Si/Al ratios at 380°C. In thermal cracking, ethene, propene, n-butane and C<sub>5</sub>+ are main products and C<sub>5</sub>+ is predominant, whereas gas fractions from catalytic cracking consist of mainly propene, n-butane and C<sub>5</sub>+. The product distribution in gaseous phase is not different upon changing the Si/Al ratios in the catalyst.

**Table 4.15** Values of %conversion and %yield obtained by catalytic cracking of HDPE over Samples HTOH-10.5-0.1-24h with different Si/Al ratios at 380°C (Condition: 10 wt% catalyst of plastic, N<sub>2</sub> flow of 20 cm<sup>3</sup>/min and reaction time of 40 min)

	Thermal	HTOH-10.5-0.1-24h-20	HTOH-10.5-0.1-24h-40	HTOH-10.5-0.1-24h-60
a <sub>s</sub> , BET(m <sup>2</sup> /g)	-	398	441	439
a <sub>2</sub> , external surface area (m <sup>2</sup> /g)	-	40	75	60
%Conversion*	0.87	75.53	83.93	83.27
% Yield*				
1. gas fraction	0.87	54.07	60.33	57.67
2. liquid fraction	0.00	21.47	23.60	25.60
- distillate oil	-	14.12	18.09	17.28
- heavy oil	-	7.35	5.51	8.32
3. residue	99.13	24.47	16.07	16.73
- solid coke	-	0.55	0.72	0.70
Total volume of liquid fraction ( cm <sup>3</sup> )	-	1.38	1.53	1.67
Liquid fraction density (g/ cm <sup>3</sup> )	-	0.77	0.77	0.77

\*Deviation within 0.8% for conversion, 0.7% for yield of gas fraction, 0.7% for yield of liquid fraction, and 0.8% for yield of residue.

Figure 4.36 shows product distribution of distillate oil obtained by the catalytic cracking of HDPE over samples HTOH-10.5-0.1-24h with different Si/Al ratios at 380°C. The major liquid products of all Si/Al ratios are distributed in the range of C<sub>7</sub> and C<sub>9</sub>. It can be concluded that Si/Al ratios in catalyst do not affect liquid product distribution. The product distribution of SUPELCO standard gasoline fraction is shown in Figure 4.37 and the major components are C<sub>7</sub> and C<sub>8</sub>. That is comparable to the distribution of distillate oil obtained in this work based on the boiling point range using n-paraffins as reference.

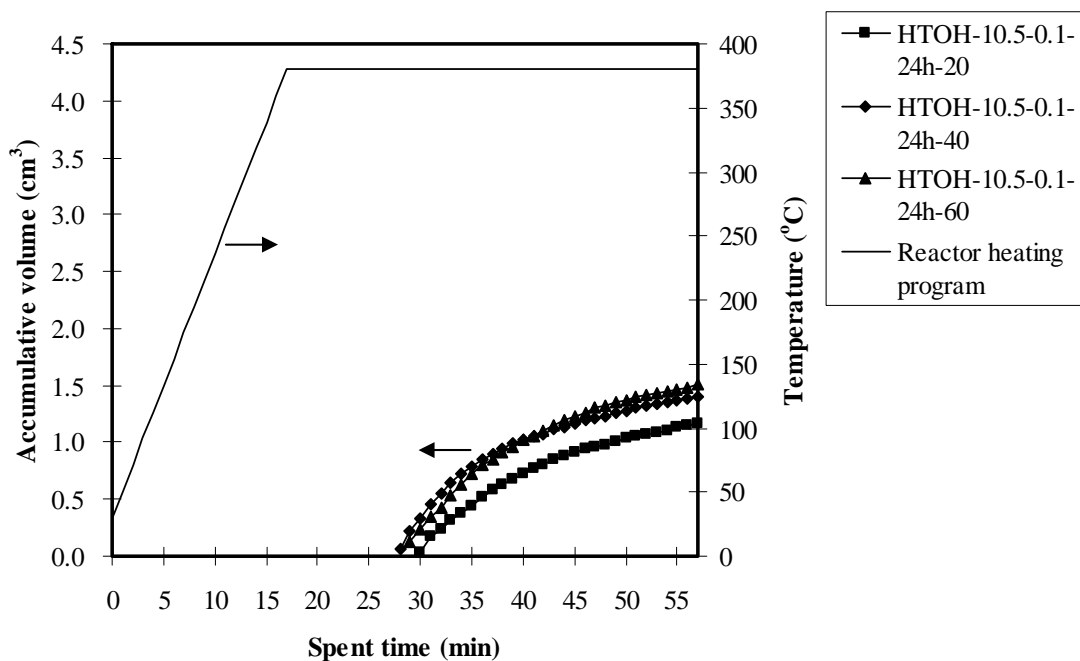


**Figure 4.34** Accumulative volume of liquid fractions obtained by catalytic cracking of HDPE over Samples HTOH-10.5-0.1-24h with different Si/Al ratio at 380°C (Condition: 10 wt% catalyst of plastic, N<sub>2</sub> flow of 20 cm<sup>3</sup>/min and reaction of 40 min).

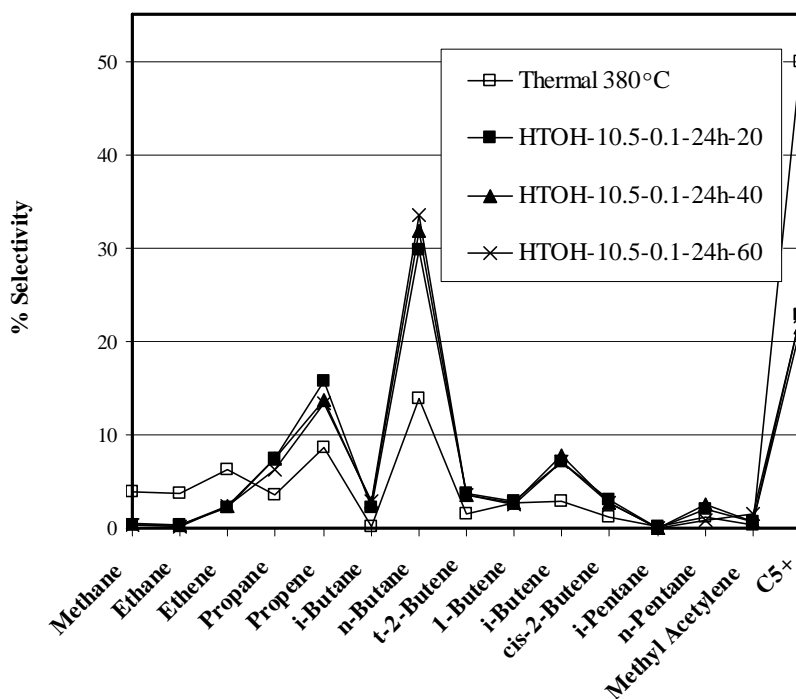


**Figure 4.35** Distribution of gas fraction obtained by thermal cracking and catalytic cracking of HDPE over Samples HTOH-10.5-0.1-24h with different Si/Al ratios at 380°C (Condition: 10 wt% catalyst of plastic, N<sub>2</sub> flow of 20 cm<sup>3</sup>/min and reaction of 40 min).

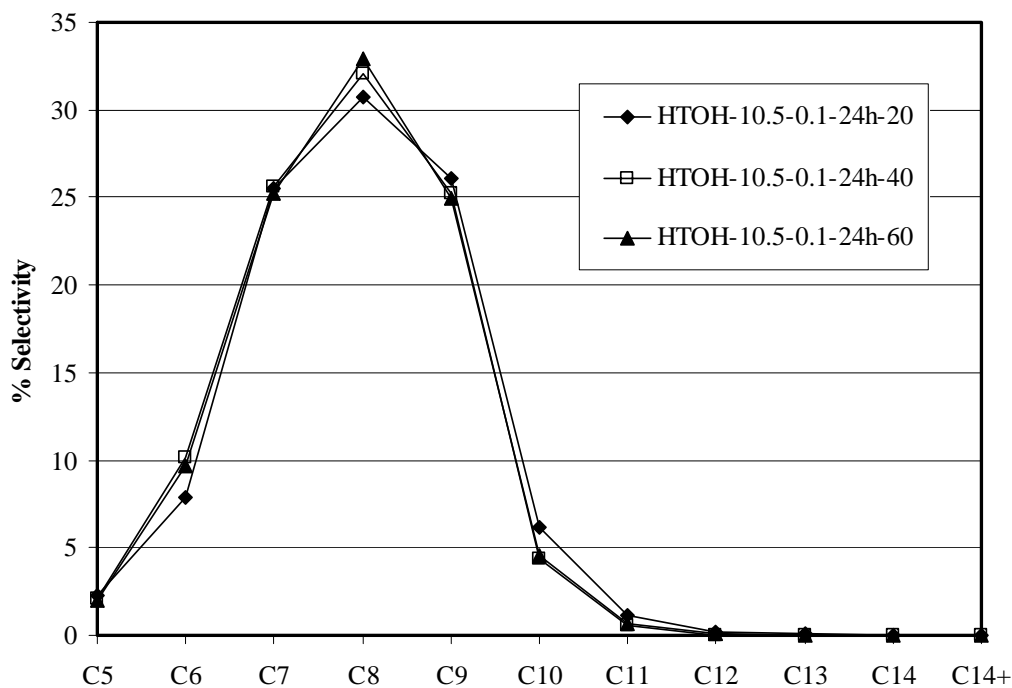


**Figure 4.36** Carbon number distribution of liquid fraction from catalytic cracking of HDPE over Samples HTOH-10.5-0.1-24h with different Si/Al ratios at 380°C (Condition: 10 wt% catalyst of plastic, N<sub>2</sub> flow of 20 cm<sup>3</sup>/min and reaction of 40 min).

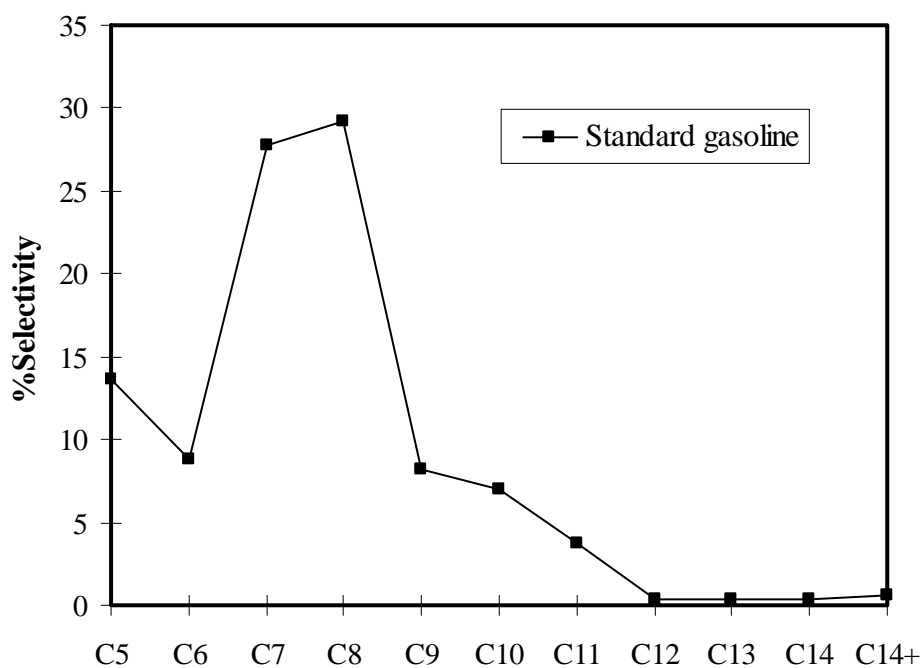


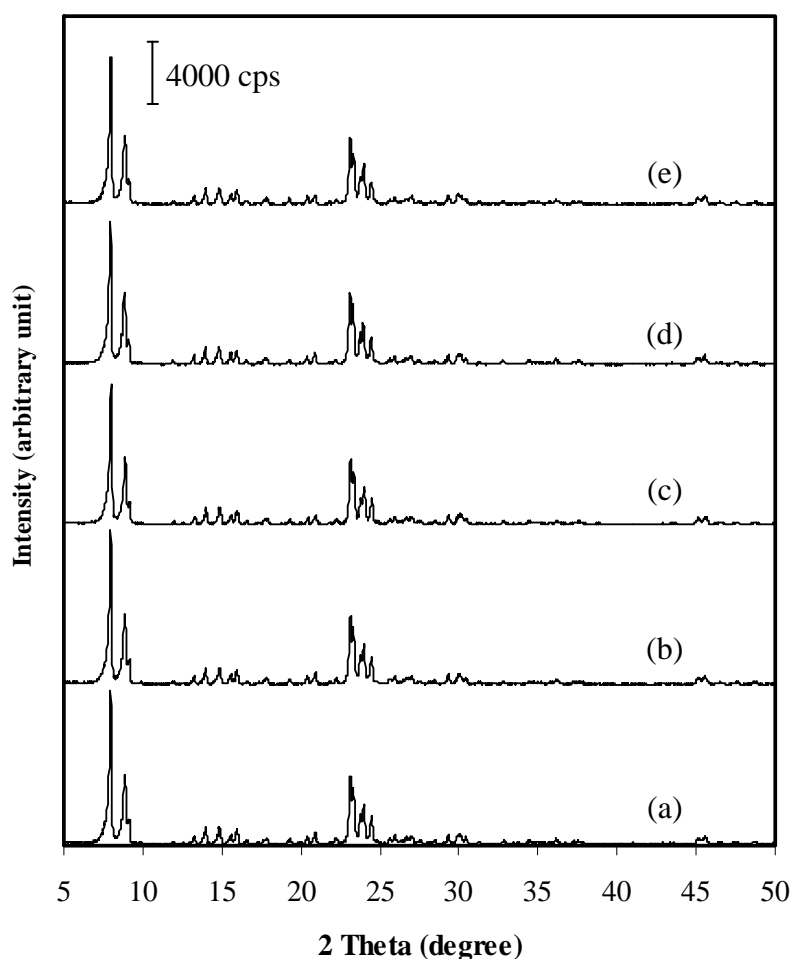
**Figure 4.37** Carbon number distribution of commercial SUPELCO standard gasoline fraction.

### 4.3.4 Reactivity of regenerated catalyst on HDPE cracking

#### 4.3.4.1 Characterization of regenerated catalyst

##### 4.3.4.1.1 XRD results

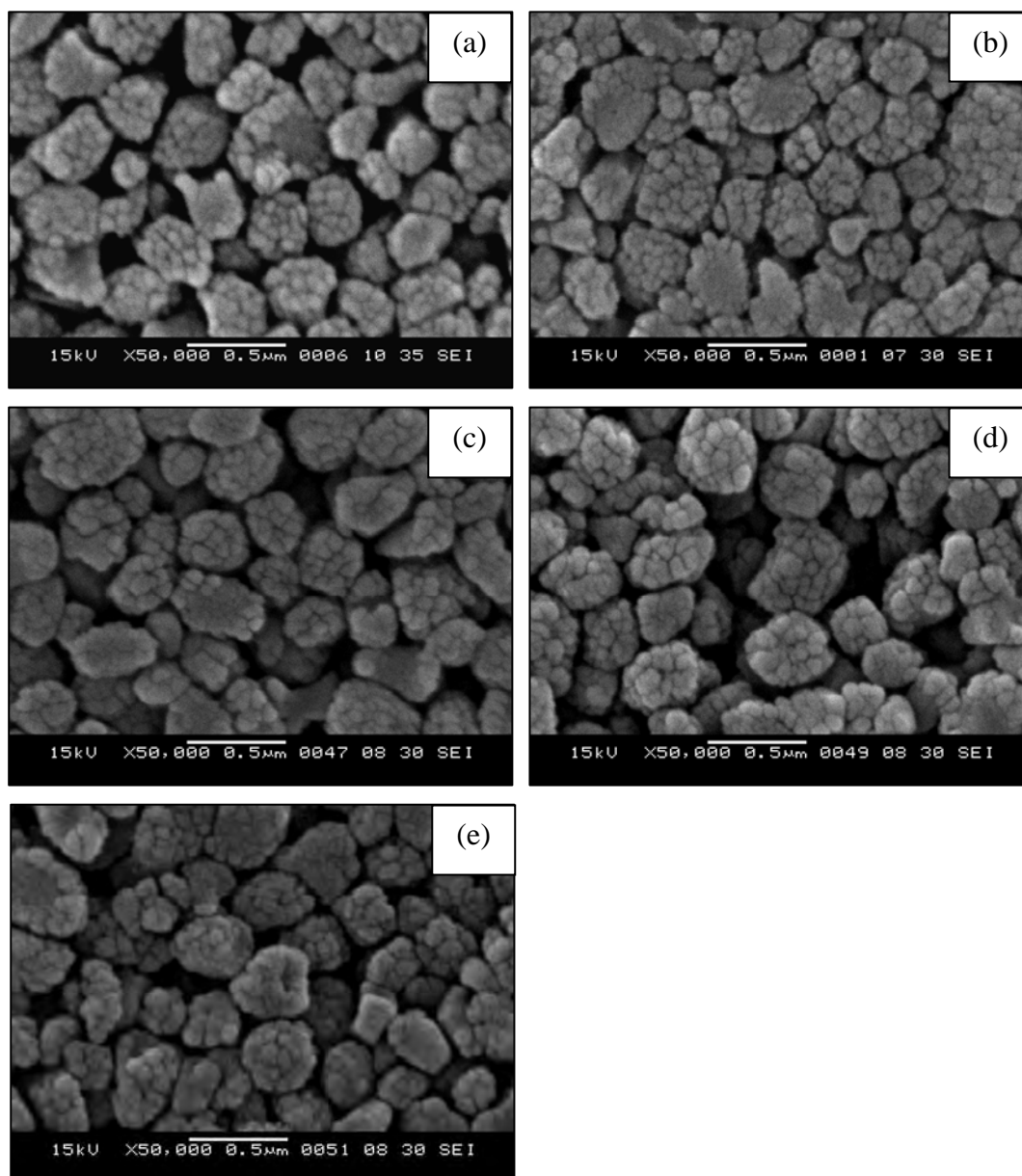
The used sample XGOH-12h became black after use due to coke deposition on the surface and in the pores. However, it easily turned to white after regeneration by calcination in a muffle furnace at 550°C for 5 h. Figure 4.38 shows the same XRD patterns of fresh XGOH-12h and the regenerated XGOH-12h catalysts. The result confirms that regenerated XGOH-12h catalysts still have a characteristic pattern of ZSM-5 with almost the same crystallinity as the unused catalyst, even if the catalysts were used repeatedly in HDPE cracking for up to four cycles and regenerated after each cycle, showing high stability of ZSM-5.



**Figure 4.38** XRD patterns of (a) fresh XGOH-12h, (b) the 1<sup>st</sup> regenerated, (c) the 2<sup>nd</sup> regenerated, (d) the 3<sup>rd</sup> regenerated and (e) the 4<sup>th</sup> regenerated XGOH-12h catalysts.

#### 4.3.4.1.2 SEM images

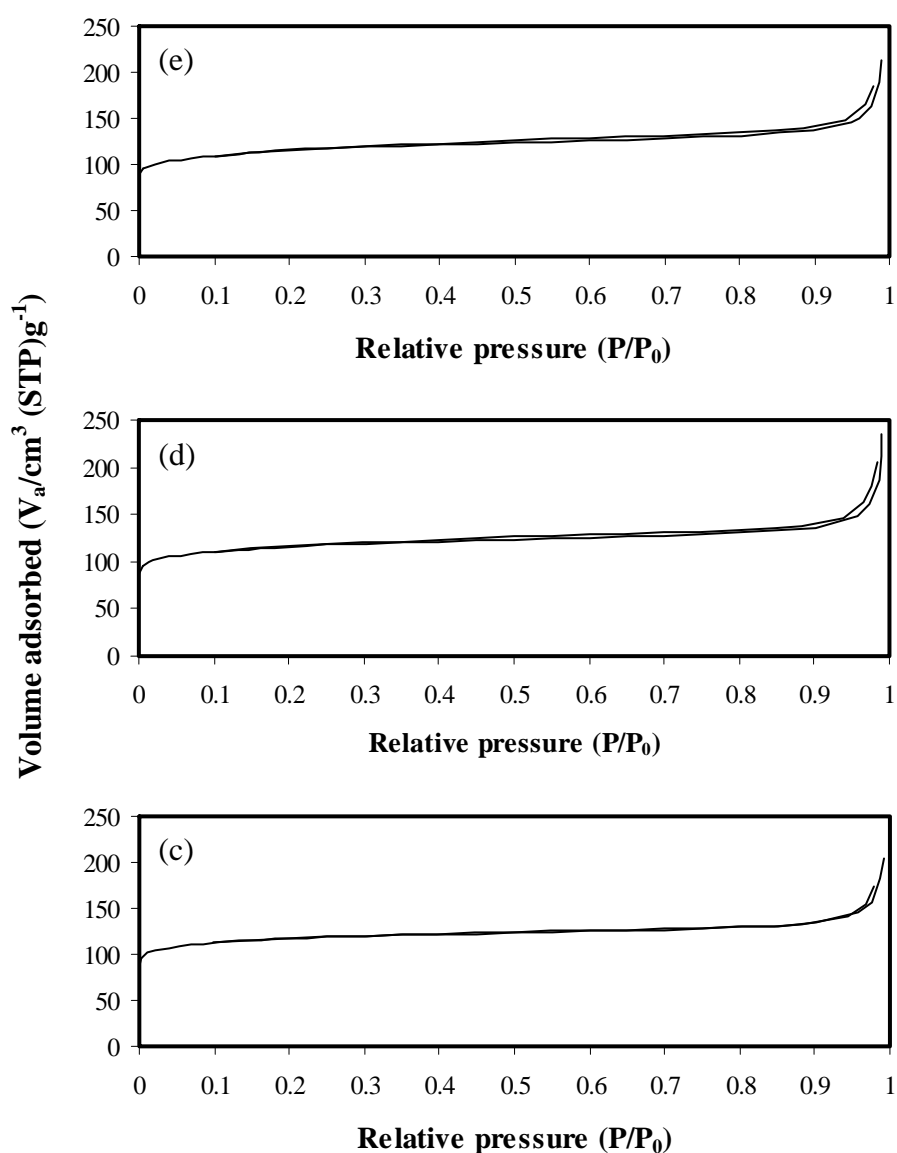
SEM images of fresh and regenerated XGOH-12h catalysts are shown in Figure 4.39. The 1<sup>st</sup> regenerated, 2<sup>nd</sup> regenerated, 3<sup>rd</sup> regenerated and 4<sup>th</sup> regenerated XGOH-12h catalysts show similar particle shape and size to the fresh catalyst.



**Figure 4.39** SEM images of fresh and regenerated XGOH-12h catalysts: (a) fresh XGOH-12h, (b) 1<sup>st</sup> regenerated, (c) 2<sup>nd</sup> regenerated, (d) 3<sup>rd</sup> regenerated and (e) 4<sup>th</sup> regenerated XGOH-12h catalysts.

#### 4.3.4.1.3 Nitrogen adsorption

The adsorption-desorption isotherms of fresh and regenerated XGOH-12h catalyst are exhibited in Figure 4.40. All samples also show the adsorption isotherms of microporous materials. The physical properties of fresh and regenerated XGOH-12h catalysts are shown in Table 4.16. The regenerated XGOH-12h catalysts exhibit slightly lower specific surface area and external surface area than the fresh catalyst.



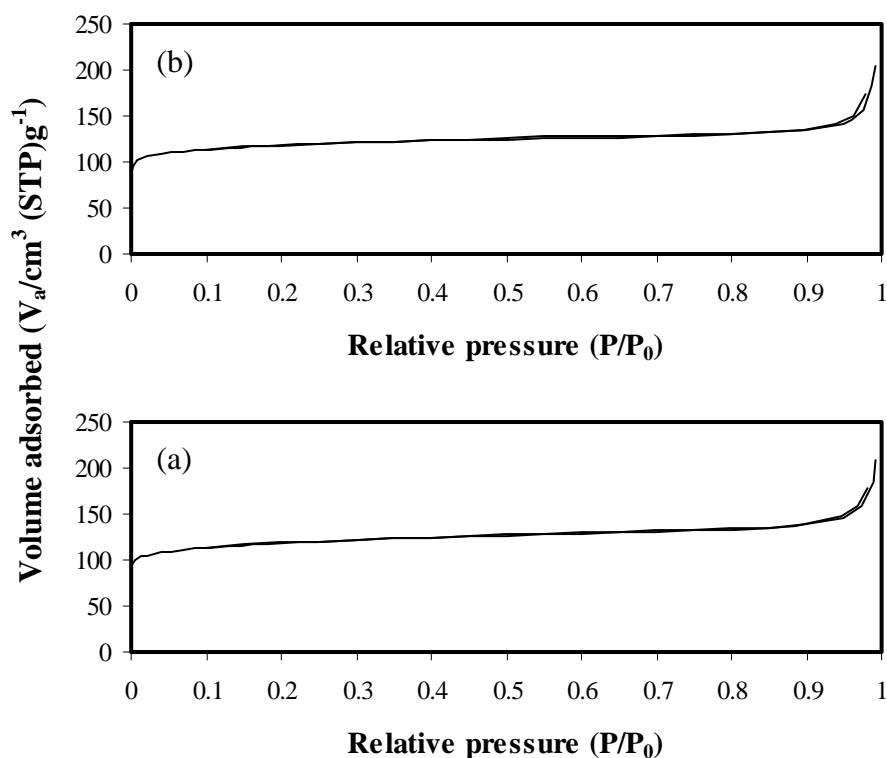


**Figure 4.40** N<sub>2</sub> adsorption-desorption isotherms of (a) fresh, (b) 1<sup>st</sup> regenerated, (c) 2<sup>nd</sup> regenerated, (d) 3<sup>rd</sup> regenerated and (e) 4<sup>th</sup> regenerated XGOH-12h catalysts.

**Table 4.16** The physical properties of fresh and regenerated XGOH-12h catalysts

Sample	S <sub>BET</sub> <sup>a</sup> (m <sup>2</sup> /g)	S <sub>ext</sub> <sup>b</sup> (m <sup>2</sup> /g)	d <sub>p</sub> <sup>c</sup> (nm)
Fresh XGOH-12h	458	47	0.6
1 <sup>st</sup> regenerated XGOH-12h	452	45	0.6
2 <sup>nd</sup> regenerated XGOH-12h	446	43	0.6
3 <sup>rd</sup> regenerated XGOH-12h	438	36	0.6
4 <sup>th</sup> regenerated XGOH-12h	432	35	0.6

<sup>a</sup> Specific surface area determined by application of BET-plot method

<sup>b</sup> External surface area determined by application of t-plot method

<sup>c</sup> Pore size distribution determined by application of MP-plot method



#### 4.3.4.2 Reactivity of regenerated catalysts on HDPE cracking

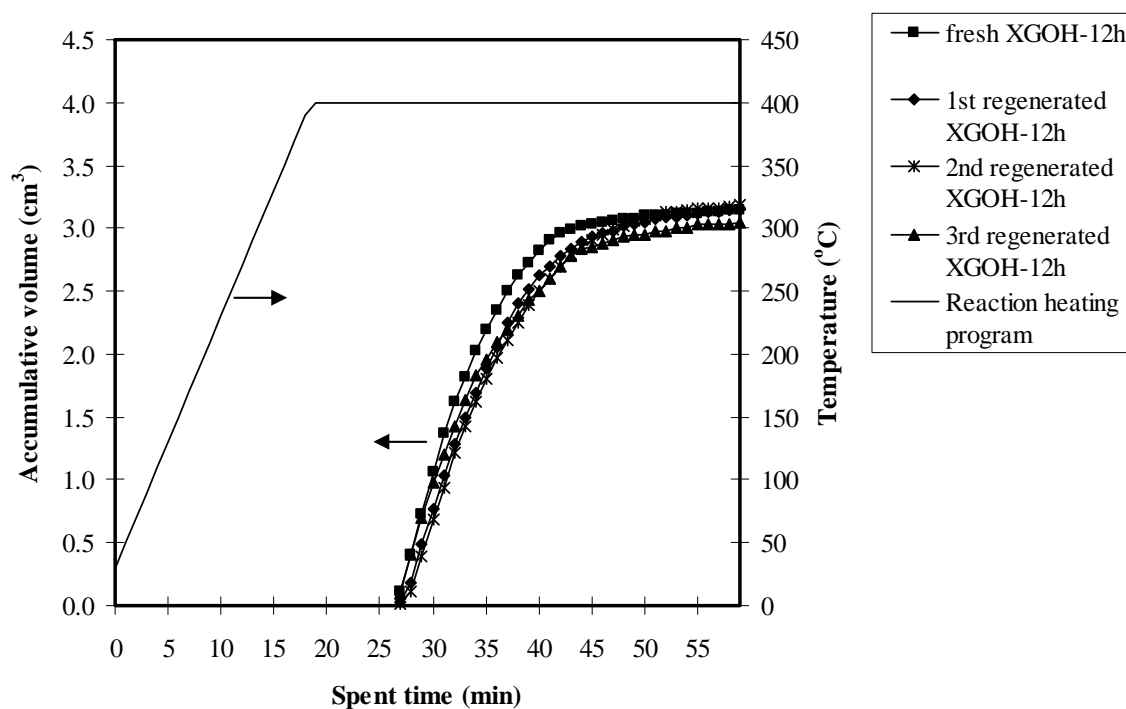
The catalytic cracking of HDPE was carried out at the optimum condition (Condition: 10 wt% catalyst of plastic, N<sub>2</sub> flow of 20 cm<sup>3</sup>/min, 400°C and reaction time of 40 min) using the XGOH-12h catalyst. The conversion and product distribution obtained are shown in Table 4.17. The conversions and product yields of the regenerated catalysts are not much different from that of the fresh catalyst. The significant differences are the yield of distillate oil, heavy oil and residue. The regenerated catalyst provided relatively lower yield of distillate oil and higher yield of heavy oil than the fresh catalyst. Relatively larger amount of residue, especially in form of wax was remained in the reactor of the regenerated catalysts rather than that of fresh catalyst. This result suggests the regenerated catalysts have lower specific surface area and external surface area than the fresh catalyst.

**Table 4.17** Values of %conversion and %yield obtained by catalytic cracking of HDPE over fresh and regenerated XGOH-12h catalysts (Condition: 10 wt% catalyst of plastic, N<sub>2</sub> flow of 20 cm<sup>3</sup>/min, 400°C and reaction time of 40 min)

	Thermal	Fresh XGOH-12h	1 <sup>st</sup> regenerated XGOH-12h	2 <sup>nd</sup> regenerated XGOH-12h	3 <sup>rd</sup> regenerated XGOH-12h
%Conversion*	3.67	96.67	96.47	95.40	92.80
% Yield*					
1. gas fraction	3.67	52.67	51.80	50.10	48.60
2. liquid fraction	0.00	44.00	46.33	45.30	44.20
- distillate oil	-	37.91	39.06	36.44	34.03
- heavy oil	-	6.09	7.27	8.86	10.17
3. residue	96.33	3.33	3.53	4.60	7.20
- solid coke	-	0.69	0.70	0.78	0.76
Total volume of liquid fraction ( cm <sup>3</sup> )	-	3.14	3.18	3.22	3.15
Liquid fraction density (g/ cm <sup>3</sup> )	-	0.70	0.70	0.71	0.71

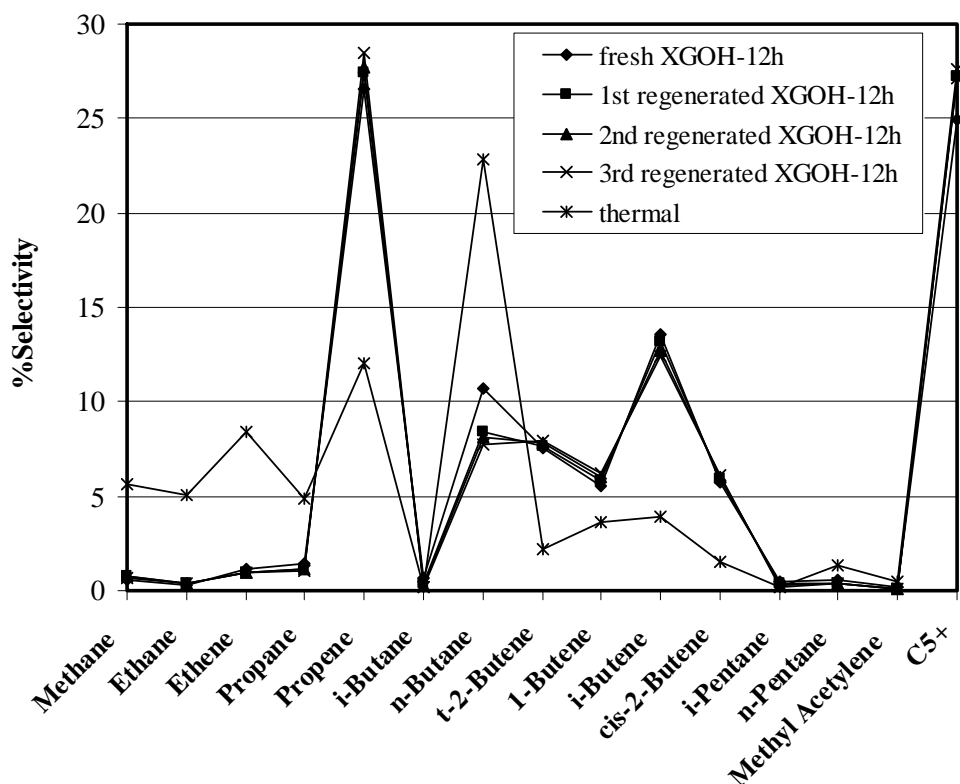
\*Deviation within 0.3% for conversion, 0.7% for yield of gas fraction, 0.5% for yield of liquid fraction, and 0.3% for yield of residue.

Figure 4.41 shows the accumulative volume of liquid fractions in the graduated cylinder. The regenerated catalyst promotes the rate of reaction slightly different to that obtained from fresh catalyst. Moreover, total amounts of liquid fraction are not much different from fresh catalyst. This shows that the catalysts can be used repeatedly at similar efficiency after regeneration.



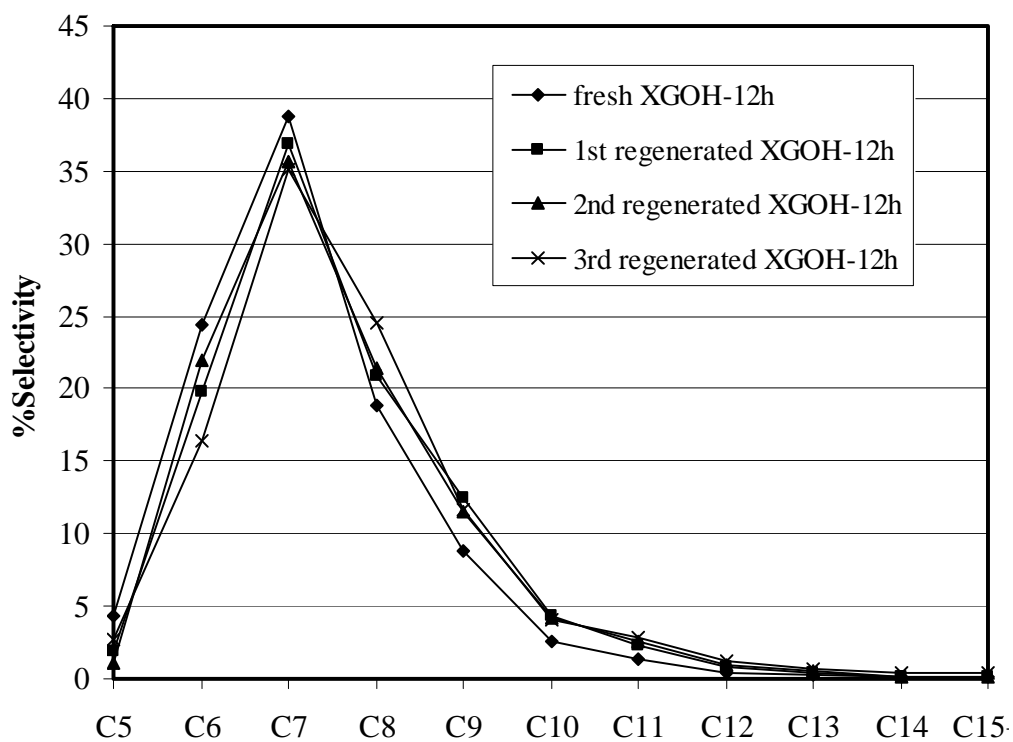
**Figure 4.41** Accumulative volume of liquid fractions obtained by catalytic cracking of HDPE over fresh and regenerated XGOH-12h catalysts at 400°C (Condition: 10 wt% catalyst of plastic, N<sub>2</sub> flow of 20 cm<sup>3</sup>/min and reaction of 40 min).

Figure 4.42 presents gas product distribution from HDPE cracking over fresh and regenerated XGOH-12h catalysts at 400°C. These results are similar to each other with the majority of gaseous product being in the propene, n-butane, i-butene and C<sub>5</sub>+. When the regenerated catalysts are used, the selectivity to C<sub>5</sub>+ increases while that to n-butane decreases.



**Figure 4.42** Distribution of gas fraction obtained by the thermal cracking and catalytic cracking of HDPE over fresh and regenerated XGOH-12h catalysts at 400°C (Condition: 10 wt% catalyst of plastic, N<sub>2</sub> flow of 20 cm<sup>3</sup>/min and reaction of 40 min).

Figure 4.43 shows product distribution of the liquid fraction obtained by the HDPE cracking using the fresh and regenerated XGOH-12h catalysts at 400°C. Both fresh and regenerated catalysts provide mainly the C<sub>6</sub> to C<sub>9</sub> range in liquid fraction.



**Figure 4.43** Carbon number distribution of liquid fractions from catalytic cracking of HDPE over fresh and regenerated XGOH-12h catalysts at 400°C (Condition: 10 wt% catalyst of plastic, N<sub>2</sub> flow of 20 cm<sup>3</sup>/min and reaction of 40 min).

## CHAPTER V

### CONCLUSION

ZSM-5 was synthesized using two different methods: hydrothermal method and xerogel method. The hydrothermal synthesis method was carried out by mixing sodium metasilicate pentahydrate solution with a sodium aluminate solution and then a solution of template, followed by crystallization at 170°C for various periods. The other so-called xerogel method is the synthesis of ZSM-5 from a freshly prepared silica xerogel mixed with aluminium isopropoxide and a solution of tetrapropylammonium hydroxide, followed by crystallization at 170°C for various periods.

For hydrothermal method, the effects of template, pH of gel, template/SiO<sub>2</sub> ratio, ultrasound irradiation or sonication, crystallization time and Si/Al ratio on formation of zeolite ZSM-5 were investigated. Tetrapropylammonium bromide and tetrapropylammonium hydroxide were used as templates in preparing ZSM-5. Tetrapropylammonium hydroxide provides smaller particle size of ZSM-5. The pH of gel of 10.5 and the template/SiO<sub>2</sub> ratio of 0.1 show the appropriate condition to synthesize ZSM-5. The application of ultrasound irradiation does not affect the structure and crystallinity but affects particle size and yield of ZSM-5. The crystallinity and particle size are not different when increasing the crystallization time from 24 to 96 h. The intensities of the reflection peaks at low angle ranging from 8°-10° increase when the Si/Al ratio increases. <sup>27</sup>Al-MAS-NMR spectra show that the aluminum atoms remain in tetrahedral oxygen coordination at the framework position. N<sub>2</sub> adsorption-desorption isotherms of all ZSM-5 catalysts exhibit a pattern of type I which is typical for microporous materials. The NH<sub>3</sub>-TPD profiles indicate that the number of acid sites decreases when aluminum content in catalyst decreases.

For xerogel method, XRD patterns show that the formation of zeolite ZSM-5 can be achieved after 6 h. With increasing crystallization time, the intensity of

characteristic peak at  $2\theta$  of  $23^\circ$  of the as-synthesized zeolite product slightly increases. Adsorption-desorption isotherms of nitrogen for all catalysts exhibits a pattern of type I which is a typical shape for micropores. The  $^{27}\text{Al}$ -MAS-NMR spectra of all samples present only tetrahedral aluminum. The signal of tetrahedral aluminum gradually decreases with the increase of crystallization time. The catalysts prepared by xerogel method have smaller particle size than the catalysts prepared by hydrothermal method. It can be concluded that the particle size strongly depends on the synthesis method.

The catalytic cracking of HDPE waste was chosen to test for the catalytic activities of ZSM-5 catalysts. The results show the efficiency of catalytic cracking of the polymer depends on physical characteristics of the catalysts. Conversion and yield by catalytic cracking are extremely higher than thermal cracking. Sample XGOH-12h prepared by xerogel method shows similar activity to the HTOH-10.5-0.1so-24h-60, which prepared by hydrothermal method. XGOH-12h shows higher liquid fraction and distillate oil than HTOH-10.5-0.1so-24h-60, while the HTOH-10.5-0.1so-24h-60 shows higher gas fraction than XGOH-12h. The conversion increases when reaction temperature increases. The initial rate of liquid fraction formation at  $400^\circ\text{C}$  is much faster than that at  $380^\circ\text{C}$  and the total volume of liquid fraction obtained at  $400^\circ\text{C}$  is greater than that at  $380^\circ\text{C}$ .

The gas fraction obtained by HDPE cracking composes mainly propene, n-butane, i-butene and  $\text{C}_5+$ . The distillate oil obtained by cracking of HDPE are mainly in the boiling point ranging from  $\text{C}_6$  to  $\text{C}_9$  which is similar to the range of standard gasoline fraction hydrocarbon based on the boiling point range using n-paraffins as reference.

The used zeolite ZSM-5 catalyst can be regenerated easily by combustion of coke in a furnace. The regenerated ZSM-5 was tested for catalytic cracking of HDPE at  $400^\circ\text{C}$ . It is found that the structure of ZSM-5 is highly stable and can be used repeatedly after regeneration. The regenerated catalysts have almost the same crystallinity as the unused catalyst. The regenerated catalysts show slightly lower specific surface area than the fresh catalyst. For HDPE cracking, the cracking activity of the regenerated catalyst still does not change significantly compared with the fresh catalyst.

**The suggestions for future work**

1. To compare ZSM-5 with other zeolite materials for catalytic cracking of HDPE and PP under the same condition.
2. To investigate the efficiency of ZSM-5 for catalytic cracking of mixed plastic containing HDPE, LDPE, PP, PS.

## REFERENCES

- [1] Feedstock recycling of plastic waste [Online]. Available from: [http://books.google.com/books?id=HUILAvuGsoQC&pg=PA2&lpg=PA2&dq=plastic+consumption&source=bl&ots=AwwDcvH1eM&sig=FpjqNyno\\_Bw8kRiqqIRBTQDVrSk&hl=th&ei=Kmi5SduKCIBPkAXmhcyNCA&sa=X&oi=book\\_result&resnum=6&ct=result#PPA2,M1](http://books.google.com/books?id=HUILAvuGsoQC&pg=PA2&lpg=PA2&dq=plastic+consumption&source=bl&ots=AwwDcvH1eM&sig=FpjqNyno_Bw8kRiqqIRBTQDVrSk&hl=th&ei=Kmi5SduKCIBPkAXmhcyNCA&sa=X&oi=book_result&resnum=6&ct=result#PPA2,M1) [2008, December 3]
- [2] Classification of plastic [Online]. Available from: [http://plastics.indiabizclub.com/info/plastic/classification\\_of\\_plastic](http://plastics.indiabizclub.com/info/plastic/classification_of_plastic) [2009, February 25]
- [3] Identify and sort the main types of plastic [Online]. Available from: <http://www.coffeecountyrecycling.com/Plastic%20Classification.pdf> [2009, January 22]
- [4] อภิพร ภายวิจิตร. *Future of Thailand petrochemical industry*. เอกสารเสวนาโต๊ะกลมคืนเหี้ยวชาววิทยา, จุฬาลงกรณ์มหาวิทยาลัย, 28 มกราคม 2548.
- [5] Marcilla, A.; Ruiz-Femenia, R.; and Hernandez, J. Thermal and catalytic pyrolysis of crosslinked polyethylene. *J. Anal. Appl. Pyrolysis*. 76(2006): 254.
- [6] Marcilla, A.; Gómez-Siurana, A.; and Berenguer, D. Study of the characteristics of different acid solids in the catalytic pyrolysis of different polymers. *Appl. Catal. A*. 301(2006): 222-231.
- [7] Aguado, J.; Serrano, D.P.; San Miguel, G.; Escola, J.M.; and Rodríguez, J.M. Catalytic activity of zeolitic and mesostructured catalysts in the cracking of pure and waste polyolefins. *J. Anal. Appl. Pyrolysis* 78(2007): 153-161.
- [8] Serrano, D.P.; Aguado, J.; Escola, J.M.; Garagorri, E.; Rodríguez, J.M.; Morselli, L.; Pallazi, G.; and Orsi, R. Feedstock recycling of agriculture plastic film wastes by catalytic cracking. *Appl. Catal. B*. 49(2004): 257-265.
- [9] Park, J.W.; Kim, J.-H.; and Seo, G. The effect of pore shape on the catalytic performance of zeolites in the liquid-phase degradation of HDPE. *Polym. Degrad. Stab.* 76(2002): 495-501.



- [10] Durmuş, A.; Naci Koç, S.; Selda Pozan, G.; and Kaşgöz, A. Thermal-catalytic degradation kinetics of polypropylene over BEA, ZSM-5 and MOR zeolites. *Appl. Catal. B.* 61(2005): 316-322.
- [11] José Geraldo A. Pacheco Filho; Emerson Cruz, Graciliano; Antonio Osimar S. Silva; Marcelo J.B. Souza; Antonio Souza Araujo. Thermo gravimetric kinetics of polypropylene degradation on ZSM-12 and ZSM-5 catalysts. *Catal. Today.* 107-108(2005): 507-512.
- [12] Kim, J.R.; Kim, Y.A.; Yoon, J.H.; Park, D.W.; and Woo, H.C. Catalytic degradation of polypropylene:effect of dealumination of clinoptilolite catalyst. 247. *Polym. Degrad. Stab.* 75(2002): 287-294.
- [13] Zhou, Q.; Wang, Y.-Z.; Tang, C.; and Zhang, Y.-H. Modifications of ZSM-5 zeolites and their applications in catalytic degradation of LDPE. *Polym. Degrad. Stab.* 80(2003): 23-30.
- [14] Marcilla, A.; Gómez, A.; Reyes-Labarta, J.A.; and Giner, A. Kinetic study of polypropylene pyrolysis using ZSM-5 and an equilibrium fluid catalytic cracking catalyst. *J. Anal. Appl. Pyrolysis* 68-69(2003): 467-480.
- [15] Saha, B.; and Goshal, A.K. Model-free kinetics analysis of ZSM-5 catalyzed pyrolysis of waste LDPE. *Thermochimica Acta* 453(2007): 120-127.
- [16] Wang, K.; and Wang, X. Comparison of catalytic performances on nanoscale HZSM-5 and microscale HZSM-5. *Microporous and Mesoporous Materials* 112(2007): 187-192.
- [17] Zhou, Q.; Zheng, L.; Wang, Y.; Zhao, G. and Wang, B. Catalytic degradation of low-density polyethylene and polypropylene using modified ZSM-5 zeolites. *Polym. Degrad. Stab.* 84(2004): 493-497.
- [18] Sakata, Y.; Uddin, A.; and Muto, A. Degradation of polyethylene and polypropylene into fuel oil by using solid acid and non-acid catalysts. *J. Anal. Appl. Pyrolysis* 51(1999): 135-155.
- [19] Manos, G.; Garforth, A.; and Dwyer, J. Catalytic degradation of high-density polyethylene over different zeolitic structures. *Ind. Eng. Res.* 39(2000): 1198-1202.
- [20] Gobin, K.; and Manos, G. Polymer degradation to fuels over microporous catalysts as a novel tertiary plastic recycling method. *Polym. Degrad. Stab.* 83(2004): 267-279.

- [21] Aguado, J.; Sotelo, J.L.; Serrano, D.P.; Callers, J.A.; and Escola, J.M. Catalytic conversion of polyolefins into liquid fuels over MCM-41: Comparison with ZSM-5 and amorphous SiO<sub>2</sub>-Al<sub>2</sub>O<sub>3</sub>. *Energy & Fuels* 11(1997): 1225.
- [22] García, R.A.; Serrano, D.P.; and Otero, D. Catalytic cracking of HDPE over hybrid zeolitic-mesoporous materials. *J. Anal. Appl. Pyrolysis* 74(2005): 379-386.
- [23] Zhang, P.; Guo, X.; Guo, H.; and Wang, X. Study of the performance of modified nano-scale ZSM-5 zeolite on olefins reduction in FCC gasoline. *J. Mol. Catal. A*. 261(2007): 139-146.
- [24] Serrano, D.P.; Aguado, J.; and Escola, J.M. Catalytic cracking of a polyolefin mixture over different acid solid catalysts. *Ind. Eng. Chem. Res.* 39 (2000): 1177.
- [25] Aguado, J.; Serrano, D.P.; San Miguel, G.; Escola, J.M.; and Rodríguez, J.M. Catalytic activity of zeolitic and mesostructured catalysts in the cracking of pure and waste polyolefin. *J. Anal. Appl. Pyrolysis* 78(2007): 153-161.
- [26] Breck, D.W. *Zeolite Molecular Sieves: Structure, Chemistry, and use*, New York: John Wiley & Sons, 1997, 3-20.
- [27] Szostak, R. *Zeolite Molecular Sieves. Principles of Synthesis and Identification*, New York Van: Nostrand Reinhold, 1989, 3-42.
- [28] Derouane, E.G. New aspects of molecular shape-selectivity: Catalytic by zeolite ZSM-5. *Studies Surface Science Catal.* 5(1980): 5.
- [29] Szostak, R. *Molecular Sieve Principles of Synthesis and Identification*, New Van Nostrand Reinhold, New York, 1988, 1-45.
- [30] Argauer, R.J.; and Landolt, G.R. Crystalline zeolite ZSM-5 and method of preparing the same. *United States Patent* 3(1972): 702-886.
- [31] Smart, L.; and Moore, E. *Solid State Chemistry*. London, Chapman & Hall University, 1992.
- [32] Derouane, E.G. New aspects of molecular shape-selectivity: Catalytic by zeolite ZSM-5. *Studies Surface Science Catal.* 5 (1980): 5.
- [33] Lewis, D.W.; Catlow, C.R.A.; and Sankar, G. Structure of Iron-substituted ZSM-5. *J. Phys. Chem.* 99(1995): 2377.

- [34] Burkett, S. L.; and Davis, M. E. Growth model of oriented crystals of zeolite Si-ZSM-5. *J. Phys. Chem.* 98(1994): 4647.
- [35] Pastore, H.O.; Munsignati, M.; Rippel, M. M.; and Bittencourt, D. Why are carbon molecular sieves interesting?. *Micropor. Mesopor. Mater.* 32 (1999): 211.
- [36] Leonid, V.A. *Elements of X-ray crystallography*, Mcgraw-hill, New York, 1997, 4-25.
- [37] Skoog, D.A. *Principles of Instrumental Analysis*, 4<sup>th</sup> ed., Harcourt Brace College Publishers, New York, 1997, 363-364.
- [38] Gabriel, B.L. *SEM: A User's Manual for Material Science*, Ohio: American Society for Metal, 1985.
- [39] Reding, G.; Mäurer, T.; and Kraushaar-Czarnetzki, B. Comparing synthesis routes to nanocrystalline zeolite ZSM-5. *Micropor. Mesopor. Mater.* 57(2003): 83-92.
- [40] Basic operating principles of the sorptomatic 1990. [Online]. Available from: <http://saf.chem.ox.ac.uk./Instruments/BET/sorpoptprin> [2008, March 12]
- [41] Analysis software user's manual, BELSORP, BEL JAPAN, INC. 57.
- [42] Elliott, P.B.; Leslie, G.J.; and Paul, P.H. The determination of pore volume and area distributions in porous substances. I Computations from nitrogen isotherms. Contribution from the multiple fellowships of Baugh and Sons Company, Mellon Institute 73(1995): 373.
- [43] Brunauer, S.; Emmett, P.M.; and Teller, E. Adsorption of gases in mutimolecular layers. The Bureau of chemistry and solids and george Washington University, 60(1938): 309.
- [44] Temperature-programmed desorption (TPD) for characterizing the acid sites on oxide surfaces-supplier data by micromeritics. [Online]. Available from: <http://www.azonano.com/details.asp?ArticleID=1475> [2006, February 12]
- [45] Hunger, M.; Schenk, U.; Breuninger, R.; Glaser, R.; and Weikamp, J. Characterization of the acid sites in MCM-41 type materials by spectroscopic and catalytic technique. *Micropor. Mesopor. Mater.* 27(1999): 261.

- [46] Nelson, W.L. Petroleum Refinery Engineering, 4<sup>th</sup> ed., Singapore: Mcgraw-hill, 1987, 759-818.
- [47] Serge Raseev Thermal and Catalytic Process in Petroleum Refining, Maecel Dekker, New York, 2003, 293-403.
- [48] Oil refinery: Cracking [Online] Available from: <http://www.schoolscience.co.uk/content/4/chemistry/petroleum/knowl/4/cracking.html> [2009, January 15]
- [49] George, O. Principle of Polymerization, 4<sup>th</sup> ed., Canada: Wiley & Sons, 2004, 209-235.
- [50] Yury, V.K. Chemical mechanisms of catalytic cracking over solid acidic catalyst: alkanes and alkenes. *Taylor & Francis* 48(2001): 85.
- [51] Scherzer, J. Octane-enhancing, zeolitic FCC catalyst: scientific and technical aspect. *Catal.* 31(1989): 83.
- [52] Greensfflder, B.S.; and Voge, H.H.; Good, G.M. Catalytic and thermal cracking of pure hydrocarbons. *Ind. Eng. Chem.* 41(1949): 2573.
- [53] Thomas, C.L. Chemistry of cracking catalysts. *Ind. Eng. Chem.* 41(1949): 2564.
- [54] Sie, S.T. Acid-catalyzed cracking of paraffinics Part2. Evidence for the protonnated cyclopropane mechanism from catalytic cracking experiments. *Ind. Eng. Chem.* 32(1993): 397.
- [55] Williams, B.A.; Babitz, S.M.; Miller, J.T.; Snurr, R.Q.; and Kung, H.H. The role of acid strength and pore diffusion in the enhanced cracking activity of steamed zeolites Y. *Apply. Catal. A.* 32(1999): 161.
- [56] Cumming, K.A.; and Wojciechowski, B.W. Hydrogen transfer, coke formation and catalyst decay and their role in the chain mechanism of catalytic cracking. *Catal. Rev. Sci. Eng.* 38(1996): 101.
- [57] Wojciechowski, B.W.; and Abbot, J. The mechanism of catalytic cracking of n-alkanes on ZSM-5 zeolite. *J. Chem. Eng.* 63(1985): 462.
- [58] Makkee, M.; Wissink, M.; and Moulijin, J.A. Gasoline conversion: reactivity towards cracking with equilibrated FCC and ZSM-5 catalysts. *Apply. Catal. A.* 223(2002): 85.
- [59] Szostak, R.; and Thomas, T. L. Preparation of ferrisilicate ZSM-5 molecular sieves. *J. Catal.* 100(1986): 555-557.

- [60] Aguado, J.; Serrano, D. P.; Escola, J. M.; Garagorri, E.; and Fernández, J. A. Catalytic conversion of polyolefins into fuels over zeolite beta. *Polym. Degrad. Stab.* 69(2000): 11-16.
- [61] Armaroli, T.; Simon, L.J.; Digne, M.; Montanari, T.; Bevilacqua, M.; Valtchev, V.; Patarin, J.; and Busca, G. Effect of crystal size and Si/Al ratio on the surface properties of HZSM-5 zeolites. *Apply. Catal. A.* 306(2006): 78-84.
- [62] Serrano, D.P.; Aguado, J.; Escola, J.M.; and Rodríguez, J.M. Influence of nanocrystalline HZSM-5 external surface on the catalytic cracking of polyolefins. *J. Anal. Appl. Pyrolysis* 74(2005): 353-360.
- [63] Yeon, Y.H.; Nam, S.S.; Kim, S.B.; and Lee, K.W. The pH effect on the preparation of MFI type ferrisilicate zeolites. *Bull. Korean Chem. Soc.* 20(1999): 781-785.
- [64] Zhang, Y.; Zhou, Y.; Liu, H.; Wang, Y.; Xu, Y.; and Wu, P. Effect of La addition on catalytic performance of PtSnNa/ZSM-5 catalyst for propane dehydrogenation. *Apply. Catal. A.* 333(2007): 202-210.
- [65] Kumar, N.; Masloboischikova, O.V.; Kustov, L.M.; Heikkilä, T.; Murzin, D.Y. Synthesis of Pt modified ZSM-5 and beta zeolite catalysts: Influence of ultrasonic irradiation and preparation methods on physico-chemical and catalytic properties in pentane isomerization. *Ultrasonics Sonochemistry* 14(2007): 122-130.
- [66] Andaç, Ö.; Tatlıer, M.; Sirkecioğlu, A.; Ece, I.; Şenatalar, A.E. Effects of ultrasound on zeolite A synthesis. *Micropor. Mesopor. Mater.* 79(2005): 225-233.
- [67] Aguado, J.; Serrano, D.P.; Escola, J.M.; and Rodríguez, J.M. Low temperature synthesis and properties of ZSM-5 aggregates formed by ultra-small nanocrystals. *Micropor. Mesopor. Mater.* 75(2004): 41-49.

## **APPENDICE**

**A-1 Calculation of Selectivity to Other Hydrocarbons****% Selectivity of gas fraction and liquid fraction**

$$\% \text{ Selectivity of X} = \frac{\text{concentration of X} \times 100}{\text{total concentration of fractions}}$$

$$\text{Concentration of X} = \frac{b \times c}{a}$$

a = Peak area of X in standard gas or liquid fraction

b = % molar of X in standard gas or liquid fraction

c = Peak area of X in sample products

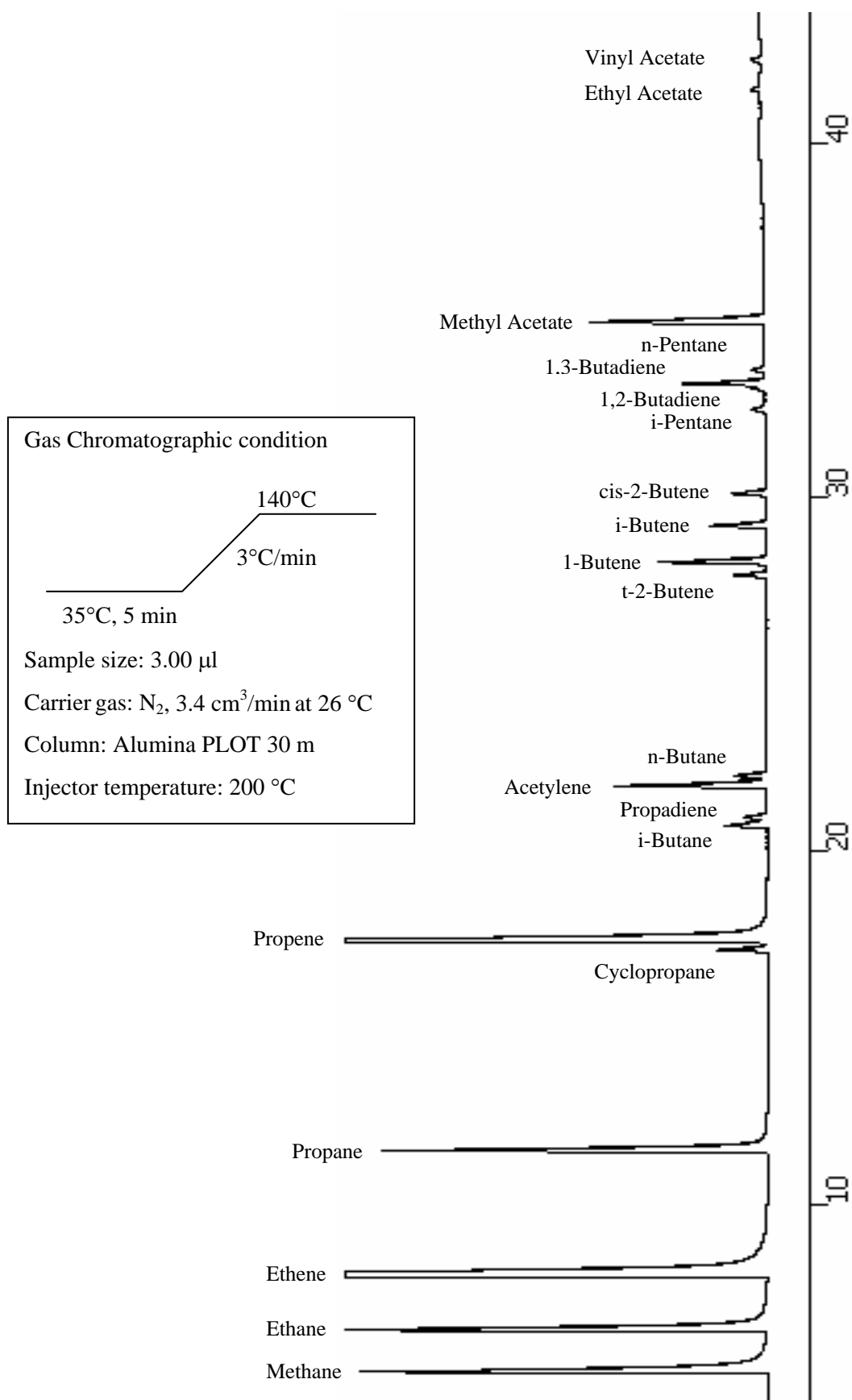


**Figure A-1** Gas chromatogram of standard mixture gas.



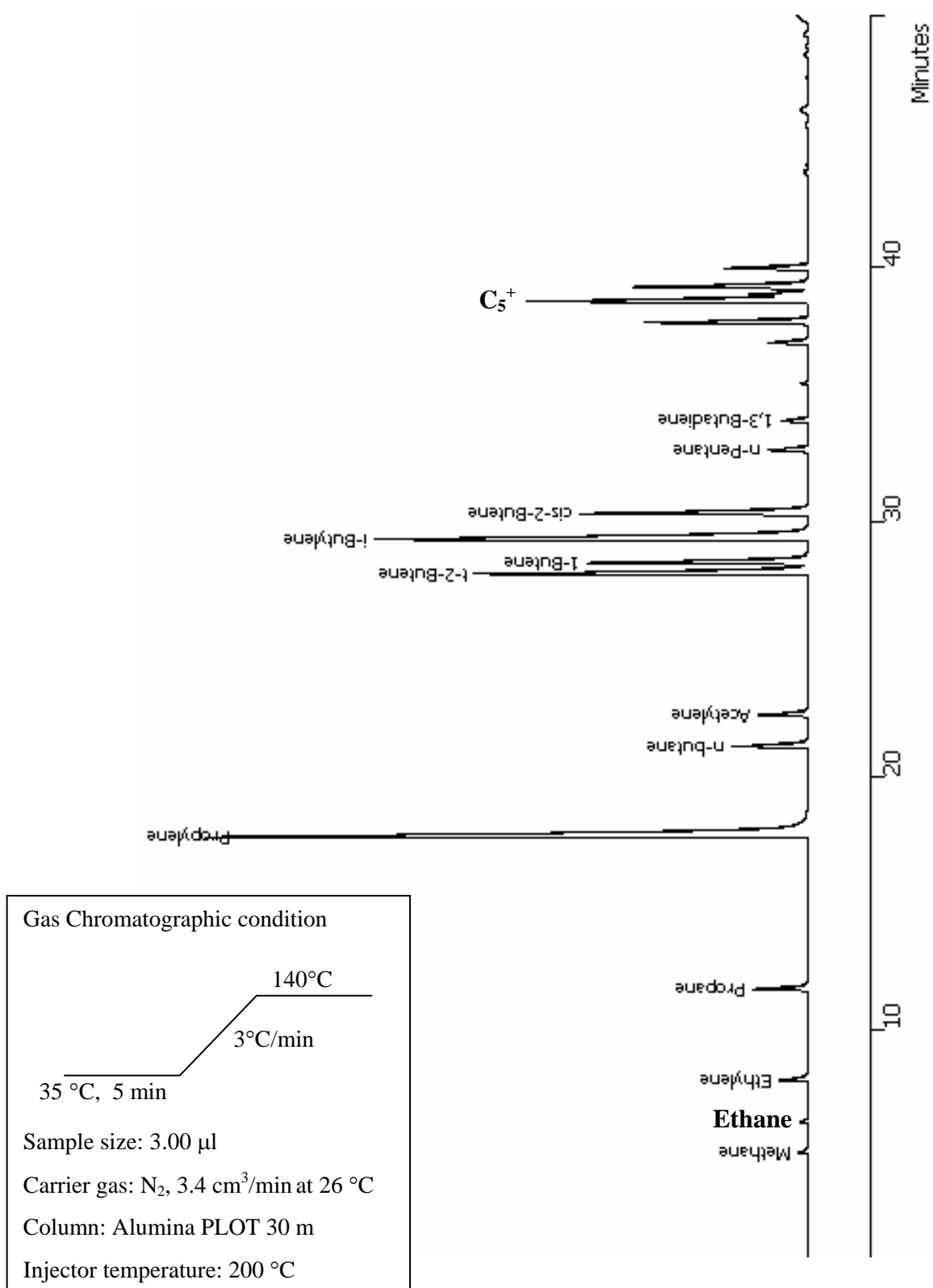


**Figure A-2** Gas chromatogram of gas product obtained from catalytic cracking of HDPE over XGOH-12h (Si/Al ratio = 60) at 400°C.

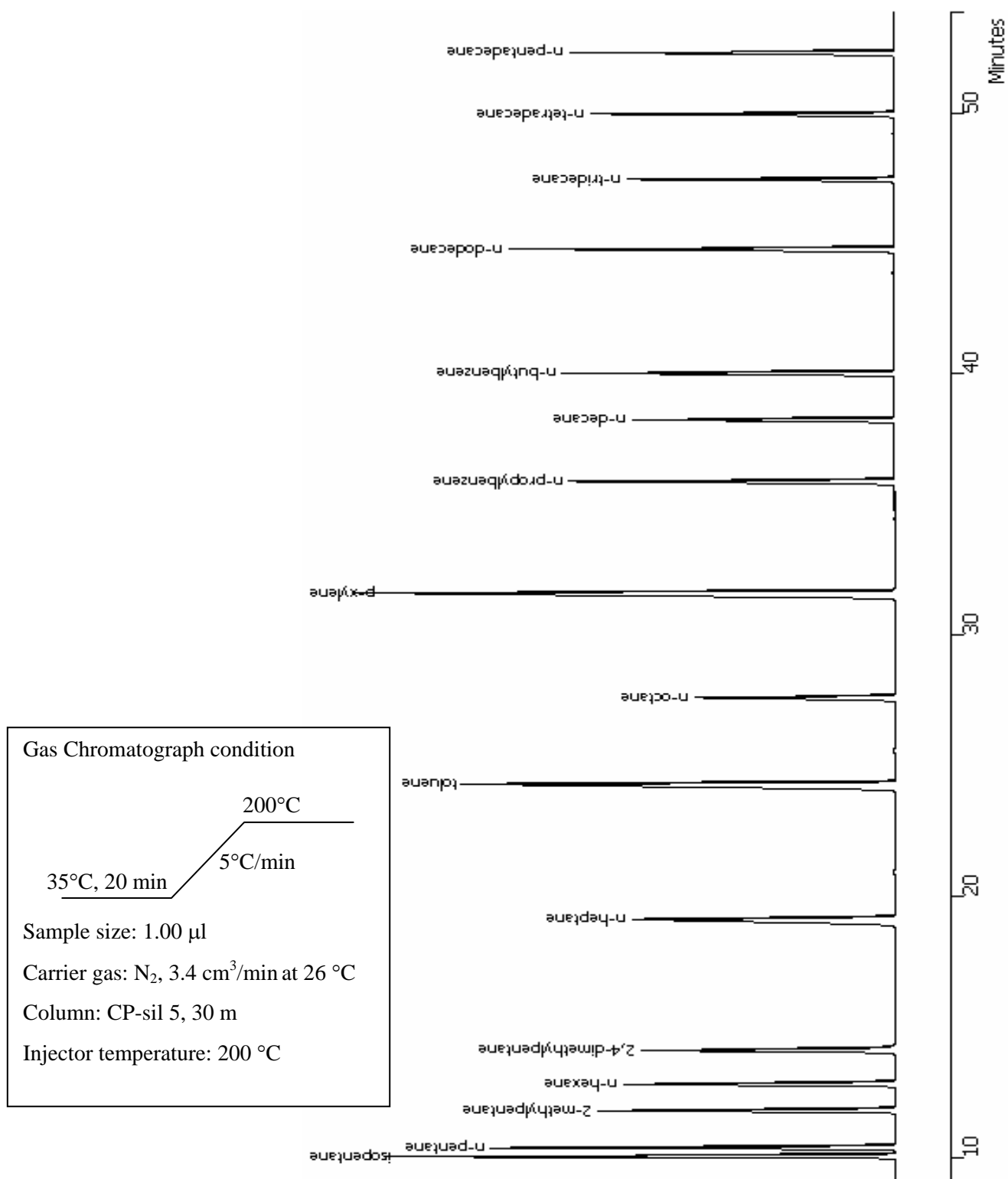


**Figure A-3** Liquid chromatogram of standard gasoline (SUPELCO).

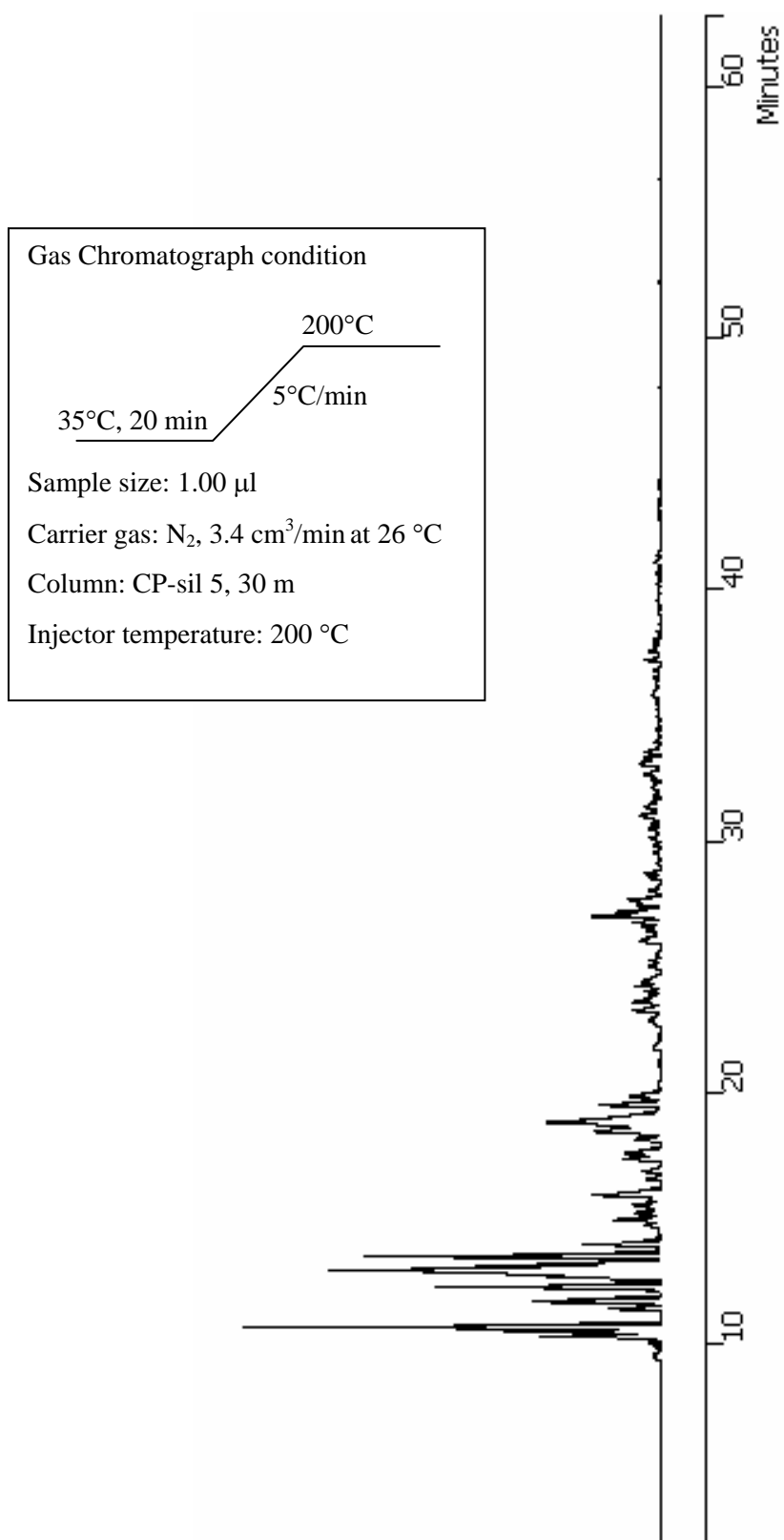


**Figure A-4** Gas chromatogram of gas product obtained from catalytic cracking of HDPE over XGOH-12h (Si/Al ratio = 60) at 400°C.

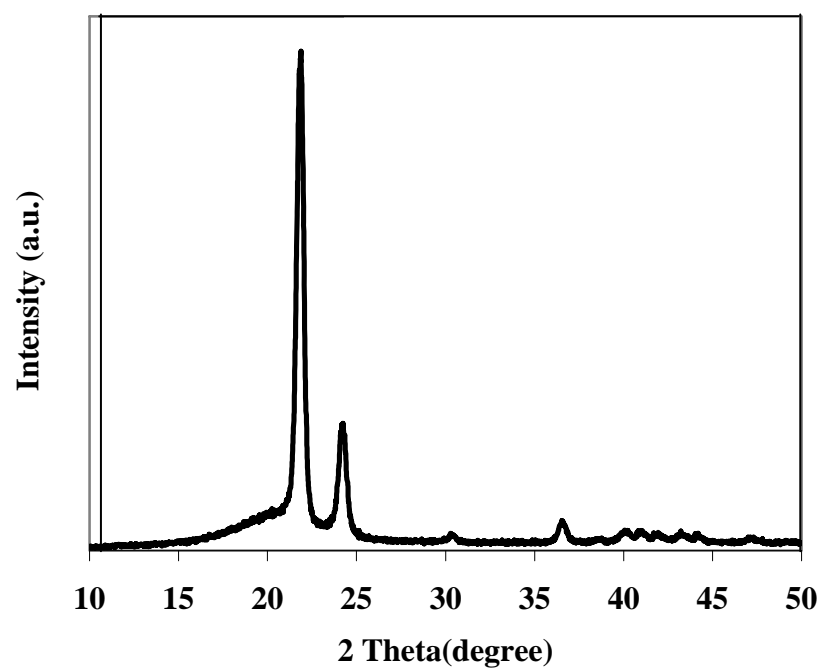


**Figure A-5** XRD pattern of a HDPE bottle used as a representation plastic waste.

## **VITAE**

Miss Sineenat Utto was born on May 27, 1983 in Kalasin, Thailand. She graduated with Bachelor's Degree in Chemistry from Faculty of Science, Mahidol University in 2005. She continued her study in Petrochemistry and Polymer Science Program, Faculty of Science, Chulalongkorn University in 2005 and completed her M.Sc. degree in 2009.